From th	ne Cécile	& Oskar	Vogt	Institute	of I	3rain	Resear	rch
	at Hein	rich Hein	e Uni	versity D)üss	eldor	f	

Cytoarchitectonic mapping of five new areas in the anterior latera
prefrontal cortex

Dissertation

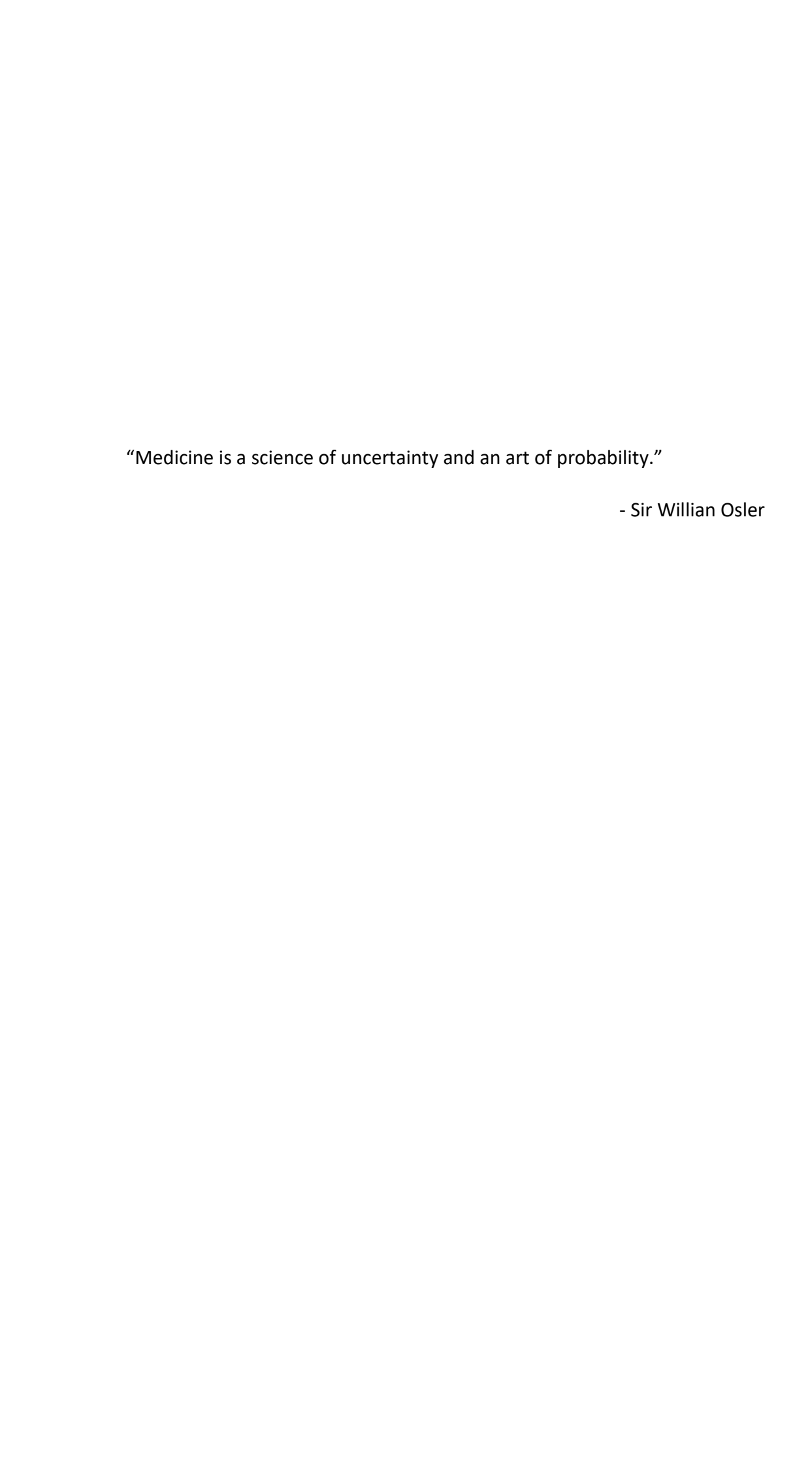
to obtain the academic title of Doctor of Philosophy (PhD) in Medical Sciences from the Faculty of Medicine at Heinrich Heine University Düsseldorf

Submitted by

Zien Zhang

2025

As an inaugural dissertation printed by permission of the Faculty of Medicine at Heinrich Heine University Düsseldorf
Signed:
Dean: Prof. Dr. med. Nikolaj Klöcker Evaminers: Prof. Dr. med. Katrin Amunts. Prof. Dr. med. Michael Sahel
Examiners: Prof. Dr. med. Katrin Amunts, Prof. Dr. med. Michael Sabel



Parts of this thesis have been published in:	
Poster, "Cytoarchitectonic mapping of five new areas in t cortex" at the 8 th Bigbrain Workshop, Padua, September	

Zusammenfassung

In der vorliegenden Studie wurden fünf neue cytoarchitektonische Areale (IMFS1, IMFS2, MFG3, IFG1 und IFG2) im lateralen präfrontalen Kortex des menschlichen Gehirns identifiziert. Digitalisierte, zellkörpergefärbte histologische Schnitte von zehn postmortem Gehirnen wurden dazu untersucht. Eine quantitative und reproduzierbare, beobachterunabhängige zytoarchitektonische Kartierungsmethode wurde angewandt, bei der der Grey Level Index (GLI) als Maß für die Zelldichte verwendet wurde. GLI-Profile, die über den Kortex liefen, erlaubten in Kombination von Bildanalyse und multivariaten statistischen Tests die Abgrenzung zytoarchitektonischer Areale sowie deren quantitative Charakterisierung. Auf Basis der unterschiedlichen räumlichen Lage der fünf neu kartierten Areale in den zehn Gehirnen wurden Wahrscheinlichkeitskarten im stereotaktischen Raum erstellt, die deren interindividuelle Variabilität widerspiegeln. Darüber hinaus wurde eine maximale Wahrscheinlichkeitskarte berechnet, um die räumliche Ausdehnung der Areale zu visualisieren und die Komplexität zu reduzieren.

Die fünf neuen Areale befinden sich im anterioren lateralen präfrontalen Kortex. Die Areale IMFS1 und IMFS2 waren hauptsächlich in der Tiefe des Sulcus frontalis intermedius lokalisiert, während sich das Areal MFG3 überwiegend auf dem rostralen Teil des Gyrus frontales medius befand. Die Areale IFG1 und IFG2 lagen auf dem rostralen Teil des Gyrus frontalis inferior. Diese Areale folgen einer dorso-ventralen sowie einer rostro-kaudalen Anordnung. Die fünf Areale konnten aufgrund ihrer zytoarchitektonischen Merkmale eindeutig unterschieden werden. Alle Areale sind granuläre isokortikale Areale und wiesen sechs kortikale Schichten mit einer ausgeprägten inneren granulären Schicht IV auf. Eine Clusteranalysen ergab, dass die Areale IMFS1, IMFS2 und IFG2 zytoarchitektonische Ähnlichkeiten mit dem lateralen orbitofrontalen Kortex (Fo5, Fo6) aufwiesen, während die Areale MFG3 und IFG1 eine stärkere Ähnlichkeit mit dem präfrontalen Kortexareal mfg5 zeigten. Alle fünf Areale unterscheiden sich deutlich von anderen präfrontalen Kortexarealen (mfg1, mfg2 und mfg4), der Broca-Region und dem frontalen Polareal Fp1.

Darüber hinaus wurde eine meta-analytische Konnektivitätsmodellierung durchgeführt, um zu untersuchen, an welchen Funktionen die neu kartierten Areale beteiligt sind. Diese waren mit verschiedenen kognitiven Funktionen assoziiert, darunter

Sprachverarbeitung, Arbeitsgedächtnis, logisches Denken, emotionale Verarbeitung sowie perzeptive und interozeptive Funktionen. Die Areale IMFS1 und MFG3 wurden primär mit dem Arbeitsgedächtnis, perzeptivem Schmerz und Verhaltensinhibition in Verbindung gebracht, während das Areal IMFS2 eine statistisch signifikante Assoziation mit perzeptivem Schmerz zeigte. Die Areale IFG1 und IFG2 wiesen eine funktionelle Lateralisation auf. Konkret waren die Areale der linken Hemisphäre an der Sprachverarbeitung beteiligt, während die rechten Areale mit emotionalen Funktionen assoziiert waren.

Die neu erstellten zytoarchitektonischen Karten der Areale IMFS1, IMFS2, MFG3, IFG1 und IFG2 werden als neuroanatomische Grundlage zukünftigen bildgebenden Studien dienen, die darauf abzielen, Struktur-Funktions-Beziehungen in komplexen kognitiven Prozessen zu entschlüsseln.

Summary

In the present study, five new cytoarchitectonic areas (IMFS1, IMFS2, MFG3, IFG1 and IFG2) were identified within the lateral prefrontal cortex of the human brain. Digitized histological sections of ten postmortem brains, stained for cell bodies, were studied. A quantitative and reproducible observer-independent cytoarchitectonic mapping approach was applied, utilizing the grey level index (GLI) as a metric for cell packing density. GLI profiles spanning the cortical ribbon facilitated the identification of borders between cytoarchitectonic areas through image analysis and multivariate statistical tests, enabling a quantitative characterization of these areas. Probability maps were generated in stereotaxic space based on the localization of these five newly identified areas in the ten individual brains, revealing their inter-subject variability. Additionally, the maximum probability map (MPM) was computed to visualize the spatial extent of these areas and reduce complexity.

The five new areas were located in the anterior lateral prefrontal cortex. Specifically, area IMFS1 and IMFS2 were primarily located in the depth of intermediate frontal sulcus, while area MFG3 was predominantly situated on the anterior part of the middle frontal gyrus. Areas IFG1 and IFG2 were mainly positioned on the anterior part of inferior frontal gyrus. These areas followed a dorsal-to-ventral as well as a rostral-to-caudal arrangement. Each of the five areas can be differentiated based on its cytoarchitectonic characteristics. All areas were classified as granular isocortical areas, exhibiting six cortical layers with a developed inner granular layer IV. Cluster analysis revealed that areas IMFS1, IMFS1 and IFG2 were cytoarchitectonically more similar to the lateral orbitofrontal cortex (Fo5, Fo6), while areas MFG3 and IFG1 exhibited greater similarity to the dorsolateral prefrontal cortex areas mfg5. Notably, all five areas were distinct from anteriorly located prefrontal cortex areas (mfg1, mfg2, and mfg4), Broca's region and the frontal pole area Fp1.

In addition, a meta-analytic connectivity modelling (MACM) was performed to investigate the functional involvement of the five newly identified areas. They were associated with various cognitive functions, including language processing, working memory, reasoning, emotional processing, as well as perceptual and interoceptive

functions. Area IMFS1 and MFG3 were primarily linked to working memory, perceptual pain, and behavioural inhibition, while area IMFS2 demonstrated a statistically significant association with perceptual pain. Importantly, areas IFG1 and IFG2 exhibited the most pronounced functional lateralization. Specifically, the left hemispheric IFG1 and IFG2 were involved in language processing, whereas their right hemispheric counterparts were associated with emotional functions.

The newly generated cytoarchitectonic maps of areas IMFS1, IMFS2, MFG3, IFG1 and IFG2 will serve as a neuroanatomical framework for future neuroimaging studies aimed at elucidating structure-function relationships in complex cognitive processes.

Abbreviations

as	ascending sulcus (ascending ramus of the lateral fissure)	ВА	Brodmann area
BD	Behavioural Domain	СВР	connectivity-based parcellations
cs	central sulcus	DA	discriminant analysis
DLPFC	dorsolateral prefrontal cortex	DMTS	delayed Match to Sample
ds	diagonal sulcus	DiFuMo	Dictionaries of Functional Modes
FDR	false discovery rate	fMRI	Functional Magnetic Resonance Imaging
Fo	orbitofrontal cortex	FOP	frontal operculum
Fp	frontal pole area	GLI	grey level index
НВР	human brain project	НСР	Human Connectome Project
hs	horizontal sulcus (horizontal ramus of the lateral fissure)	ifs	inferior frontal sulcus
imfs	intermediate frontal sulcus	imfs-h	horizontal part of the intermediate frontal sulcus
imfs-v	vertical part of the intermediate frontal sulcus	IFG/ ifg	inferior frontal gyrus
iprs	inferior precentral sulcus	Ifms	lateral frontomarginal sulcus
LPFC	lateral prefrontal cortex	MACM	meta-analytic connectivity modelling
MFG/ mfg	middle frontal gyrus	MD	Mahalanobis distance
MNI	montreal neurological institute	MPFC	medial prefrontal cortex
MPM	maximum probability map	MRI	magnetic resonance imaging
MRIs	magnetic resonance images	Op	Area opercularis
OPFC	orbital prefrontal cortex	PC	Paradigm Classes

PET	Positron Emission Tomography	PFC	prefrontal cortex
pimfs	paraintermediate frontal sulcus	pimfs-d	paraintermediate frontal sulcus, dorsal
pimfs-v	paraintermediate frontal sulcus, ventral	pmfs	posterior middle frontal sulcus
prs	precentral sulcus	rs- fNIRS	resting-state functional near- infrared spectroscopy
ROI	region of interest	SD	standard deviation
SFG/	superior frontal gyrus	sfs	superior frontal sulcus
sfg sfs-a	anterior branch of superior frontal sulcus	sfs-p	posterior branch of superior frontal sulcus
sprs	superior precentral sulcus	ts	triangular sulcus
VLPFC	ventrolateral prefrontal cortex		

Table of contents

1	Intr	oduc	tion ·····	1
	1.1	Cyto	parchitecture ·····	1
	1.2	Pref	frontal Cortex: Structures and Functions ·····	4
	1.2	.1	Development of the prefrontal cortex	4
	1.2	.2	Structure of the lateral prefrontal cortex	5
	1.2	.3	Mapping of the prefrontal Cortex	9
	1.2	.3.1 R	eview of previous cytoarchitectural maps of the human prefrontal cortex	9
	1.2	.3.2 L	imitations of existing cytoarchitectonic maps	12
	1.2	.4	Functions and dysfunctions of the lateral prefrontal cortex	13
	1.3	Aim	s of the study ·····	· 17
2	Ма	terial	s and Methods·····	· 19
	2.1	Hist	ological processing of post-mortem brains	· 19
	2.2		erver-independent detection of cytoarchitectonic borders using the grey level	
	index			
	2.3		umetric analysis of delineated areas ······	
	2.4		rarchical clustering of mean areal GLI profiles ······	
	2.5		onstruction of cortical areas and probabilistic maps ······	
	2.6		ctional analytics·····	
3	Res			
	3.1	Cyto	parchitectonic characteristics and borders ······	· 27
	3.1	.1	Cytoarchitecture of areas IMFS1, IMFS2, MFG3, IFG1 and IFG2	29
	3.1	.2	Borders to neighboring areas	39
	3.2		antification of cytoarchitectonic differences and similarities of new areas and	
			g areas of the prefrontal cortex ······	
	3.3		vidual localization of areas within single brains ·······	
	3.3		Sulcal pattern	52
	3.3		The localization of areas	53
	3.4		bability maps and maximum probability maps ······	
	3.5	Volu	umes of areas IMFS1, IMFS2, MFG3, IFG1 and IFG2 ·······	· 62
	3.6 conne		ctional characterization of the cytoarchitectonic areas by meta-analytic y modelling······	. 64
	3.6 her	.1 nisph	Behavioural Domains of areas IMFS1, IMFS2, MFG3, IFG1 and IFG2 on both	65
	3.6	•	Paradigm Classes of areas IMFS1, IMFS2, MFG3, IFG1 and IFG2 on both	65
4		•	on	
-	יכוט	しいりりに	711	U.)

4.1 The newly defined five areas in the context of previous cytoarchitectonic				
4.1.1 Comparison with the map of Petrides and Pandya		Comparison with the map of Petrides and Pandya	70	
4.1.2		Comparison with other classical maps	72	
	4.1.3	Interpretation of the cluster analysis results	73	
	4.2 Var	iability in brains ·····	······ 75	
	4.2.1	Sulcal variability	75	
	4.2.2	Volumetric variability	75	
	4.3 Stru	ictural-Functional properties of areas IMFS1, IMFS2, MFG3, IFG1 and IFG2 $\cdot\cdot$	······ 78	
	4.3.1 IFG2	Relationship of structure and function of areas IMFS1, IMFS2, MFG3, IFG1 78	. and	
	4.3.2	Functional lateralization	83	
5	Conclusi	on	······ 86	
6	Reference	References8		
7	' Appendi	Appendix9		

1 Introduction

1.1 Cytoarchitecture

The cerebral cortex functions as the primary integrative and executive center of the human central nervous system (Brodmann 1909, Shi et al 2012). Cortical areas can be distinguished based on their microstructural properties (e.g., cytoarchitecture, myeloarchitecture, and receptor architecture), functional characteristics, and connectivity patterns (Zilles and Amunts 2010). Cytoarchitecture describes the spatial distribution of cell bodies, the presence or absence of particular cell types, their size, arrangement in layers and columns. It is a major principle of microstructural brain organization which have a high relevance for the interpretation of functional neuroimaging results (Amunts and Zilles 2015, Amunts et al 2020). The neocortex of the human brain exhibits a laminar structure. It comprises six distinct layers (with the exception of motor cortex), which can be identified and characterized using Nissl-stained sections. These layers, from the surface to the deeper cortical regions, are as follows: (I) Lamina molecularis, (II) Lamina granularis externa, (III) Lamina pyramidalis externa, (IV) Lamina granularis interna, (V) Lamina pyramidalis interna and (VI) Lamina multiformis (Brodmann 1909) (Figure 1).

Each layer shows distinct cytoarchitectonic characteristics:

- I. The lamina molecularis contains very few neurons.
- II. The lamina granularis externa consists of small, densely packed cell bodies even though most cells of this layer belong to small pyramidal neurons.
- III. The lamina pyramidalis externa is a thick layer in which pyramidal cells size increase from the upper to deeper part.
- IV. The lamina granularis interna is composed of densely packed, nonpyramidal and small pyramidal cells.
- V. The lamina pyramidalis interna primarily contains medium to large sized, loosely packed pyramidal cells.
- VI. The lamina multiformis is characterized by relatively tightly packed, spindle-shaped cells.

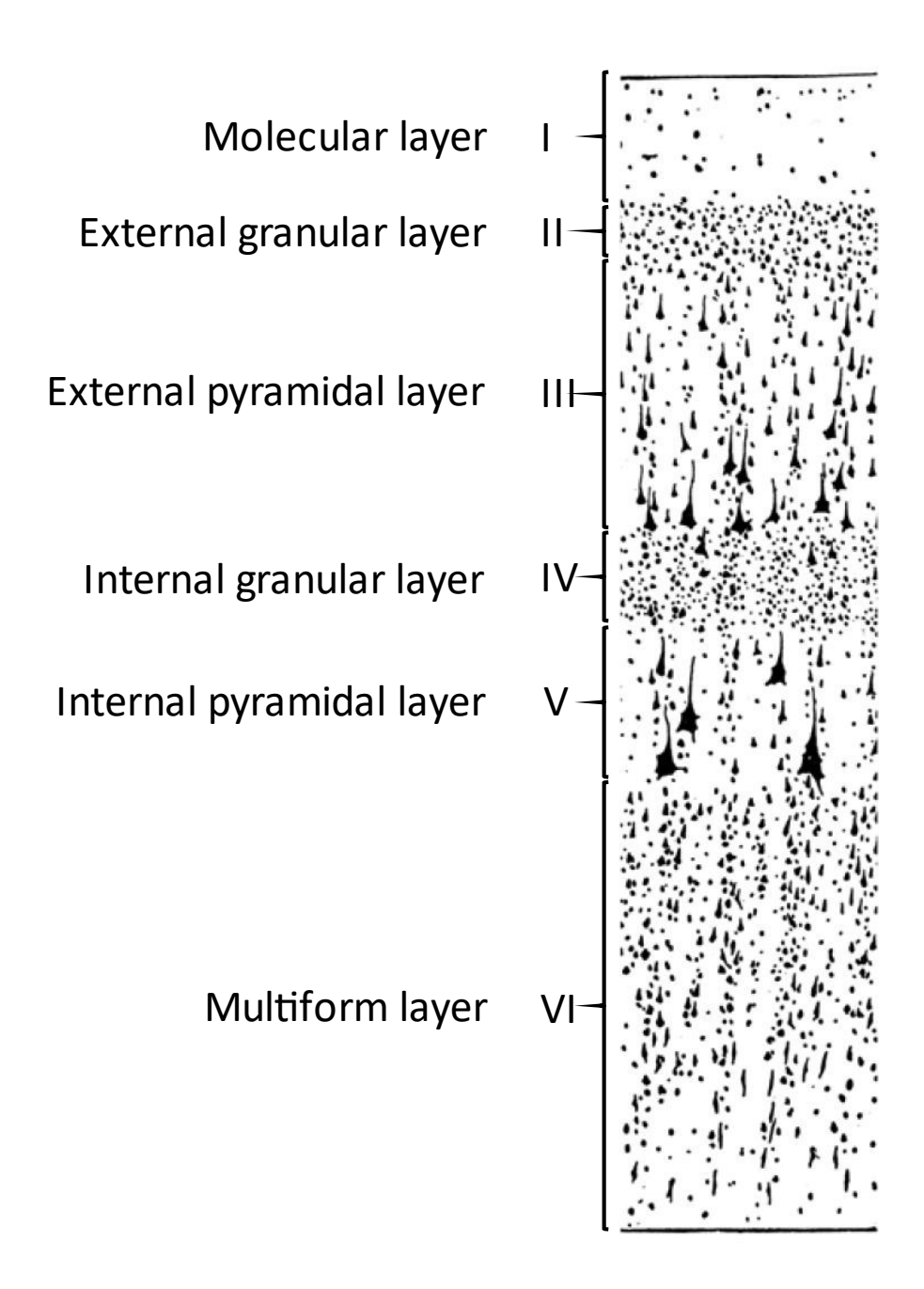


Fig. 1: Schematic of cytoarchitecture of the prefrontal cortex (PFC) in human brain

The laminar pattern of the human neocortex, visualized in Nissl-stained sections of an adult human brain, displays six cortical layers. The figure is adapted from Brodmann (Brodmann 1909).

Cytoarchitectonic studies of the human cerebral cortex began in the late 19th century. The first published map, by Campbell (1905), divided the cortex into several general regions (Campbell 1905). Subsequently, numerous cytoarchitectonic maps of the human cerebral cortex were produced by various investigators. Among the most notable maps from that period are those by Brodmann (Brodmann 1909), von Economo and Koskinas (von Economo and Koskinas 1925), Sarkissov et al. (Sarkissov et al 1955), and Petrides and Pandya (Petrides and Pandya 1999). In all these maps, the cortex is parcellated into a series of non-overlapping areas or fields. For example, Brodmann's map distinguishes 43 sharply delineated areas, with area 52 being the highest-numbered area; the total of 43 areas results from the absence of areas numbered 12-16 and 48-51 (Brodmann 1909, Zilles and Amunts 2010). Von Economo and Koskinas, as well as Sarkissov, further subdivided several of Brodmann's areas into smaller units, introducing many transitional zones within them, thereby resulting in a greater total number of fields than originally defined by Brodmann (Brodmann 1909, von Economo and Koskinas 1925, Sarkissov et al. 1955, Nieuwenhuys et al 2007). Furthermore, there are other cytoarchitectonic maps with fewer areas, such as Campbell's (12 areas in total) (Campbell 1905), Bailey and von Bonin's (8 areas in total) (Bailey 1951).

The architecture of the prefrontal cortex (PFC) has been studied in the context of whole-brain cytoarchitectonic mapping efforts conducted by several influential researchers. Investigators such as Beck (Beck 1949), Rajkowska and Goldman-Rakic (Rajkowska and Goldman-Rakic 1995), Amunts et al. (Amunts et al 1999), Semendeferi et al. and Petrides and Pandya (Petrides and Pandya 1999, Petrides et al 2012) systematically mapped the human cerebral cortex and, thereby providing detailed insights into the structure of the prefrontal cortex. Their work, along with other studies, has significantly advanced our understanding of the prefrontal cortex's complex architecture, offering insights into its organization and function. The following sections will provide an in-depth introduction of the structure, function, and cytoarchitectonic organization of this region.

1.2 Prefrontal Cortex: Structures and Functions

1.2.1 Development of the prefrontal cortex

The prefrontal cortex is a late-developing region of the neocortex and is known as the association cortex of the frontal lobe (Preuss and Wise 2022). It is both cytoarchitectonically and functionally diverse and considered to be the substrate for the highest cognitive functions, having been extensively studied in humans and nonhuman primates (Haber et al 2022, Levy 2024).

In humans, the PFC has expanded dramatically compared to that of other primates, occupying approximately one-third of the total neocortex (Carlén 2017). It is believed to be the last region of the brain to reach full maturity (Teffer and Semendeferi 2012). The development of both the axons and dendrites in frontal areas appears to lag chronologically behind that of other cortical areas during the perinatally period (Flechsig 1927, Tau and Peterson 2010). Evolutionarily, the cerebral cortex has advanced by increasing its surface area and by the introduction of new cytoarchitectonic areas (Fuster 2002, Kolk and Rakic 2022). All neurons in the PFC are generated between embryonic (E) day 40 and 90 within the 165-day gestational period in macaque monkeys (Bourgeois et al 1994, Kolk and Rakic 2022). The structural development of the PFC begins with a massive expansion of the most proximal part of the developing neural tube and then progresses in the dorsal telencephalon, situated between two older structures: the laterally positioned olfactory (piriform) pallium and the medially positioned hippocampal pallium, under the influence of the Fgf family (Fuster 2002, Kolk and Rakic 2022).

1.2.2 Structure of the lateral prefrontal cortex

The PFC exhibits a complex sulcus pattern and can be divided into three major regions: lateral (LPFC), medial (MPFC) and orbital (OPFC) (Figure 2) (Nieuwenhuys et al. 2007). These regions are reciprocally connected with each other as well as with the anterior and dorsal thalamus nuclei. Compared to other prefrontal regions, the LPFC exhibits a later and more extensive evolutionary expansion in terms of surface morphology. Additionally, the LPFC projects to the basal ganglia and is extensively interconnected with the association cortices of the occipital, temporal, and parietal lobes. In contrast, the medial and orbital frontal regions (MPFC and OPFC), are connected to the hypothalamus and other limbic structures, with some of these connections occurring indirectly via the thalamus (Fuster 2002).

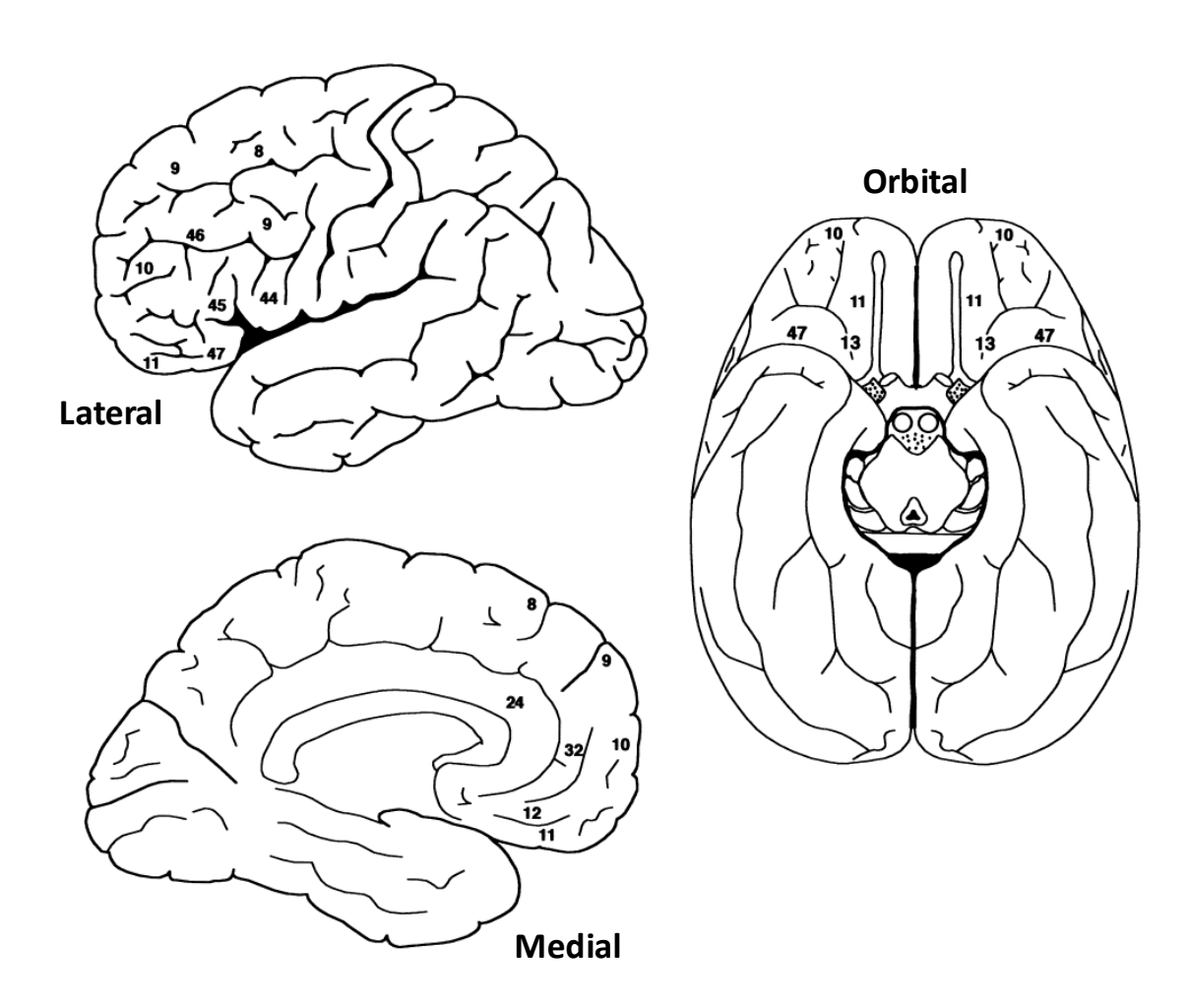


Fig. 2: Schematic of three views of the prefrontal cortex in human brain

Three views of the prefrontal cortex are shown with numbered areas corresponding to Brodmann's cytoarchitectonic map. The figure is adapted from Fuster (2002).

The lateral surface of the prefrontal cortex is marked by three horizontally oriented gyri: the superior, middle, and inferior frontal gyri, along with the frontopolar region. The primary sulci, including the superior and inferior frontal sulci, serve as key landmarks of the LPFC (see **Figure 3**).

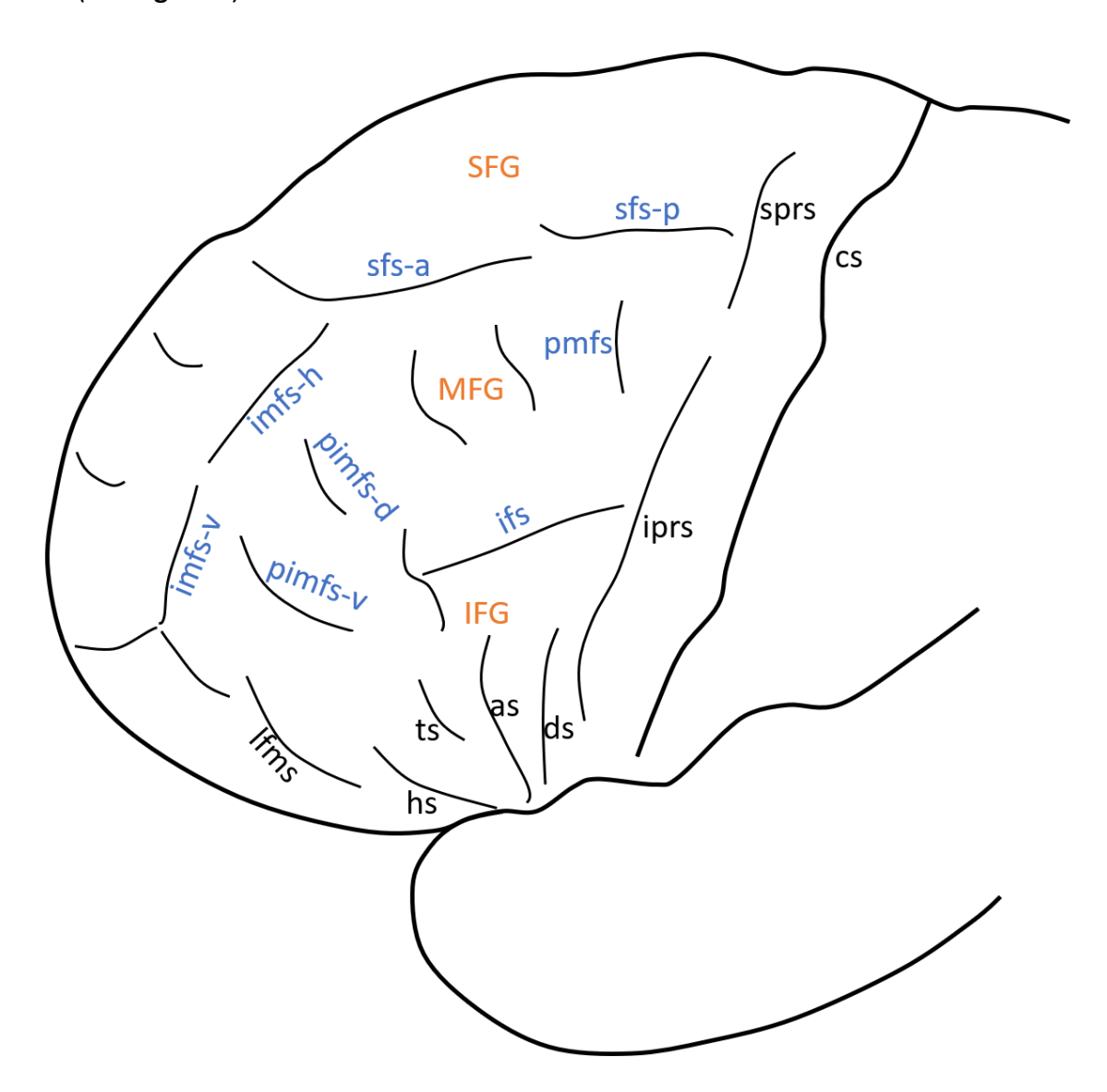


Fig. 3: The schematic of the lateral surface of the human brain with main anatomical landmarks

Three horizontally directed gyri, SFG, MFG and IFG occupy the major part of the lateral prefrontal cortex. Abbreviations: as, ascending sulcus (ascending ramus of the lateral fissure); cs, central sulcus; ds, diagonal sulcus; hs, horizontal sulcus (horizontal ramus of the lateral fissure); IFG, inferior frontal gyrus; ifs, inferior frontal sulcus; imfs-h, horizontal part of the intermediate frontal sulcus;

imfs-v, vertical part of the intermediate frontal sulcus; iprs, inferior precentral sulcus; Ifms, lateral frontomarginal sulcus; MFG, middle frontal gyrus; pmfs, posterior middle frontal sulcus; pimfs-d, paraintermediate frontal sulcus, dorsal; pimfs-v, paraintermediate frontal sulcus, ventral; SFG, superior frontal gyrus; sfs-a, anterior branch of superior frontal sulcus; sfs-p, posterior branch of superior frontal sulcus; sprs, superior precentral sulcus; ts, triangular sulcus. This schema is based on (Petrides and Pandya 2012, Petrides 2018).

The anterior sulcal pattern surrounding the middle frontal gyrus (mfg) and the sulci within its region show considerable complexity. Superiorly and anteriorly, the mfg is segregated by the superior frontal sulcus (sfs), while its inferior boundary is defined by the inferior frontal sulcus (ifs). However, due to the ifs typically not extending to the anterior part of the frontal lobe, the anterior-inferior boundary of the mfg is formed by the frontomarginal sulcus or lateral orbital sulcus. The anterior portion of the mfg is located within a deep sulcus, referred to as the middle frontal sulcus (mfs) or the intermediate frontal sulcus (imfs) (Ono et al 1990, Petrides 2013, Amiez et al 2023), though the intermediate frontal sulcus is also sometimes termed as infs (Petrides and Pandya 2012). This sulcus originates in the rostral part of the middle frontal gyrus, initially extending horizontally (imfs-h) before veering ventrally (imfs-v) to meet the medial frontomarginal sulcus. Lateral to the intermediate frontal sulcus, another set of short sulci are found: the paraintermediate frontal sulci (pimfs), which are divided into dorsal (pimfs-d) and ventral (pimfs-v) parts. The posterior middle frontal gyrus (pmfs) contains three of these sulci: the anterior (pmfs-a), intermediate (pmfs-i), and posterior (pmfs-p) components. These components exhibit considerable variability in their direction and may merge, creating complex and often confusing patterns.

The inferior frontal gyrus (ifg) can be divided into three distinct regions along a caudorostral axis: Pars opercularis, Pars triangularis, and Pars orbitalis. The posterior border of the ifg is delineated by the precentral sulcus (prs). The anterior boundary extends from the anterior tip of the inferior frontal sulcus to the frontomarginal sulcus or lateral orbital sulcus. The ifs typically extends rostrally to approximately the midportion of the dorsal edge of the pars triangularis. Due to individual variability, the lateral frontomarginal sulcus (Ifms) and lateral orbital sulcus may occasionally appear as sides branches of the ifs, further complicating the identification of frontal sulci (Ono et al. 1990). Thus, traditional macro landmarks are not

sufficiently reliable for guiding current functional imaging studies. Therefore, it is necessary to carefully differentiate the anterior portions of the mfg and ifg, as well as their surrounding sulci, through meticulous examination and the redefinition of their respective regions.

The prefrontal cortex can be differentiated based on its laminar organization, the presence of granule cells, glial composition, and afferent and efferent connectivity (Zald 2007, Bruno et al 2022, Bruno et al 2024). It can be subdivided into distinct cytoarchitectonic areas according to variations in cell size, cell type, and the structural arrangement of cortical layers, including differences in cell density, the presence or absence of specific layers, and variations in layer thickness (Petrides et al. 2012). The fundamental architectural characteristics shared across all cortical layers include cellular stratification and consistent patterns of connectivity (Fuster 2015). The cellular and fibrous architecture of the prefrontal cortex adheres to the general structural organization observed across neocortical regions, exemplified in human by the microscopic morphology of the isocortex. The lateral prefrontal cortex is classified as homotypical isocortex, exhibiting clear lamination with a well-developed internal granular layer (IV), which distinguishes it from the rest of the frontal cortex. This layer becomes progressively thicker and more defined as the cortex transitions toward the frontal pole (Fuster 2015).

1.2.3 Mapping of the prefrontal Cortex

1.2.3.1 Review of previous cytoarchitectural maps of the human prefrontal cortex

The extensive "Regio frontalis" in Brodmann's map encompasses areas 8, 9, 10, 11, 44, 45, 46 and 47, which, as a whole, largely corresponds to what is now referred to as the prefrontal cortex (Judaš et al 2012, Carlén 2017). Classical cytoarchitectonic maps of the human prefrontal cortex, produced by various investigators in the early twentieth century, exhibit similarities in gross topography but differ in size, shape, and precise localization of specific regions within the prefrontal cortex. In Brodmann's map, area 9 (BA9) and area 46 (BA46) are situated in the dorsolateral prefrontal cortex (DLPFC). Specifically, BA9 occupies the superior frontal gyrus (sfg) and caudal portion of the middle part frontal gyrus, while BA46 is located in the remaining portion of the mfg and the ifg, bordered ventrally by BA45, rostrally by BA10, and dorsally and caudally by BA9 (see **Figure 4A**) (Brodmann 1909).

In contrast, while area 9 and area 46 are also mapped onto the sfg and mfg in the cytoarchitectonic maps of Sarkissov et al. (Sarkissov et al. 1955) and von Economo and Koskinas (von Economo and Koskinas 1925), area 46 (labeled as FDΔ in the map of von Economo and Koskinas) is depicted as an "island" within area 9, lacking a ventral border with area 45 – differing notably from Brodmann's map (see **Figure 4B, C**). Furthermore, the superior border of area 46 with adjacent cortical areas varies within the middle and superior frontal sulci, as does its inferior boundary within the upper wall of the inferior frontal sulcus (Rajkowska and Goldman-Rakic 1995).

Moreover, some researchers have identified a so-called transitional type of cortex. Rajkowska and Goldman-Rakic designated area 9-46 on the middle frontal gyrus of the human brain, which exhibits cytoarchitectonic features of both areas 9 and 46. Additionally, they reported subtle differences between the rostral and caudal portions of area 46 (Rajkowska and Goldman-Rakic 1995).

Petrides and Pandya described similar transitional areas, observing that the cytoarchitecture of the portion of the sfg designated as area 9 differs from that of that of the mfg, which is also labelled as area 9 in the maps of Brodmann and Sarkissov et al. Notably, the structure area 9 in the mfg more closely resembles area 46. Consequently, they designated this portion as area 9/46 to reflect its architectural similarity to area 46 and to acknowledge that the corresponding region in macaque monkey cortex was

region and part of area 46 by Walker (Walker 1940). Additionally, the map of Petrides and Pandya identified subdivisions within this transitional region, specifically the ventral (9/46v) and dorsal (9/46d) portions of area 9/46 (see **Figure 4D**) (Petrides and Pandya 1999). Furthermore, Walker and subsequent researchers investigating the frontal cortex in nonhuman primates observed that the region labelled as area 46 is not homogeneous and can be further subdivided (e.g., Barbas & Pandya, 1989; Preuss & Goldman-Rakic, 1991)(Walker 1940, Preuss and Goldman-Rakic 1991).

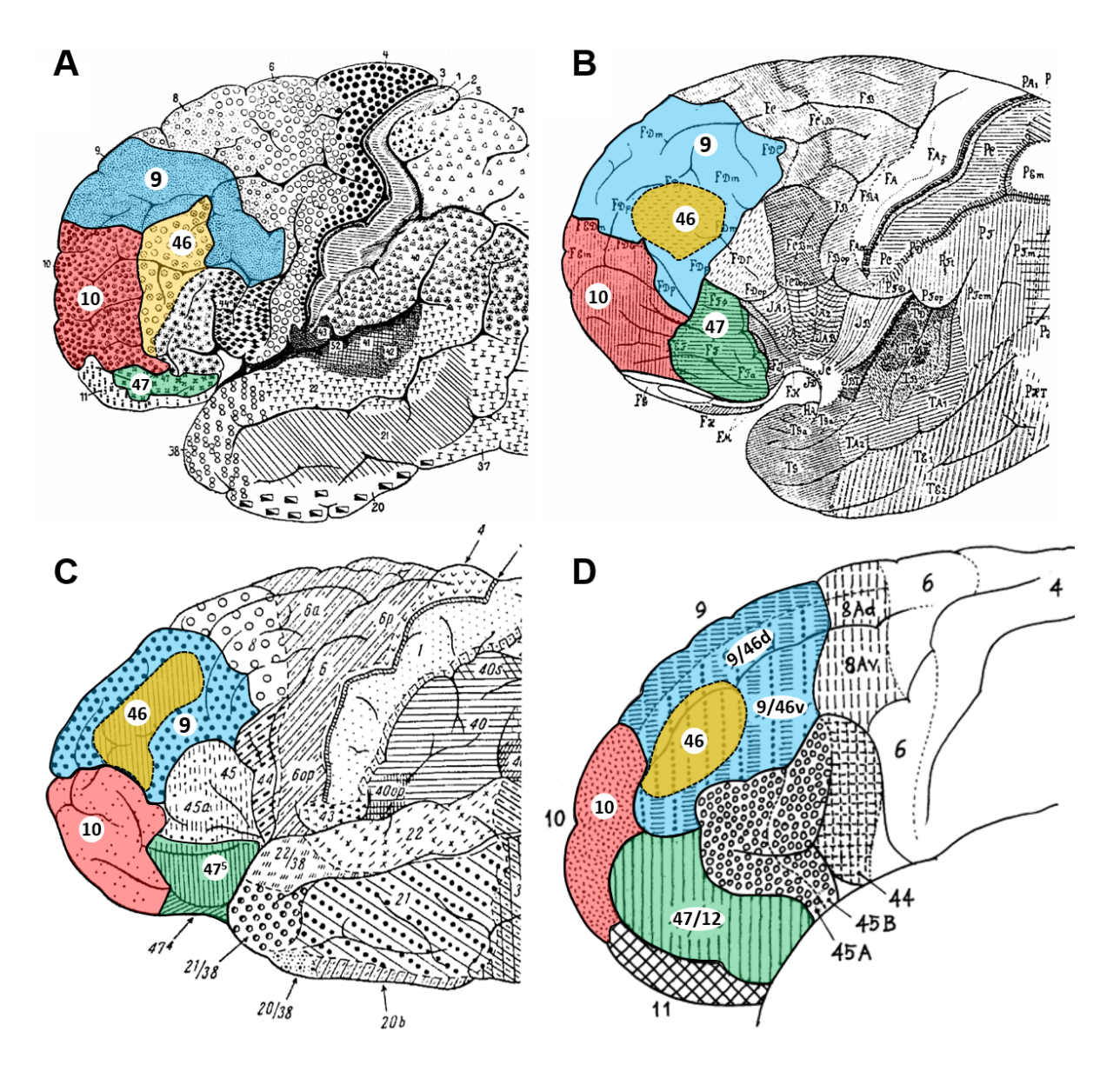


Fig. 4: Previous maps pf the prefrontal cortex

Several lateral prefrontal areas and frontal pole were shown in the adapted cytoarchitectonic maps labelled by (A) (Brodmann 1909), (B) (von Economo and Koskinas 1925), (C) (Sarkissov et al. 1955),

and (D) (Petrides and Pandya 1999). Associated areas are marked with corresponding color coding for clarity: area 9 (blue), area 10 (transparent red), area 46 (yellow), and area 47 (green).

The cortical region located rostroventral to area 45 and caudal to area10 is designated as area 47 in classical maps of the human brain. The region occupies the most rostral part of the ifg (pars orbitalis) and extends into the caudal portion of the orbitofrontal cortex (Beck 1949, Sarkissov et al. 1955). Brodmann noted that the architecture of this region was heterogenous, suggesting the existence of subdivisions (Brodmann 1909). Indeed, Sarkissov et al. (Sarkissov et al. 1955) and Kononova (Kononova 1935) further divided this large and heterogenous region into five distinct parts. Petrides and Pandya later redefined the portion of this region that lies rostral and ventral to area 45, extending to the lateral orbital sulcus, as area 47/12, to reflect its similarity to Walker's ventrolateral area 12 in the macaque brain. Meanwhile, the remaining portion of classical area 47, which occupies the caudal orbitofrontal cortex, exhibits structural characteristics comparable to those of orbitofrontal area 13 in nonhuman primates (Walker 1940, Petrides and Pandya 1999, Petrides and Pandya 2012).

1.2.3.2 Limitations of existing cytoarchitectonic maps

As previously described, available cytoarchitectonic maps exhibit considerably inconsistencies in terms of localization, extent, and nomenclature of cortical areas. Furthermore, these maps are typically represented as two-dimensional schematic drawings that illustrate only superficially exposed regions. Given the structural complexity of the frontal cortex – characterized by numerous deeply folded sulci – the precise localization and extent of cortical areas within these sulci remain undefined (Zilles et al 1997). Consequently, these hidden areas are not adequately represented in traditional cytoarchitectonic maps.

Additionally, two-dimensional representations do not facilitate direct comparisons with functional imaging studies, whereas superimposing datasets in a three-dimensional (3D) framework is essential for such analyses (Zilles and Amunts 2010). Although magnetic resonance imaging (MRI)-based cortical parcellations have provided highly detailed segmentation of the prefrontal cortex, the corresponding microstructural and cytoarchitectonic correlates remain to be fully elucidated (Bruno et al. 2022).

Furthermore, the macroanatomical landmarks reviewed in the present paper also present significant challenges. Sulcal and gyral patterns exhibit substantial interindividual variability, and many cytoarchitectonic borders do not align precisely with sulcal landmarks (Amunts et al 2007). Past investigators did not adequately address differences in architectonic definitions across studies or the inherent variability between individuals. Therefore, previous cytoarchitectonic maps have several limitations and are not sufficiently reliable for contemporary functional imaging research.

1.2.4 Functions and dysfunctions of the lateral prefrontal cortex

The investigation of frontal cortex function began with Fritsch and Hitzig's examination of motor cortex organization in dogs and Ferrier's studies of the frontal cortex in monkeys during the 1880s (Kolb 2024). Research in the mid-20th century predominantly focused on motor functions, with limited understanding of the frontal cortex's role in other domains. Consequently, cognitive studies at the time largely concentrated on the parietal and temporal cortical regions, with minimal attention on the frontal cortex. The first systematic investigations into the effects of prefrontal lesions in non-human primates emerged around 1950, subsequently leading to a surge of research on the prefrontal cortex and its role in cognitive behaviour in humans (Kolb 2024).

The prefrontal cortex is functionally heterogeneous. Substantial evidence indicates that, as a whole, the PFC plays a critical role in the representation and organization of behavioural, linguistic, and cognitive processes (Fuster 1988, Fuster 2002). The LPFC is primarily involved in language processing and executive function, whereas the OPFC and MPFC primarily contribute to cognitive regulation and emotional control. The anterior LPFC is particularly important for motor preparation (Vogt et al 2007), planning (Levy 2023), language control (Vingerhoets et al 2003, Abutalebi et al 2009), and music perception (Hyde et al 2011). Additionally, it serves as a primary site for sensory integration from the posterior cortex, facilitating the development of executive memory networks (Petrides 2005, Mizuno et al 2008, Levy 2023) and higher-order cognitive functions (Fuster 2002). The LPFC involves two functional regions along both the rostral-caudal and dorsal-ventral axes: the dorsolateral prefrontal cortex and the ventrolateral prefrontal cortex (VLPFC) (Nieuwenhuys et al 2008). The DLPFC primarily encompasses the superior and middle frontal gyri, whereas the VLPFC is predominantly located within the inferior frontal gyrus (Petrides 2005).

A substantial body of literature has explored the functional organization of the human brain. The functions of each cortical area are determined by its extrinsic connections and intrinsic properties, with its unique cytoarchitecture potentially reflecting these properties indirectly (Passingham et al 2002). Passingham et al. further proposed that each cytoarchitectonic area had a specialized set of extrinsic inputs and outputs, termed a "connectional fingerprint", which critically defined its functional capabilities (Passingham et al. 2002). Early applications of diffusion imaging provided foundational advances in

mapping anatomical connectivity in vivo. For example, Behrens et al. pioneered a probability tractography algorithm to trace connections between the thalamus and cerebral cortex in living humans (Behrens et al 2003). By classifying thalamic voxels based on their highest probability of connectivity to specific cortical regions (e.g., prefrontal, motor, and somatosensory cortices), they subdivided the thalamus into subregions that aligned with histologically defined nuclei in non-human primates. This work provided the first quantitative evidence that diffusion data could reliably infer connectivity between gray matter structures and demonstrated the reproducibility of such parcellations across individuals. Later, analogous approaches based on resting-state functional connectivity has been introduced (Kim et al 2010). Based on these methodological innovations, systematic connectivity-based parcellation (CBP) was introduced as a method to subdivide a region of interest (ROI) into functionally distinct subregions (Eickhoff et al 2015). This approach has been applied to map functional subdivisions in various regions of the human brain, including the ventromedial frontal cortex (Chase et al 2020), frontal pole (Ray et al 2015), and inferior frontal cortex (Sebastian et al 2016, Bulut 2022).

Furthermore, recent advances in functional brain mapping have developed high-resolution atlases such as the Dictionaries of Functional Modes (DiFuMo) (Dadi et al 2020). This approach employs sparse dictionary learning on a large-scale aggregation of 2192 functional Magnetic Resonance Imaging (fMRI) datasets (2.4TB in total) spanning 27 studies, including task-based and resting-state functional signals. Compared to traditional hard parcellation approaches, DiFuMo preserves functional gradients while substantially improving computational efficiency and interpretability (Dadi et al. 2020).

Another method of parcellating the human cerebral cortex is the multi-modal parcellation, which was developed using multi-modal MRI data from the Human Connectome Project (HCP) combined with an objective semi-automated neuroanatomical approach (Glasser et al 2016). This parcellation delineated 180 distinct cortical areas per hemisphere, including 13 areas in the dorsolateral prefrontal cortex, 8 areas in the inferior frontal cortex, and 11 areas in the orbital and polar frontal cortex. The defined borders of these areas correspond to differences in functional characteristics, cortical architecture, connectivity profiles, and topographical features. A systematic review of MRI-based frontal lobe parcellation summarized functional imaging and lesion studies related to the DLPFC, demonstrating that

the DLPFC is responsible for working memory, attentional control, cognitive flexibility, planning and intelligence. While differentiation within the DLPFC is evident, the functional boundaries of the region vary across experiments (Cox et al 2014).

Another MRI-based parcellation method was introduced to subdivide the entire human frontal cortex into 11 subregions in the study by Crespo-Facorro et al. (Crespo-Facorro et al 1999). Three subregions, superior frontal gyrus (SFG), middle frontal gyrus (MFG), and inferior frontal gyrus (IFG), were delineated by integrating tracings from both coronal and transaxial slices. The SFG is involved in cognition activities and is considered a functionally heterogenous frontal subregion. The MFG is associated with various cognitive functions, including working memory, decision making, and sensory perception. Meanwhile, the IFG is primarily dedicated to speech processing, and reductions in its gray matter volume have been observed in schizophrenia (Suga et al 2010).

Several studies have further examined the functional organization of the left inferior frontal gyrus. The left ifg is associated with both word comprehension and production (Klaus and Hartwigsen 2019, Goldstein et al 2025), whereas the right ifg is primarily involved in response inhibition (Suda et al 2020, Wu et al 2025). Friederici et al. identified two functionally distinct subregions within the left IFG: Broca's area (BA 44/45) and the frontal operculum (FOP), both of which support different aspects of syntactic processing (Friederici et al 2006). Broca's area support syntax integration by processing hierarchical dependencies via its connections to the posterior temporal cortex, while the FOP tracks local sequence structures through anterior temporal connections. Moreover, another functional segregation has been observed. The dorsal portion of the left ifg is activated during phonological verbal fluency tasks and the ventral portion is engaged in semantic verbal fluency tasks (Costafreda et al 2006). These findings highlight how structural connectivity shapes the functional specialization within the IFG, without proposing new anatomical subdivisions. Additionally, MRI and histological analyses have distinguished the pars triangularis and pars orbitalis near the anterior horizontal ramus of the lateral fissure (Uylings et al 2010).

In conclusion, these findings support the feasibility of a functionally meaningful parcellation of the lateral prefrontal cortex. However, the synthesis and interpretation of

these functional subdivisions remain challenging due to the lack of consensus on the methodological criteria used to delineate the frontal regions across studies (Cox et al. 2014).

Building upon the MRI-based functional parcellation methods described earlier, it is important to highlight how structural abnormalities or lesions within the LPFC can significantly impact various psychiatric, behavioural, and neurological disorders. These impairments are not only observed in clinical conditions but also in normal developmental and aging processes (Convit et al 2001, Salat et al 2001, Yucel et al 2008, Cox et al. 2014). Cognitive impairment (e.g., loss of initiative, decreased motivation) and dysexecutive symptoms (e.g., behavioural slowness, stuttering) are commonly observed in patients with damage to the DLPFC (Pirau and Lui 2018, Catani 2019). DLPFC lesions may also exacerbate depressive symptoms (Koenigs and Grafman 2009) and are strongly associated with conditions such as schizophrenia (Jones 2001, Petralia et al 2020), obsessive-compulsive disorder (Ahmari and Rauch 2022), and bipolar disorder (Zhang et al 2020). Disorders such as reduced spontaneous speech (Catani 2019), anxiety (Yokoyama et al 2015), and depression (Brody et al 2001) are linked to alterations in the VLPFC and its associated circuitry.

1.3 Aims of the study

Given the key role of the LPFC in cognitive functions and its strong association with neurological disorders, this region has become a focal point of our research. At the same time, due to the limitations of existing cytoarchitectonic maps in accurately delineating the prefrontal cortex, generating probability cytoarchitectonic maps in established reference spaces offers a robust approach that accounts for interindividual variability and enhances the comparability of functional imaging studies with microstructural data (Zilles and Amunts 2010).

A quantitative, reliable and reproducible cytoarchitectonic mapping approach for defining cortical borders has been applied to numerous brain regions. Using this method, our group has identified several distinct areas within the lateral prefrontal cortex (Amunts et al. 2020). For instance, Bruno et al. demonstrated that the human DLPFC exhibits a finer level of differentiation than previously assumed, identifying nine novel cytoarchitectonic areas using this mapping approach (Bruno et al. 2022, Bruno et al. 2024). However, the relationships between these areas in the DLPFC and their specific functions remain incompletely understood.

Hence, this study aimed to delineate remaining unmapped regions of the LPFC (unexplored gaps, "GapMap Frontal-I", and dorsal portion of "GapMap Frontal-to-Temporal-I") (see Figure 5), in the Julich-Brain Atlas to enhance our understanding of their microstructural organization and provide a cytoarchitectonic reference for functional studies. These regions primarily include areas within the mfg and ifg, along with the adjacent sulci bordering previously delineated areas such as frontal pole area Fp1 (Bludau et al 2014), the lateral orbitofrontal cortex (Fo5, Fo6) (Wojtasik et al 2020), additional DLPFC areas (SFS1, SFS2, MFG1, MFG2, MFG4, MFG5) (Bruno et al. 2022, Bruno et al. 2024), and areas of the Broca region (area 45) (Amunts et al. 1999).

Probabilistic maps for each identified area will be constructed in standard stereotaxic spaces to establish a reference framework for future functional and multimodal investigations, facilitating a deeper understanding of the functional and structural organization of the brain in both health and disease at the level of individual cortical areas. Furthermore, volumetric analyses and cell body fraction measurements will be

systematically conducted to assess potential interhemispheric and sex-related differences (Amunts et al. 2020).

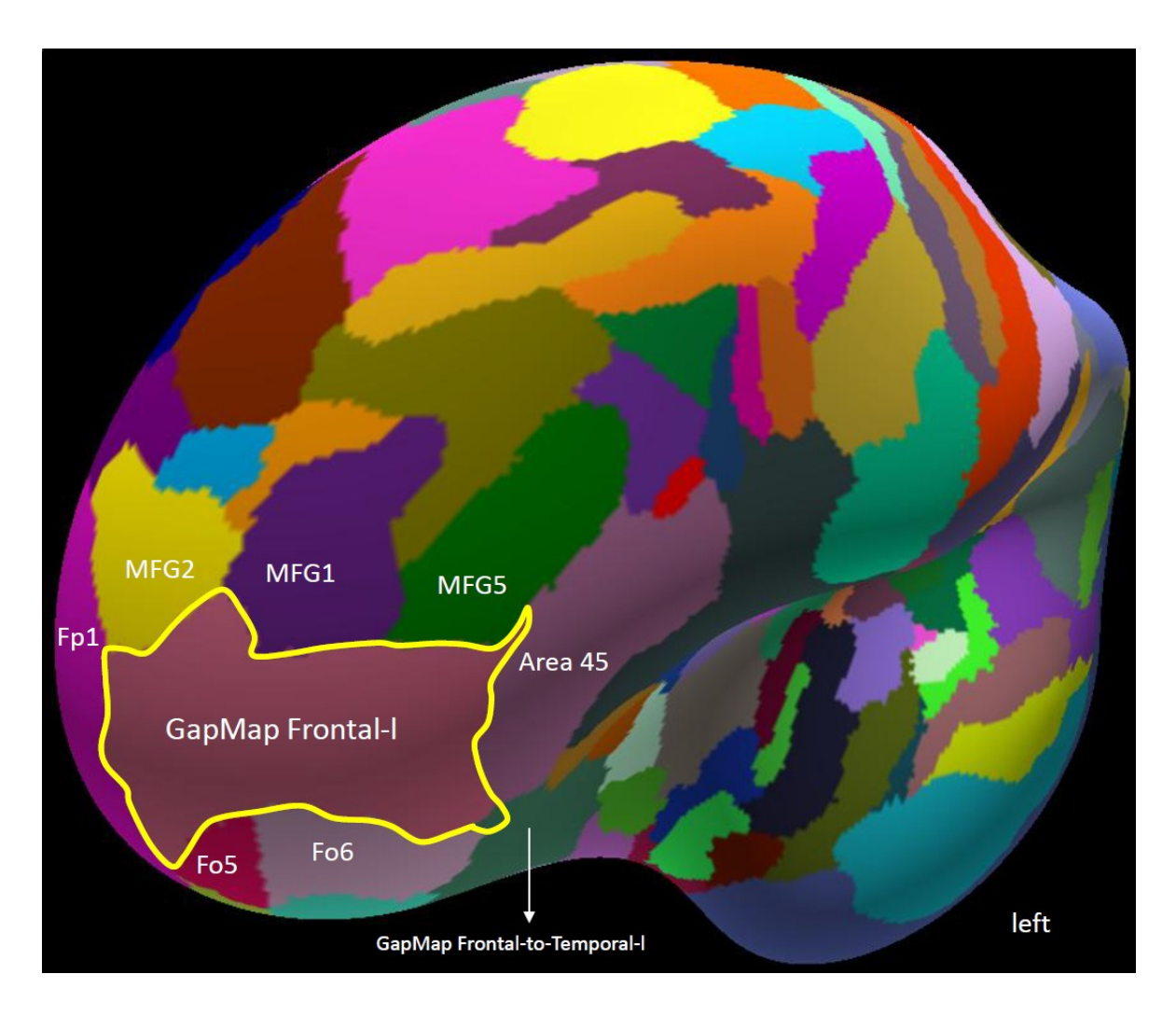


Fig. 5: Unmapped regions ("GapMap Frontal-I", and "GapMap Frontal-to-Temporal-I") with adjacent areas in the lateral prefrontal cortex

Details are included within EBRAINS (https://ebrains.eu/services/human-brain-atlas).

2 Materials and Methods

2.1 Histological processing of post-mortem brains

Ten human brains (five females, five males, post-mortem delay < 24 h), including two Bigbrain datasets (BC20 and BC21), were obtained through the body donor programs of the Institute of Anatomy, University Hospital and Heinrich Heine University Düsseldorf, Germany (see Table 1). All specimens were collected and processed in accordance with the ethical guidelines of the local ethics committee, with written informed consent obtained prior to donation (ethics approval number 2023-2632). No neurological or psychiatric disorders were reported in the clinical records. Histological processing and image analysis were performed as previously described in detail (Amunts et al. 2020). In short, MRI was conducted using a T1-weighted 3D FLASH sequence on a Siemens 1.5 Tesla scanner (Erlangen, Germany) to capture the initial morphology and dimensions of the brains. These MRI scans were subsequently utilized for distortions correction and to facilitate the generation of 3D reconstructions of the histological sections. The brains were fixed in either formalin or Bodian solution, embedded in paraffin, and serially sectioned at 20-μm intervals in the coronal plane using a microtome. The total number of sections obtained per brain ranged from approximately 6000 to 7500, depending on individual brain size. Each 15th section was mounted on a gelatine-covered glass slide and stained for cell bodies using a modified Merker method (Merker 1983). The histological sections were digitized, and every 15th to 60th section was used for cytoarchitectonic analysis.

Brain no.	Gender	Age (years)	Cause of death	Fresh weight (g)
BC01	Female	79	Carcinoma of the bladder	1350
BC04	Male	75	Acute glomerulonephritis	1349
BC05	Female	59	Cardiorespiratory	1142
			insufficiency	
BC08	Female	72	Renal failure	1216
BC09	Female	79	Cardiorespiratory	1110
			insufficiency	
BC10	Female	85	Mesenteric infarction	1046
BC11	Male	74	Myocardial infarction	1381
BC13	Male	39	drowning	1234
BC20	Male	65	Cardiorespiratory	1392
			insufficiency	
BC21	Male	30	Bronchopneumonia	1409

Table 1: List of post-mortem brains that were used for cytoarchitectonic analysis (all cutting planes coronal)

2.2 Observer-independent detection of cytoarchitectonic borders using the grey level index (GLI)

Cortical areas differ regarding their laminar cell packing density. The localization of cytoarchitectonic borders between cortical regions was determined through an observer-independent approach, incorporating image analysis combined with multivariate statistical techniques (Schleicher et al 1999, Schleicher et al 2005, Schleicher et al 2009) (see **Figure 6**). The histological sections containing the region of interest were scanned using a high throughput brightfield microscope (TissueScope LE120, Huron Digital Pathology) to generate images with a resolution of 1 μ m/pixel (~8 Gb per image, 8 bit) (Bruno et al. 2024). The images were accessible via the Section Tracer Online Tool (Amunts et al. 2020). Each ROI encompassed the lateral and ventral parts of the frontal cortex, spanning from the frontal-marginal sulcus to the horizontal ramus of the lateral fissure (Ono et al. 1990).

The GLI images were generated from the digitized ROIs using in-house written Matlab-based scripts (The MathWorks, Inc., Natick, MA, USA) (Schleicher et al. 2009, Bludau et al.

2014). In a square measuring field of 16 × 16 pixels, the GLI estimates the volume fraction of cell bodies (Wree et al 1982) and characterizes the cytoarchitectonic organization (Bludau et al. 2014). Subsequently, GLI profiles were extracted along traverses extending from the border between layer I/II (outer contour line, 0% cortical depth) and the layer VI/white matter border (inner contour line, 100% cortical depth). These profiles characterized cell density in layers II-VI. Two GLI profiles extracted from different cortical areas differ in shape. Comparative analysis of GLI profiles across different cortical areas can be conducted (Jones et al 2000, Schleicher et al. 2009) (see Figure 6). The shape of the GLI profile was quantified using 10 feature vectors, i.e. mean GLI, standard deviation, skewness and kurtosis, cortical depth of the center of gravity, and the analogous parameters of the profile's first derivatives (Schleicher et al. 2009). To measure dissimilarity between laminar cell densities, the Mahalanobis distance (MD) was calculated between neighboring blocks of GLI profiles using the sliding window procedure. As the window moved across the cortical ribbon, distances were calculated at each profile's position. Peaks in this function indicated areal borders between two adjacent regions. Borders were defined based on identifying consistent patterns across multiple block sizes and in a minimum of three consecutive histological sections (Mahalanobis et al 1949, Schleicher and Zilles 1990). The Hoteling's T2-test with Bonferroni correction for multiple comparisons (p<0.001) was used to test the significance of the borders (Schleicher et al. 1999).

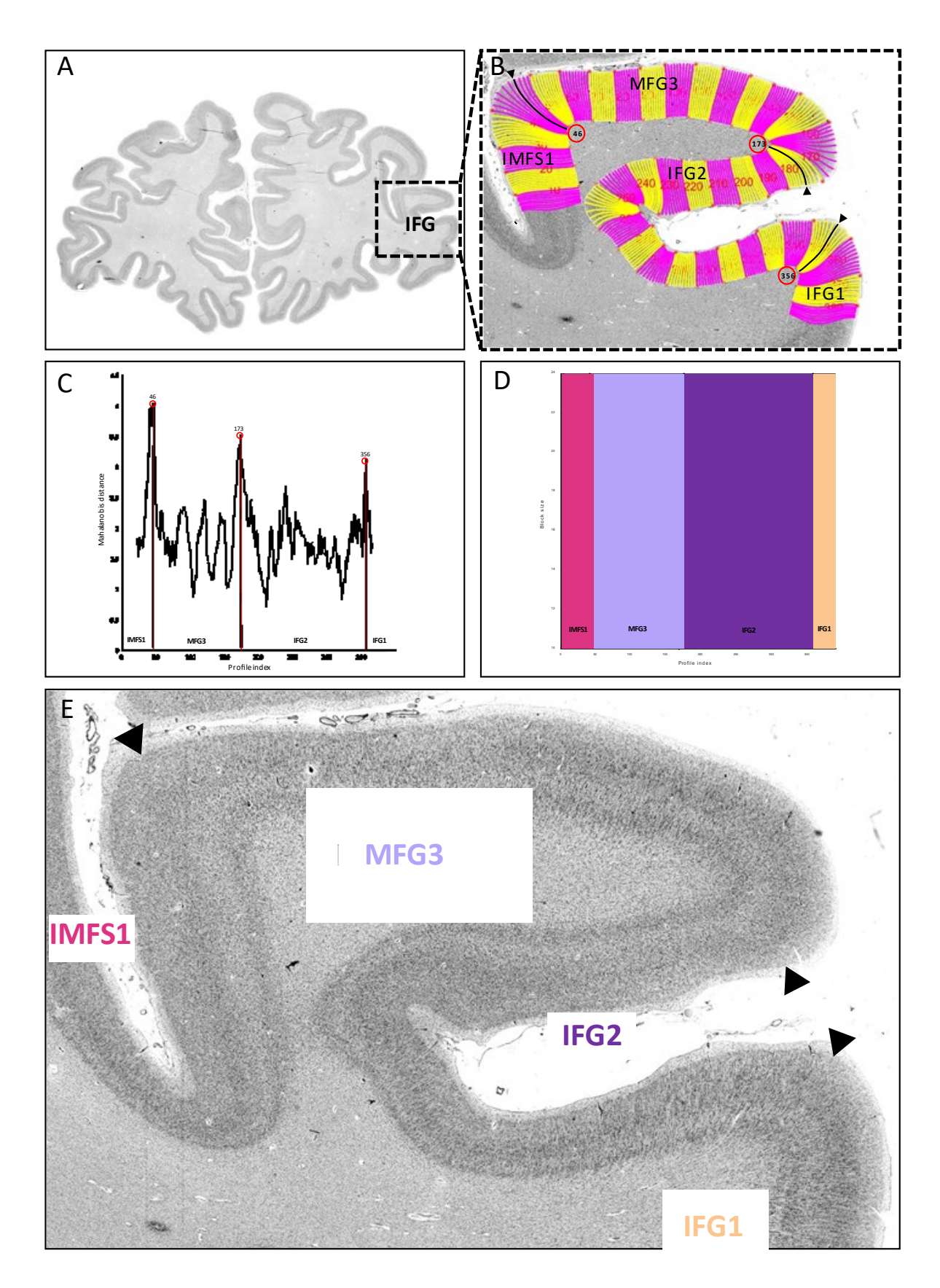


Fig. 6: Observer-independent mapping approach

Coronally cut section with cell body stained from one of the ten brains (BCO1) with rectangular region of interest (ROI, box) (A). The profiles of areas were extracted between the outer contour line and inner contour lines (B). Significant maxima of the Mahalanobis distance were detected with different block size (n=10-24) (D) and at profile numbers 46, 173, and 356 are plotted against the profile index (labeled with red circles) (C). These positions indicate the laminar pattern changes between IMFS1, MFG3, IFG2 and IFG1(B, E). The corresponding maxima of the MD function are accepted as borders marked with black arrowheads (E).

2.3 Volumetric analysis of delineated areas

In order to compensate shrinkage resulting from histological processing, a unique correction factor was established for each post-mortem brain. This factor was determined by comparing the fresh volume of the brain to its volume after histological processing. The volumes were individually corrected for shrinkage (Amunts et al 2007). To compare area volumes across brains of varying sizes, normalization was performed using the individual whole-brain volume (Bludau et al. 2014) to avoid bias, such as that arising from physiologically differences, e.g., larger brain volumes in male humans. The normalized volumes of the newly identified areas were then analysed and compared across brains to examine interhemispheric and gender differences. This was achieved using a pairwise Monte Carlo permutation test (p<0.05) and a Matlab tool (Bludau et al. 2014).

2.4 Hierarchical clustering of mean areal GLI profiles

Hierarchical cluster analysis was conducted to detect similarities and differences between the new areas (IMFS1, IMFS2, MFG3, IFG1 and IFG2) and the neighbouring frontal pole areas (Fp1, Fp2) (Bludau et al. 2014), DLPFC areas (MFG1, MFG2, MFG4, and MFG5) (Bruno et al. 2022, Bruno et al. 2024), areas 44 and 45 of Broca's region (Amunts et al 2004), and lateral orbitofrontal cortex(Fo5, Fo6) (Wojtasik et al. 2020). For each area and hemisphere, 15-20 profiles were extracted from three sections, resulting in approximately 45 profiles per hemisphere and 900 profiles in total for each area. The sections were selected to be free of histological artifacts, large vessels and not tangentially cut. Based on a mean GLI profiles for each area, feature vectors were calculated. A hierarchical cluster analysis and discriminant analyses were performed using the Euclidean distance and the Ward-linking

approach (Ward Jr 1963) with Matlab (The MathWorks, Inc., Natick, MA, USA). The error ellipse in our discriminant analysis (DA) script includes all data points with a maximum Mahalanobis distance of 1.0 from the group mean. This distance is calculated by measuring how far each data point is from the mean, while also accounting for the spread and orientation of the data (i.e., the covariance). A large Euclidean distance implies significant cytoarchitectural differences and a low structural similarity, and vice versa. The results were visualized using a dendrogram.

2.5 Reconstruction of cortical areas and probabilistic maps

Border positions were labeled in digitized sections, and a closed polygon (contour line) delineated each area extent within each section using the in-house software "Section Tracer Online Tool" (Amunts et al. 2020). Subsequently, the new areas were 3Dreconstructed based on the structural MRI 3D data set of the fixed brain prior to sectioning, along with high-resolution flatbed scans of the stained histological section (Amunts et al. 1999). We defined the main sulci of the frontal lobe within each individual hemisphere. Manual lines were drawn on the cortical surface to define sulci based on the most recent schematic of the lateral prefrontal cortex by Amiez (Amiez et al. 2023) and Petrides (Petrides 2013), as well as from our own expertise in defining these components from our previously published work (Amunts et al 2022). The 3D-reconstructed maps of each brain were then transferred to the single-subject MNI-Colin27 template of the Montreal Neurological Institute and the non-linear asymmetric MNI152 2009c (ICBM152casym) template (Evans et al 2012). The areas of all 10 brains were then superimposed in these reference brain templates, and the probability maps were calculated in each stereotaxic space (Amunts et al. 2020). The probability maps illustrate the cortical area's inter-subject variability at specific positions within the reference brain. The probabilities were represented using a color spectrum, ranging from dark blue to red, denoting low to high probabilities, respectively. The centers of gravity of areas IMFS1, IMFS2, MFG3, IFG2 and IFG1 were calculated. In the next step, the maximum probability map (MPM) was generated to reduce complexity and visualize the extent of areas comparable to Brodmann's map. Each voxel in the reference brain was assigned to the cytoarchitectonic area with the highest probability at that position (Eickhoff et al 2005). The maps for all areas are available for access through the Julich Brain Cytoarchitectonic Atlas (https://iulich-brain-atlas. which are included within EBRAINS (https://ebrains.eu/services/human-brain-atlas).

2.6 Functional analytics

The involvement of the newly mapped areas in the different functions of the PFC was studied by performing a meta-analytic connectivity modelling (MACM), which is commonly used to investigate the functional connectivity of anatomically defined seed regions (Eickhoff et al 2010, Robinson et al 2010, Minkova et al 2017). MACM leverages the advantages of the high degree of standardization inherent in neuroimaging data dissemination, including the widespread use of standardized coordinate systems (e.g., Talairach, MNI) and the development of databases dedicated to storing such information. The fundamental concept of MACM involves initially identifying all experiments within a database that activate a specific brain region (seed) or volumes of interest (VOI), followed by testing for the convergence of activation foci across these experiments (Hoffstaedter et al 2014). Convergence across activation foci refers to the degree of consistency or overlap in the specific brain region that activated across multiple experiments. In other words, this convergence assesses whether the activation foci reported in different studies cluster in particular brain regions, suggesting that these areas may share similar functions or roles across different tasks or conditions. In MACM analysis, this convergence is tested through statistical methods to reveal whether a particular brain region is consistently associated with a specific set of functions. Since experiments are selected based on activation within the seed region, the highest convergence is expected to occur within the seed itself (Hoffstaedter et al. 2014).

To identify studies reporting neural activation within the newly defined region, the BrainMap database [www.brainmap.org (Fox and Lancaster 2002, Laird et al 2005)] was used in this procedure, which was originally conceived in 1987 and stored over 20,000 neuroimaging experiments. The MPM of areas IMFS1, IMFS2, MFG3, IFG1 and IFG2 on both hemispheres in MNI and ICBM 152 reference spaces were defined as VOIs. The search specifically targeted coordinates activated within at least one seed region, thereby eliminating potential nomenclature biases arising from inconsistent naming of regions

across experiments. Only studies involving healthy subjects using fMRI and positron emission tomography (PET) were selected. First, we identified all experiments that featured at least one focus of activation within the newly defined regions (in MNI-space). Second, we identified all experiments in which the considered seed was activated. This step was based on the reported activation coordinates (Eickhoff et al 2009, Eickhoff et al 2012).

Each experiment in the BrainMap database is associated with a specific "Behavioural Domain" (BD) and "Paradigm Classes" (PC). The specific BD is classified based on the experimental design's intent and includes six main categories (cognition, emotion, perception, interoception, action, and pharmacology) along with their subcategories (e.g., action.preparation, cognition.language.speech, emotion.negative.fear), as guided by the BrainMap coding scheme (Laird et al. 2005). Paradigm Classes refer to the experimental tasks in each specific experiment, such as viewing, naming, chewing, or reading (for all behavioural items, see https://brainmap.org/taxonomy/paradigms/). Based on this coding scheme, the frequency of all BD and PC in IMFS1, IMFS2, MFG3, IFG1 and IFG2 was compared to their appearance in the entire database. Bar charts visualized activated 26 behavioural domains and paradigm classes for each examined VOI, along with their respective probability likelihood ratios. The significance of the local occurrence of a certain domain or class was tested using the χ^2 test (significance at p<0.05). The possible functions of areas were determined by the significant frequency of occurrence. If significance was achieved (p < 0.05), a binomial test assessed the over- or under-representation of the domain or class, including its specific subdivisions. Both forward and reverse characterizations were performed: forward analysis tested whether a given task was more likely to activate the seed region than random activation, while reverse analysis tested whether activation in the seed region predicted the associated task, behavioural domain, or paradigm class. In addition, the results were corrected for multiple comparisons by applying the false discovery rate (FDR) (Laird et al. 2005).

3 Results

Five new areas were defined by analyzing the cytoarchitecture in serial sections of ten human post-mortem brains, including the two BigBrains, using the observer-independent mapping approach. The areas were named according to their approximate macroanatomical localization: IMFS1 (intermediate frontal sulcus 1), IMFS2 (intermediate frontal sulcus 2), MFG3 (middle frontal gyrus 3), IFG1 (inferior frontal gyrus 1) and IFG2 (inferior frontal gyrus 2). They were arranged in both dorsal-to-ventral and rostral-to-caudal orientations.

3.1 Cytoarchitectonic characteristics and borders

All areas IMFS1, IMFS2, MFG3, IFG1 and IFG2 were granular isocortical areas, exhibiting six cortical layers with a developed inner granular layer IV. However, their individual cytoarchitectonic characteristics, such as size, cell density, and arrangement of neurons within cortical layers differentiated them from one another (summarized in **Table 2** and **Figure 7**).

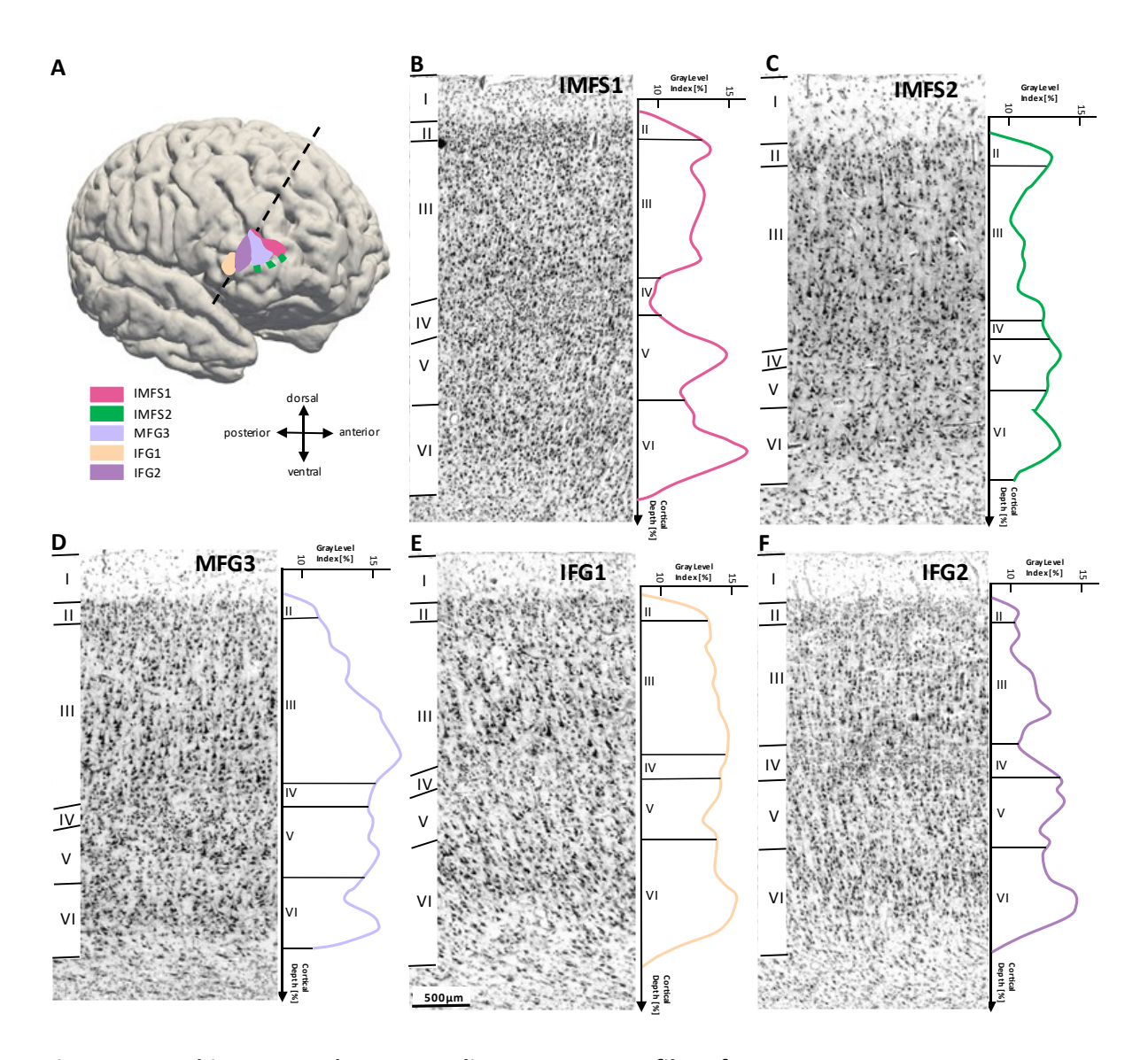


Fig. 7: Cytoarchitecture and corresponding mean GLI-profiles of areas IMFS1, IMFS2, MFG3, IFG1 and IFG2

The GLI represents the cytoarchitectonic organization. The statistical image analysis was based on GLI profiles. The lateral overview (A) illustrates area localizations and orientations of brain BC01. Colored lines indicate mean GLI-profiles. Area IMFS1 was characterized by a cell dense layer III with medium—sized pyramidal cells and a well-developed layer IV compared to the neighboring areas IMFS2 and MFG3. Layer V lacked clear subdivisions, and its border with layer VI was blurry (B). Area IMFS2 was distinguished by a thin, indistinct layer IV and loosely packed layer III and layer V (C). Area MFG3 exhibited large pyramidal cells in the deeper portion of layer III and the upper part of layer V. Layer VI had a sharply defined border with the white matter (D). The most defining cytoarchitectonic feature of area IFG1 was its thin layer IV, resulting from large pyramidal cells in the deeper portion of layer III (E). Area IFG2 was characterized by a relatively homogenous cell size

across all layers, a broad, well-developed layer IV, and blurry transition to white matter (F). The scale bar (500µm) in (E) applies to panels B-F.

3.1.1 Cytoarchitecture of areas IMFS1, IMFS2, MFG3, IFG1 and IFG2

In detail, area IMFS1 showed densely packed cells and a relatively homogenous cytoarchitecture, due to the absence of large pyramidal cells in layers III and V. Layer II was prominent, cell dense, and sharply bordered from layer III. Small to medium-sized pyramidal cells populated layer III, with a blurred transition to layer IV (Figure 7B). Layer IV was well-developed compared to area IMFS2 (Figure 8A) and area MFG3 (Figure 9A), which was the defining cytoarchitectonic feature of area IMFS1. Layer V lacked clear subdivisions, contained no large pyramidal cells, and exhibited a diffuse boundary with layer VI. The cell-rich and broad layer VI showed a blurry transition to the white matter.

Area IMFS2 featured a thin layer II with a diffuse border to layer III. Layer III and layer V were loosely packed and contained medium to large pyramidal cells. A subtle gradient in pyramidal cell size was observed within layer III, increasing from its upper to lower parts. Layer IV was present but considerably thinner than in area IMFS1 (Figure 8A) and area MFG3 (Figure 10A). The pyramidal cells in the deeper portion of layer III were larger than those in the infragranular layers V and VI, which appeared pale (Figure 7C). The whitematter boundary was sharply distinguished, contrasting distinctly with adjacent areas IMFS1 (Figure 8A).

The main characteristics feature of area MFG3 was the presence of large pyramidal cells in the deeper portion of layer III and the upper portion of layer V, with a distinct layer IV compared to adjacent area IMFS2 (Figure 10A). Layer II was narrow with clear borders separating it from layer III. There was a gradient in cell arrangement throughout layer III, with medium- to large-sized neurons and a higher cell density (local maximum in GLI profile, see Figure 7D) than that observed in area IMFS2. Layer IV was distinct but thinner than that of area IMFS1 (Figure 9A). Layers V and VI contained medium- to large-sized pyramidal cells, and the white-matter border was sharper than in area IMFS1 and IFG2 (Figure 12A).

The most distinct feature for identifying area IFG1 was the presence of prominent large pyramidal cells in the deeper portion of layer III, which were more loosely packed and larger

in size compared to those in area IFG2 (**Figure 11A**). Layer II was thin with an indistinct transition to layer III. Layer IV was clearly defined, exhibiting a sharp border with layer III, but it was thinner than in areas IMFS1, MFG3, and IFG2. The medium- to large-sized pyramidal cells in layer V showed no sub-lamination and were loosely packed, while the prominent, cell dense, and broad layer VI exhibited a sharper border than that of area IFG2 (**Figure 7E, F**).

Area IFG2 was mainly characterized by densely arranged cells, especially in the supragranular layers as well as layers IV and VI. Layer II was thick and transitioned sharply to the cell-rich layer III. Medium-sized cells were present throughout layer III, which had a smaller cell size compared to area IFG1 (Figure 11A) and area MFG3 (Figure 12A). Layer IV was well defined, with distinct borders separating it from the adjacent layers III and V. Layer V, composed of small- to medium-sized neurons, lacked sub-lamination into Va and Vb. Compared to the adjacent area MFG3, layer VI exhibited a higher cell density, consisting of medium-sized pyramidal cells, and showed a diffuse transition to the white matter (Figure 7F, Figure 12A).

Area		Cytoarchitectonic characteristics
IMFS1	II	Cell dense and thick with clear border to
		layer III
	III	Densely packed, small to medium-sized
		pyramidal cells in layer III
	IV	Well-developed layer IV, thicker than
		IMFS2 and MFG3
	V	Not sub-dividable, blurry border with layer
		VI
	VI	No large pyramidal cells and blurry
		transition to white matter
IMFS2	II	Thin and blurry border to layer III
		compared to IMFS1
	Ш	Loosely packed and larger cell size than in
		IMFS1
	IV	Visible but thinner than in MFG3

	V	Pale layer V with medium to large	
		pyramidal cells	
	VI	Sharp border with white matter	
MFG3	II	Narrow with clear border to layer III	
	Ш	Pyramidal cell gradient along layer III with	
		medium- to large-sized neurons in deeper	
		layer III, higher cell dense than in IMFS2	
	IV	Thin with clear border with layer III and V	
	V	Medium to large pyramidal cells	
	VI	sharp border to white matter	
IFG1	II	Thin with an indistinct border to layer III	
	III	Prominent with large pyramidal cells in	
		deeper layer III, more loosely packed and	
		larger cell size compared to IFG2	
	IV	Definable but few cells than in IMFS1,	
		MFG3 and IFG2	
	V	Loosely packed	
	VI	Prominent, cell dense and broad	
IFG2	II	Thick and sharp border with layer III	
	Ш	High cell density with small to medium-	
		sized cells across layer III, smaller cell size	
		than IFG1 and MFG3	
	IV	Densely packed and well-definable	
	V	Small to medium pyramidal cells	
	VI	Cell dense with medium-sized pyramidal	
		cells, blurry white-matter border compared	
		to MFG3	
Fo5ª		Densely cell packing than in IMFS2	
		Lower cell density layer II and more	
		prominent layer V and VI than in IFG2	
		Smaller cell size in deeper layer III than in	
		MFG3 and IFG1	
Fo6 ^a		Sparsely cell packing than in IFG2	
		Layer IV is not as broad as in IFG2	

	Layer V are well developed compared to
	IFG1
	More broader layer V and VI than in MFG3
	Clear transition to white matter
MFG1 ^b	Broader layer IV than in MFG3 but not as
	dense as compared to IMFS1
	Prominent layer VI with large cells and
	blurry border to white matter
MFG2 ^b	Uniform appearance due to homogenous
	cell density
	Dense, prominent layer II than in MFG3
	and IMFS2 but not as in IMFS1
	Broad, well-developed layer IV
	Sharp border between layer VI and white
	matter
MFG4 ^c	Prominent layer II with a blurry border to
	layer III
	Cell dense layer III
	Well-developed layer IV but not as broad
	as in IMFS1
MFG5 ^c	High cell density with a gradient in cell size
	to layer IIIc
	Visible, thinner layer IV than in IFG2 but
	broader than in MFG3
	Thinner and less cell density layer V and
	layer VI than in IFG2
	Sharp border to white matter
Fp1 ^d	Sharp border between layers I, II and III
	Dense layer II and deeper layer III
	Cell size in deeper layer III is larger than
	IMFS1
	Layer IV is not as broad as in IMFS1 but
	more pronounced than in IMFS2

45 ^e	Thinner layer II and layer IV compared to
	IFG2 but thicker layer II than in IFG1
	Larger pyramidal cells in deep layer IIIc and
	layer VI compared to IFG2
	White matter transition not as sharp as in
	IFG1 and IFG2
Op9 ^f	Cell size in deeper layer III is not as large as
	in IFG1
	Layer IV is visible but less developed than
	in IFG1
	Prominent layer VI
	White matter transition not as sharp as in
	IFG1

Table 2: Cytoarchitectonic characteristics of anterior prefrontal areas IMFS1, IMFS2, MFG3, IFG1 and IFG2 and neighboring areas Fo5, Fo6, MFG1, MFG2, MFG4, MFG5, Fp1, 45 and Op9

IMFS, intermediate frontal sulcus; MFG, middle frontal gyrus; IFG, inferior frontal gyrus; Fo, orbitofrontal cortex; Fp, frontal pole; Op, operculum. Labels denote the following references: a, (Wojtasik et al. 2020); b, (Bruno et al. 2022); c, (Bruno et al. 2024); d, (Bludau et al. 2014); e, (Amunts et al. 1999); f, (Saal et al 2021).

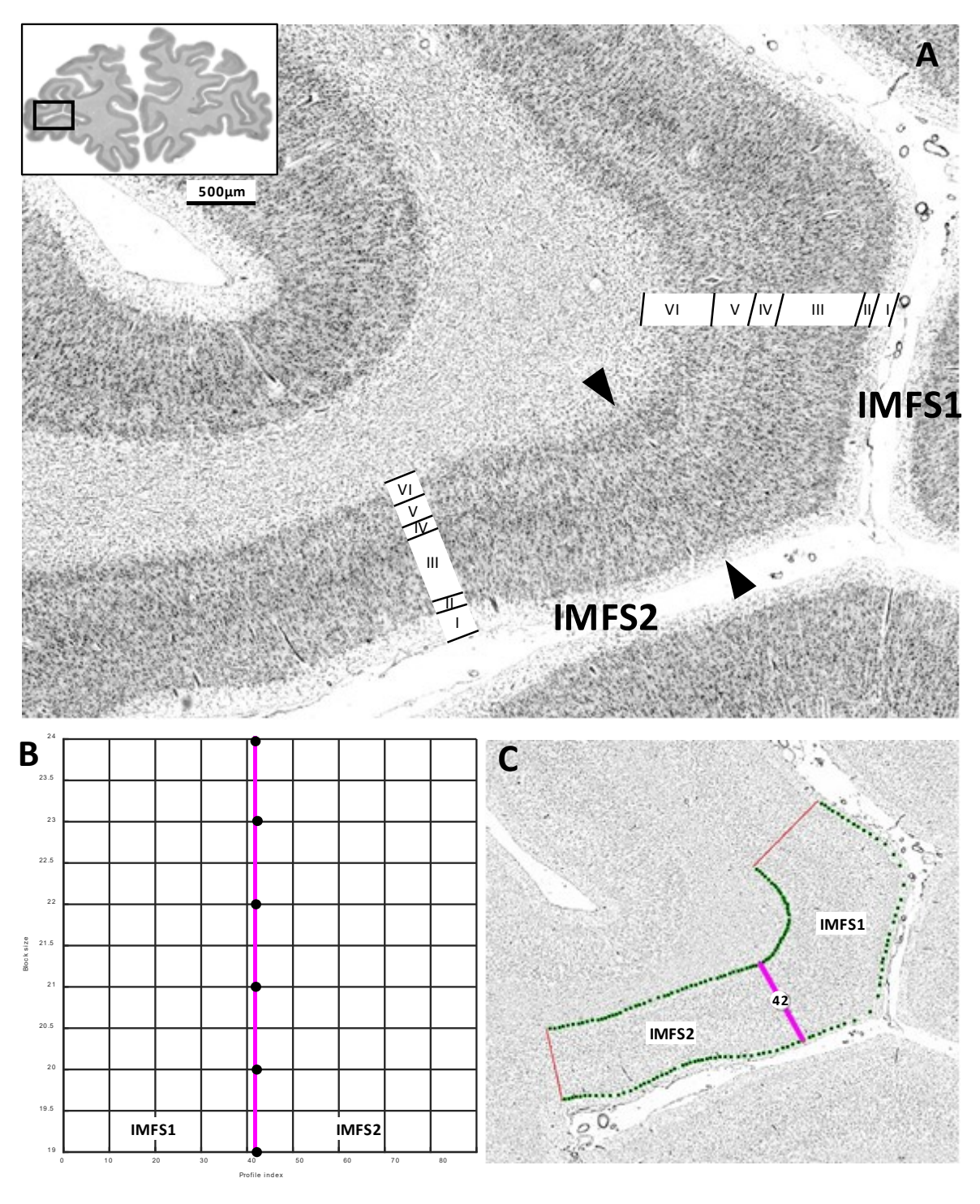


Fig. 8: Cytoarchitectonic border of IMFS1 and IMFS2 (A) with quantified border detection and dot blot illustrating the position of significant peaks plotted against the block size

Brain code: BC01. Section number: 6601. Hemisphere: left. Roman numbers indicate the cortical layers. Scale bar: 500µm. Notice that layer II is less densely packed, and layer III is more loosely arranged in IMFS2 than in IMFS1. Layer IV is thicker and more developed in IMFS1 compared to in IMFS2; however, both areas exhibit a granular structure. While both areas display a pale layer V, the infragranular layers (V and VI) are broader in IMFS1 than in IMFS2. Lamination and columnar

organization are more distinct in IMFS1. (B) Dot blot illustrating block size and profile index. Dots indicated the profile index where the Mahalanobis distance reached statistical significance. (C) Inverted GLI image following quantified border detection. A significant border was marked by a pink line, along with the corresponding profile number at which each border was identified.

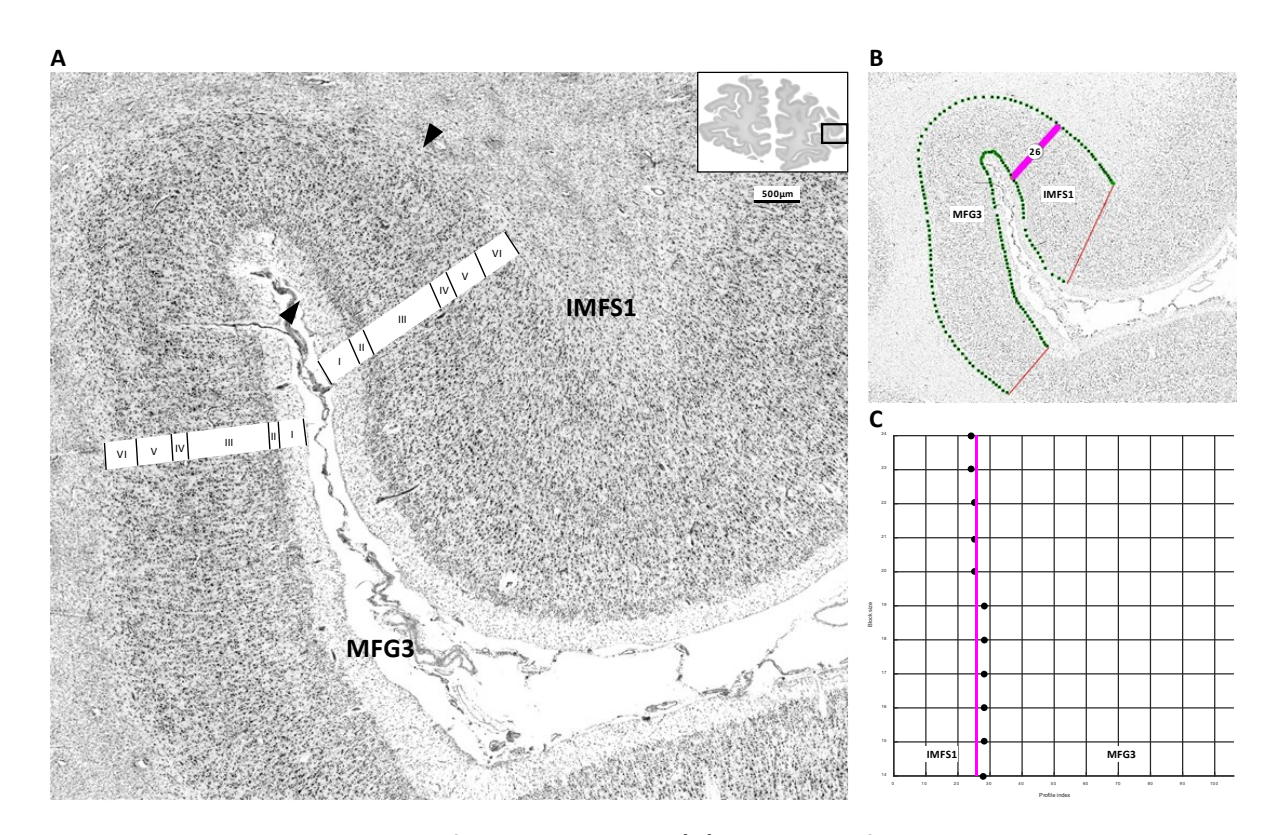


Fig. 9: Cytoarchitectonic border of IMFS1 and MFG3 (A) with quantified border detection and dot blot illustrating the position of significant peaks plotted against the block size

Brain code: BC20. Section number: 6691. Hemisphere: right. Roman numbers indicate the cortical layers. Scale bar: 500µm. Notably, layer II is denser in IMFS1, whereas pyramidal cells are bigger and more prominent in MFG3. Layer IV is broader in IMFS1 compared to MFG3; however, both areas present a granular structure. Lamination and columnar organization are more distinct in IMFS1. (B) Inverted GLI image with quantified border detection. A significant border was labeled by a pink line, along with the corresponding profile number at which each border was identified. (C) Dot blot illustrating block size and profile index. Dots indicate that the significant maxima of the MD function for different block sizes are identified at the profile positions where the cytoarchitectonic border lies between two areas.

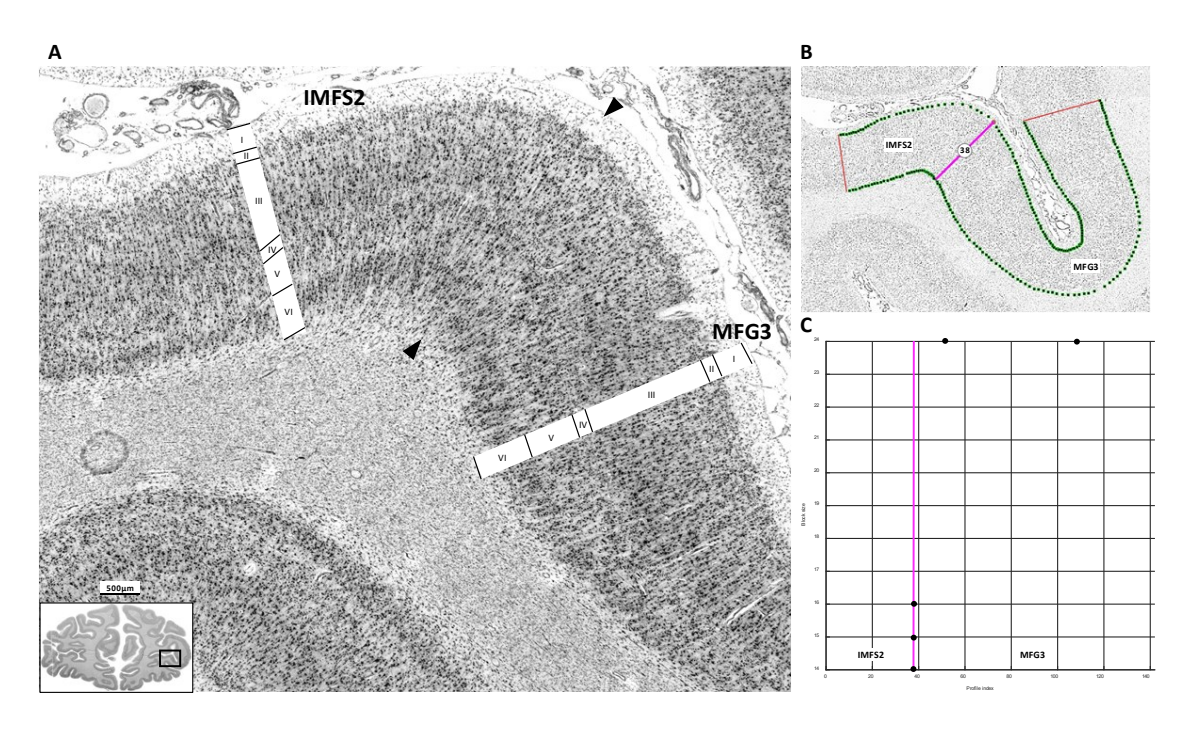


Fig. 10: Cytoarchitectonic border of IMFS2 and MFG3 (A) with quantified border detection and dot blot illustrating the position of significant peaks plotted against the block size

Brain code: BC11. Section number: 6751. Hemisphere: right. Roman numbers indicate the cortical layers. Scale bar: 500µm. Notice that layer II is less dense in IMFS2 than in MFG3. Large pyramidal cells are present in the deeper part of layer III, and layer IV is definable in both areas. In MFG3, upper layer V contains prominent large pyramidal cells. Layer VI is less dense in IMFS2. Both areas exhibit a sharply border with the white matter. Lamination and columnar organization are more distinct in MFG3. (B) The identified border detection was shown in the inverted GLI image. A significant border was marked by a pink line, along with the corresponding profile number at which each border was identified. (C) Dot blot depicting block size and profile index. Dots suggest that the significant maxima of the MD function for different block sizes are found at the profile positions where the cytoarchitectonic border lies between two areas.

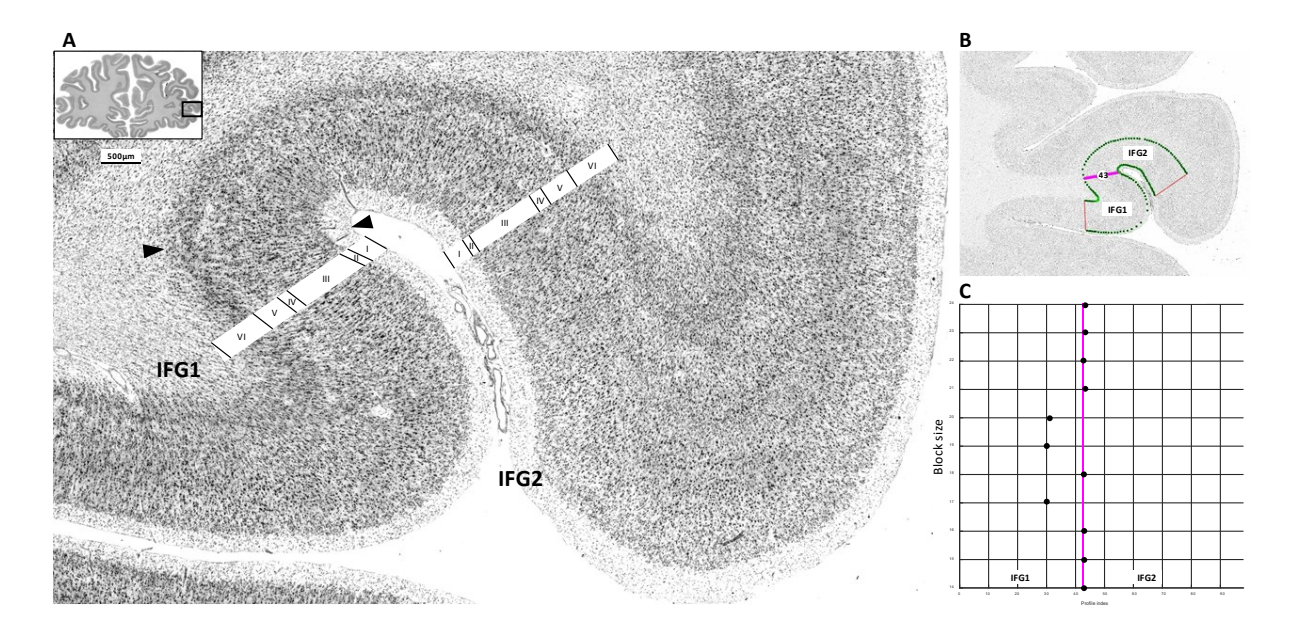


Fig. 11: Cytoarchitectonic border of IFG1 and IFG2 (A) with quantified border detection and dot blot illustrating the position of significant peaks plotted against the block size

Brain code: BC11. Section number: 6496. Hemisphere: right. Roman numbers indicate the cortical layers. Scale bar: 500µm. Notice that layer II is less dense in IFG1 than in IFG2. Large pyramidal cells are present in the deeper part of layer III, and layer IV is less dense in IFG1. Both areas exhibit prominent infragranular layers (V, VI), while the cell size is smaller in IFG2. Lamination and columnar organization are distinct in both areas. (B) Inverted GLI image with the quantified border detection. A significant border was labeled by a pink line, along with the corresponding profile number at which each border was identified. (C) Dot blot representing block size and profile index. Dots indicate that the significant maxima of the MD function for different block sizes are found at the profile positions where the cytoarchitectonic border lies between two areas.

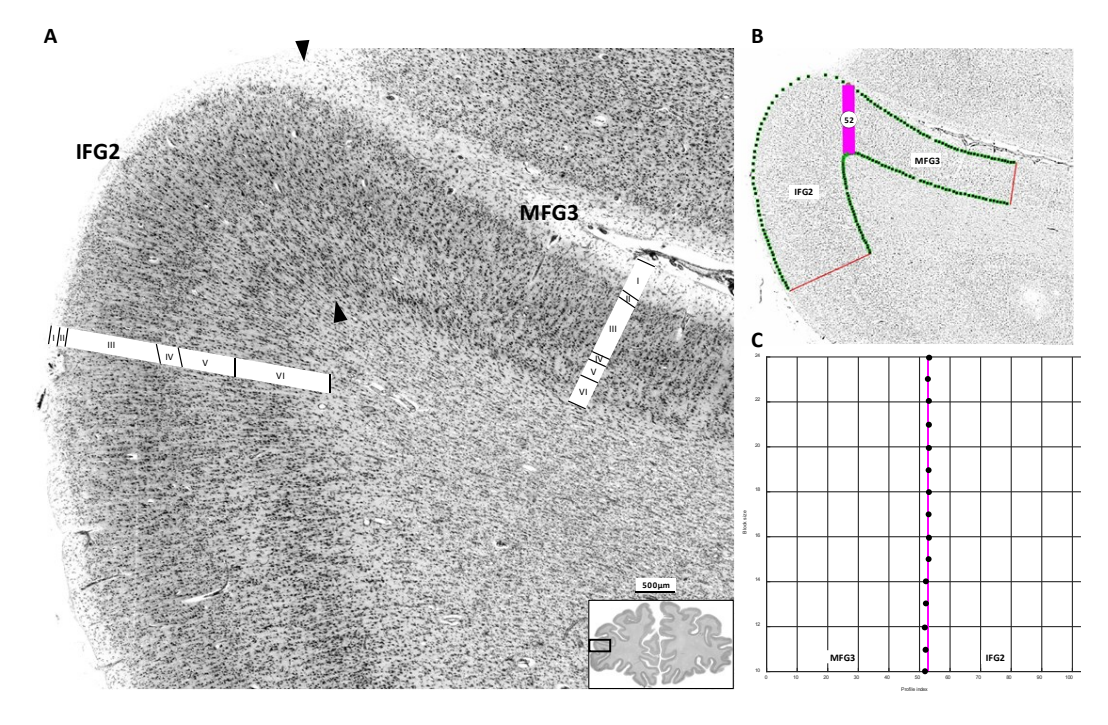


Fig. 12: Cytoarchitectonic border of IFG2 and MFG3 (A) with quantified border detection and dot blot illustrating the position of significant peaks plotted against the block size

Brain code: BCO1. Section number: 6211. Hemisphere: left. Roman numbers indicate the cortical layers. Scale bar: 500µm. Notice that layer II is less dense in both areas. Large pyramidal cells in the deeper part of layer III and layer V are more prominent, with larger cells size in MFG3 than in IFG2. Layer IV is dense and broad in IFG2, while it remains visible in MFG3. Layer VI is broad in IFG2, with a blurry transition to the white matter. Lamination and columnar organization are more distinct in IFG2. (B) Inverted GLI image with the quantified border detection. A significant border was marked by a pink line, along with the corresponding profile number at which each border was identified. (C) Dot blot illustrating block size and profile index. Dots show that the significant maxima of the MD function for different block sizes are identified at the profile positions where the cytoarchitectonic border lies between two areas.

3.1.2 Borders to neighboring areas

The cytoarchitecture of areas IMFS1, IMFS2, MFG3, IFG1 and IFG2 differed from their neighboring areas (see **Table 2**). The frontopolar area 1 (Fp1) lied rostral to IMFS1 and IMFS2 (Bludau et al. 2014). Similar to IMFS1, Fp1 had a dense layer II with a sharp border to layer III, though the pyramidal cells in the deeper part of layer III in Fp1 were larger. Layer IV of Fp1 was not as broad as in IMFS1 but more prominent than in IMFS2 (**Figure 13**). The pyramidal cells in layer V of Fp1 were larger than those in IMFS2, and its white-matter-boundary was more distinct compared to that of IMFS1.

In their dorsal aspect, the newly delineated areas shared borders with previously mapped areas, such as middle frontal gyrus area 1 (MFG1), middle frontal gyrus area 2 (MFG2) (Bruno et al. 2022), middle frontal gyrus area 4 (MFG4), and middle frontal gyrus 5 (MFG5) (Bruno et al. 2024), which were located in the mfg.

In contrast to MFG3, area MFG1 presented a dense layer II with larger pyramidal cell in deeper layers III and V. Layer IV of MFG1 was less dense than in IMFS1 (**Figure 14**) as well as in MFG3. MFG1 displayed a prominent layer VI with large cells and a blurry border to white matter, distinguishing it from MFG3.

Similar to IMFS1, area MFG2 had a relatively uniform appearance with a dense layer II and a well-developed layer IV, lacking large pyramidal cells in deeper layers III and V. However, layers III and VI were slightly more prominent in IMFS1 than in MFG2. Compared to MFG3 (**Figure 15**) and IMFS2, layers II and IV were more prominent in MFG2, while the cell size in deeper layers III and V was smaller.

Area MFG4 exhibited a prominent layer II, similar to IMFS1, but with a relatively blurry border to layer III. Layer IV of MFG4 was well developed, though not as broad as in IMFS1 (**Figure 16**). The infragranular layers (layer V and VI) of MFG4 was brighter than those in IMFS1.

Area MFG5 displayed a high cell density with a gradient of cell size in layer III. The pyramidal cells size in deeper layer III of MFG5 was smaller than in MFG3 (**Figure 17**) but larger than in IFG2. Layer IV was visible, thinner than in IFG2 but broader than in MFG3. Additionally, the cell density of the infragranular layers (layer V and VI) was lower, and there was a sharper border to the white matter compared to IFG2.

In their ventral process, the newly delineated areas also shared borders with previously mapped areas, such as areas Fo5 and Fo6 (Wojtasik et al. 2020), located on the lateral orbitofrontal cortex. Area Fo5 was rostral to area Fo6, which connected to areas IMFS2, MFG3, and IFG2 dorsally. Compared to IMFS2, area Fo5 manifested a dense layer II with smaller pyramidal cells in layer III. However, Fo5 had a lower cell density in layer II and smaller cell sizes in layer III compared to MFG3 (**Figure 18**). Moreover, layer IV was more cell-rich in Fo5 than in IMFS2, though not as broad as in IFG2. The pyramidal cells in layer V of area Fo5 were smaller than in area MFG3, and the white-matter-boundary was distinct compared to area IFG2.

Compared to Fo5, Fo6, and MFG3, IFG2 expressed similar characteristics in appearance. However, they can still be differentiated based on detailed cytoarchitectonic features. Fo6 had a less dense layer II with a clear border to layer III compared to IFG2 (**Figure 19**). Layer III was less dense than in MFG3 but similar to IFG1. Layer IV was not as broad as in IFG2 but wider than in MFG3. Fewer large pyramidal cells were present in layers V and VI than in IFG1 and MFG3, with a clear boundary to white matter.

Posterodorsally to areas IFG1 and IFG2, area 45 of Broca's region (Amunts et al. 2004) was located on the surface of the ifg. The main characteristic features of area 45 included large pyramidal cells in deeper layer III, a less pronounced layer IV, and a blurred transition into the white matter compared to IFG2 (**Figure 20**). Compared to IFG1, the primarily identifying criteria for area 45 were large pyramidal cells in deep layer III, a higher cell density in layer II and a more prominent layer V with large pyramidal cells.

Posteroventrally to area IFG1, area opercularis Op9 (Saal 2019) was located in the depth of the lateral fissure. Op9 demonstrated a less dense layer II and lacks large pyramidal cells in deeper layer III compared to IFG1. Layer IV was visible but poorly developed, with a blurred border to layer V, in contrast to IFG1. The prominent layer VI to white matter transition was not as sharp as in IFG1 (**Figure 21**).

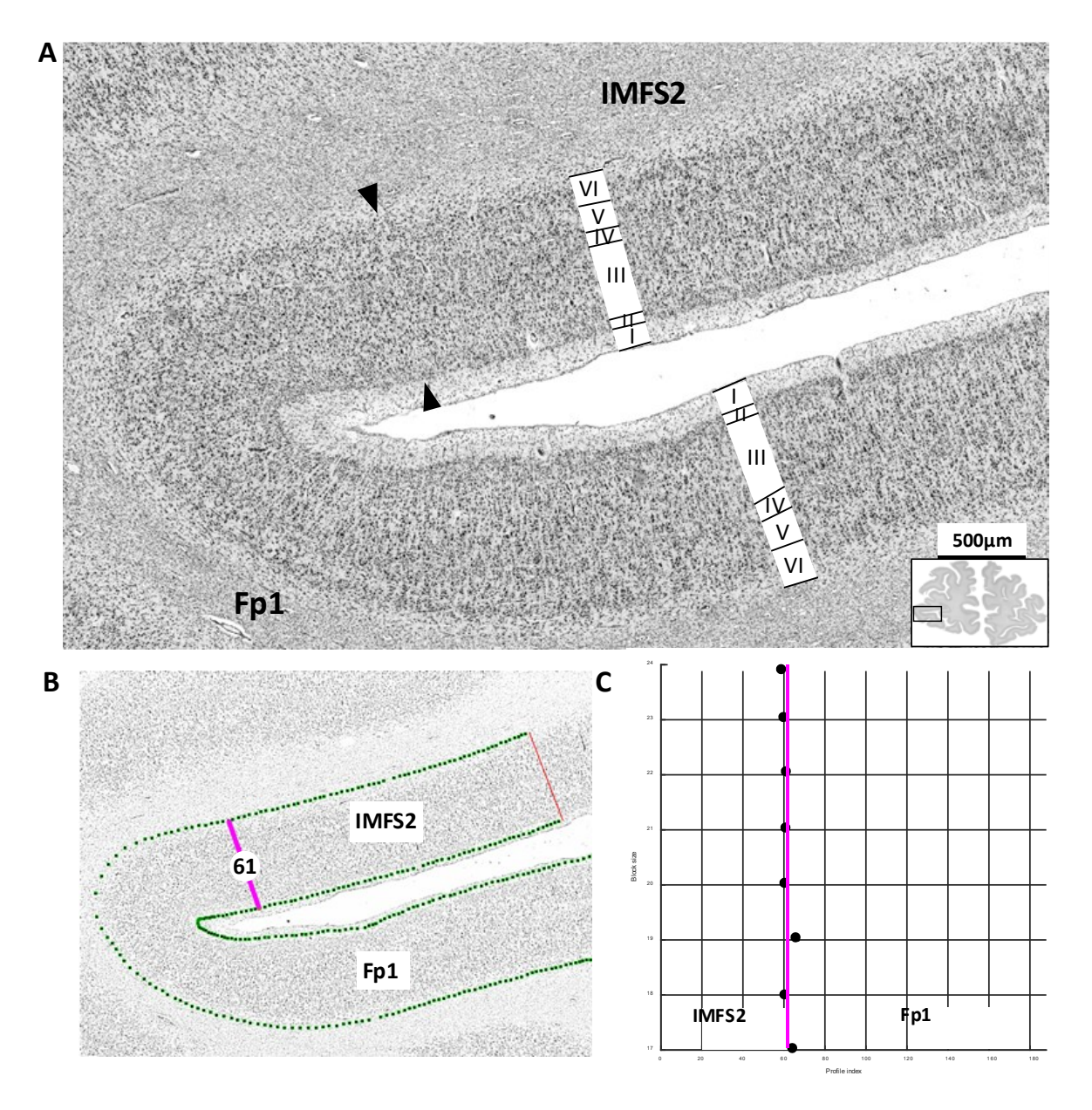


Fig. 13: Cytoarchitectonic border of IMFS2 and Fp1 (A) with quantified border detection and dot blot illustrating the position of significant peaks plotted against the block size

Brain code: BC20. Section number: 6751. Hemisphere: left. Roman numbers indicate the cortical layers. Scale bar: 500µm. Notice that layer II is less dense in IMFS2. Large pyramidal cells are presented in deeper layer III in both areas, but layer III is denser in Fp1. Layer IV was more prominent in Fp1(Bludau et al. 2014), and the pyramidal cells in layer V are larger than IMFS2. Both areas exhibit a distinct boundary to the white matter. (B) Inverted GLI image with identified border detection. A significant border was marked by a pink line, along with the corresponding profile number at which each border was identified. (C) Dot blot showing block size and profile index. Dots represent that the significant maxima of the MD function for different block sizes are found at the profile positions where the cytoarchitectonic border lies between two areas.

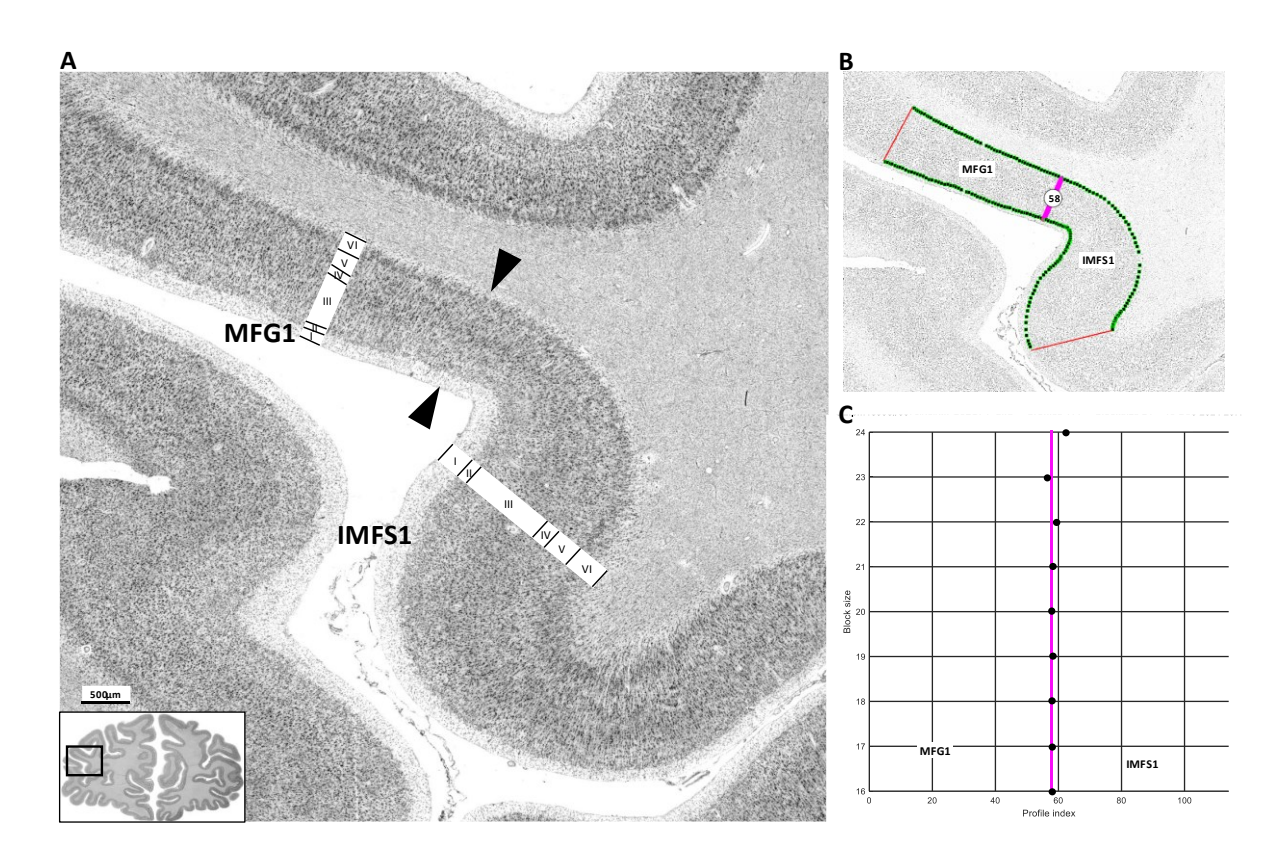


Fig. 14: Cytoarchitectonic border of IMFS1 and MFG1 (A) with quantified border detection and dot blot illustrating the position of significant peaks plotted against the block size

Brain code: BC11. Section number: 6676. Hemisphere: left. Roman numbers indicate the cortical layers. Scale bar: 500µm. Notice that layer II is dense in both areas. MFG1 (Bruno et al. 2022) has larger pyramidal cells in deeper layer III, while its layer IV is less dense than in IMFS1. Layer VI exhibits a sharper boundary to the white matter in MFG1 compared to IMFS1. Lamination and the visibility of columns are more distinct in IMFS1. (B) Inverted GLI image with the identified border detection. A significant border was marked by a pink line, along with the corresponding profile number at which each border was identified. (C) Dot blot depicting block size and profile index. Dots indicate that the significant maxima of the MD function for different block sizes are identified at the profile positions where the cytoarchitectonic border lies between two areas.

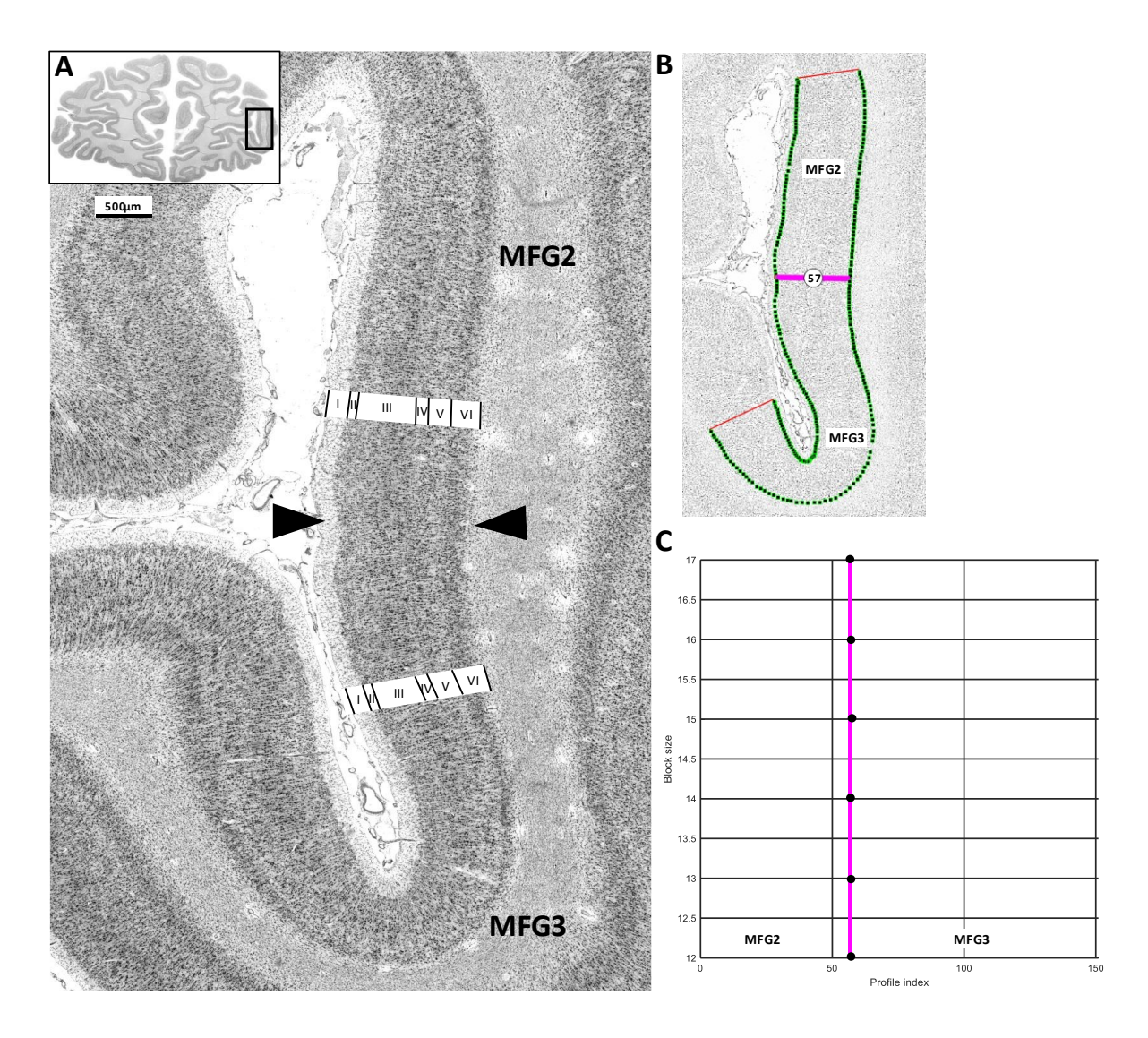


Fig. 15: Cytoarchitectonic border of MFG2 and MFG3 (A) with quantified border detection and dot blot illustrating the position of significant peaks plotted against the block size

Brain code: BC11. Section number: 6811. Hemisphere: right. Roman numbers indicate the cortical layers. Scale bar: 500µm. Notice that MFG2 (Bruno et al. 2022)has a homogeneous appearance, with a dense layer II and blurry border to layer III. The pyramidal cell size in deeper layer III is smaller, while layer IV is more prominent in MFG2 than in MFG3. Layers V and VI lack large pyramidal cells in MFG2, and there is a sharp border to the white matter. Lamination and the visibility of columns are more distinct in MFG2. (B) The identified border detection was shown in the inverted GLI image. A Significant border was marked by a pink line, along with the corresponding profile number at which each border was identified. (C) Dot blot representing block size and profile index. Dots indicate that the significant maxima of the MD function for different block sizes are identified at the profile positions where the cytoarchitectonic border lies between two areas.

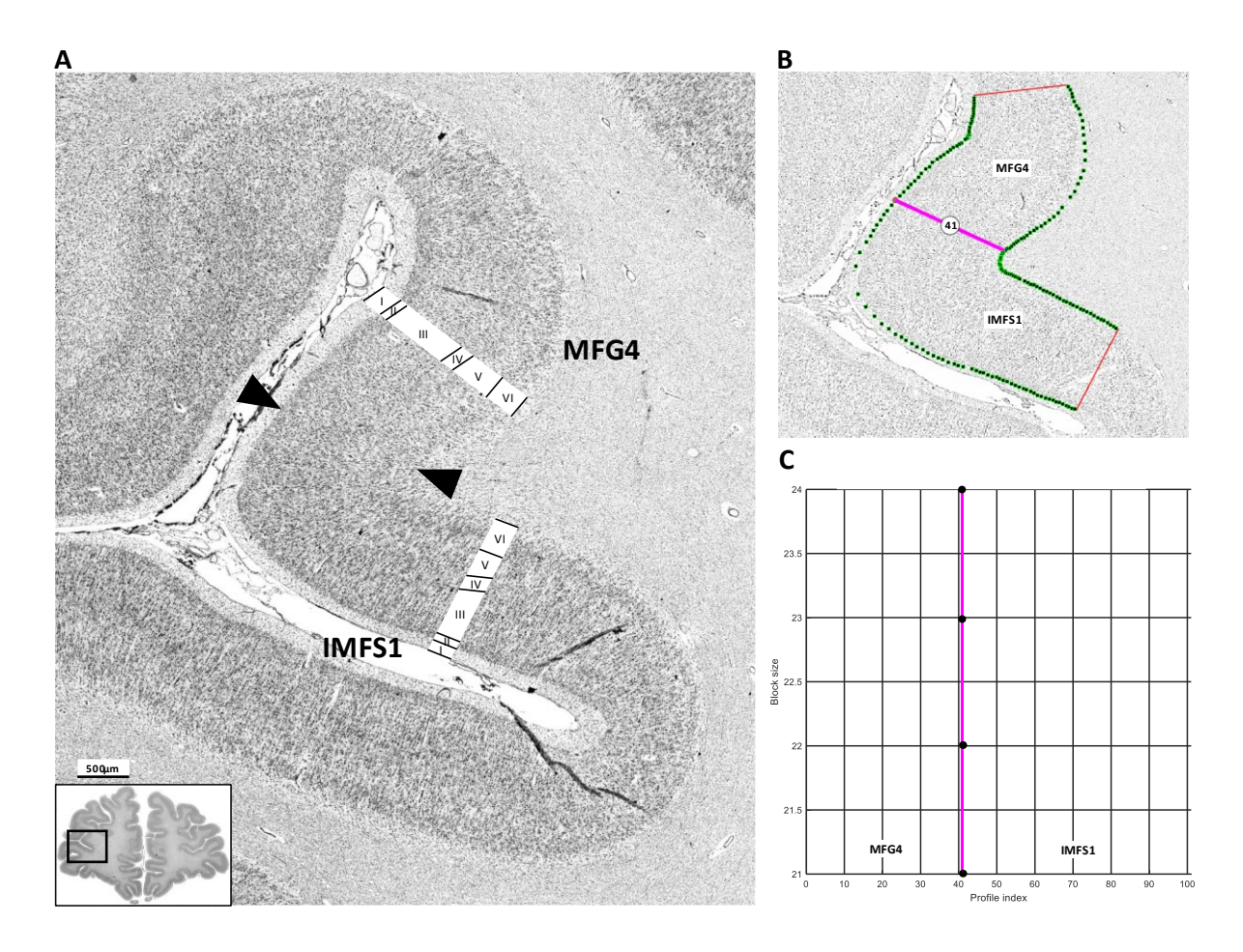


Fig. 16: Cytoarchitectonic border of IMFS1 and MFG4 (A) with quantified border detection and dot blot illustrating the position of significant peaks plotted against the block size

Brain code: BCO9. Section number: 6316. Hemisphere: left. Roman numbers indicate the cortical layers. Scale bar: 500µm. Notice that layer II is dense in both areas, with a relatively blurry border to layer III in MFG4 (Bruno et al. 2024). Layer IV of MFG4 is well developed but not as broad as in IMFS1. The infragranular layers (layer V and VI) of MFG4 are brighter than in IMFS1. Lamination and the visibility of columns are more distinct in IMFS1. (B) Inverted GLI image with the identified border detection. A significant border was marked by a pink line, along with the corresponding profile number at which each border was identified. (C) Dot blot illustrating block size and profile index. Dots demonstrate that the significant maxima of the MD function for different block sizes are found at the profile positions where the cytoarchitectonic border lies between two areas.

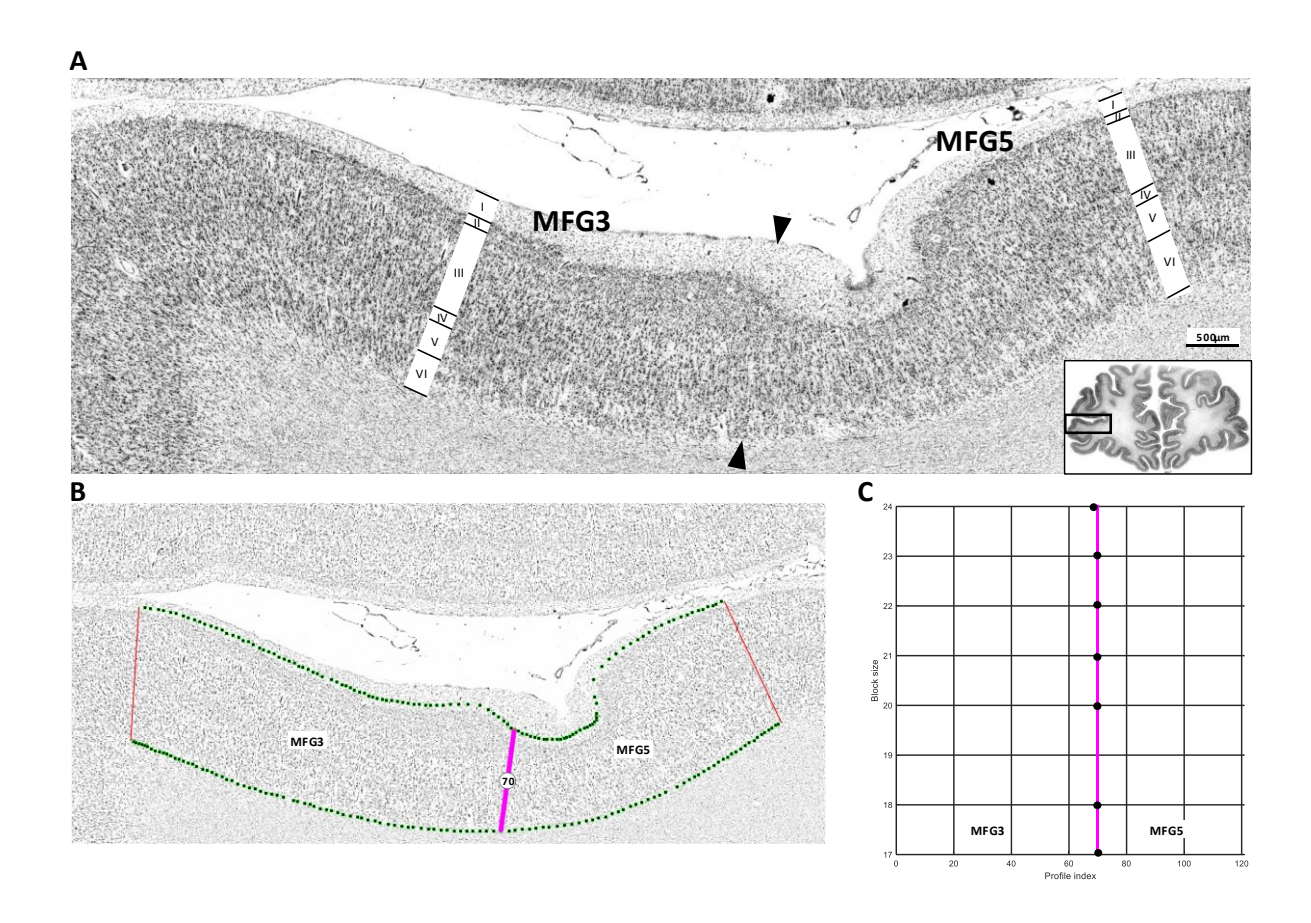


Fig. 17: Cytoarchitectonic border of MFG3 and MFG5 (A) with quantified border detection and dot blot illustrating the position of significant peaks plotted against the block size

Brain code: BC09. Section number: 6076. Hemisphere: left. Roman numbers indicate the cortical layers. Scale bar: 500µm. Notice that MFG5 (Bruno et al. 2024) has a less dense layer II with smaller pyramidal cells in deeper layer III compared to MFG3. Layer IV of MFG5 is slightly broader than in MFG3. Layers V and VI are brighter in MFG5, with a sharp boundary to white matter compared to MFG3. (B) Inverted GLI image with the quantified border detection. A significant border was marked by a pink line, along with the corresponding profile number at which each border was identified. (C) Dot blot depicting block size and profile index. Dots indicate that the significant maxima of the MD function for different block sizes are found at the profile positions where the cytoarchitectonic border lies between two areas.

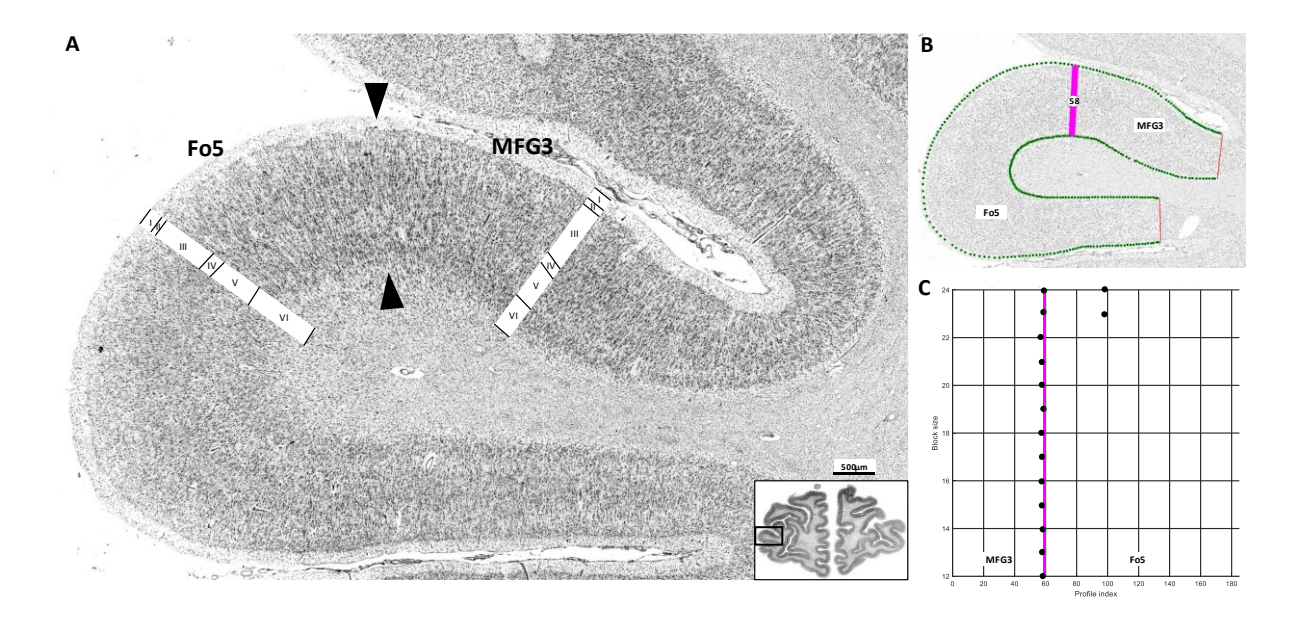


Fig. 18: Cytoarchitectonic border of MFG3 and Fo5 (A) with quantified border detection and dot blot illustrating the position of significant peaks plotted against the block size

Brain code: BCO9. Section number: 6721. Hemisphere: left. Roman numbers indicate the cortical layers. Scale bar: 500µm. Notice that area Fo5 (Wojtasik et al. 2020) has a less dense layer II and smaller pyramidal cell size in layer III compared to MFG3. Layer IV is more prominent in Fo5, and the cell size in layer V is not as large as in MFG3. The prominent layer VI, without large pyramidal cells, has a blurry transition to white matter in Fo5 compared to MFG3. (B) Inverted GLI image with the quantified border detection. A significant border was marked by a pink line, along with the corresponding profile number at which each border was identified. (C) Dot blot illustrating block size and profile index. Dots suggest that the significant maxima of the MD function for different block sizes are found at profile positions where the cytoarchitectonic border lies between two areas.

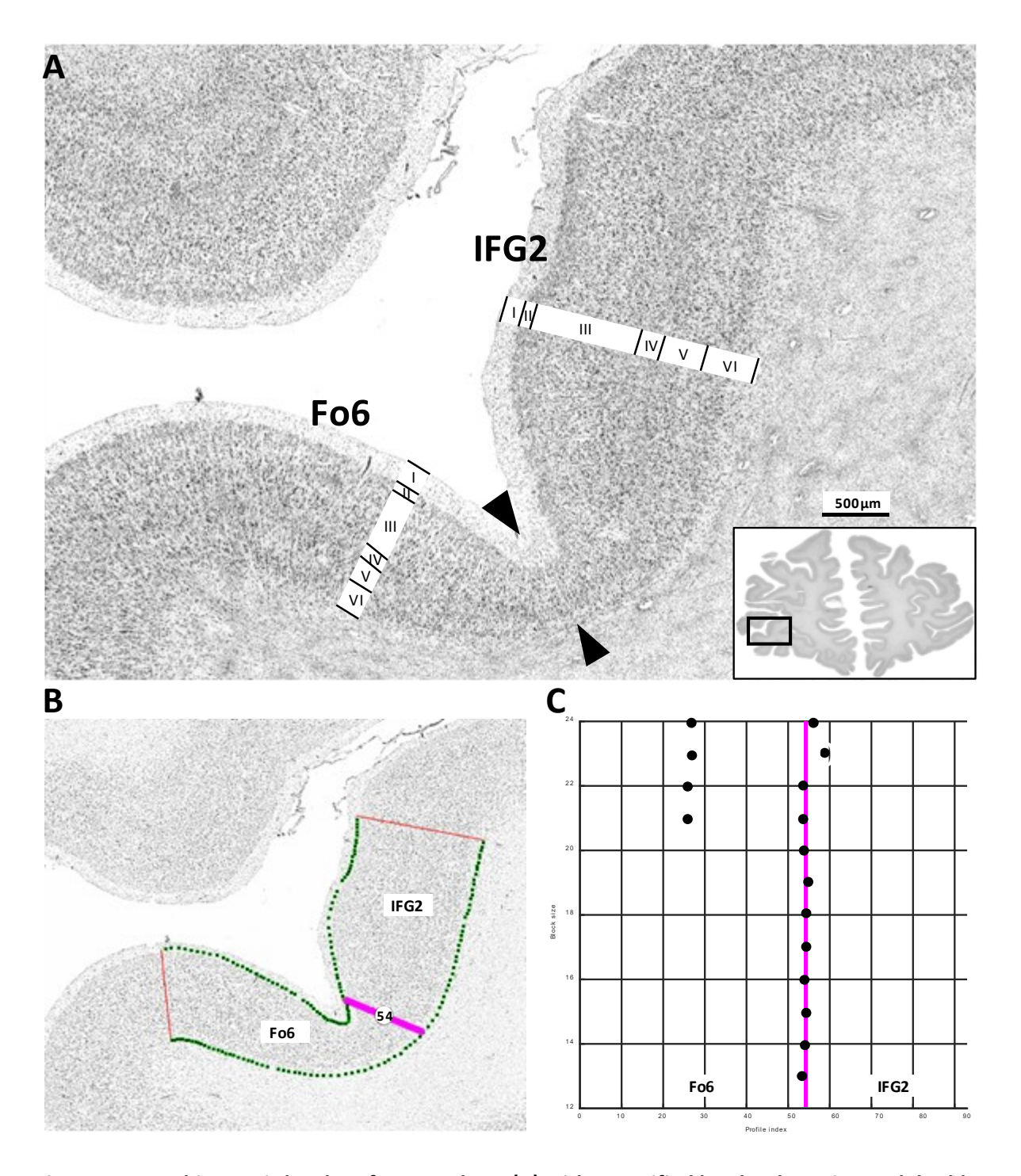


Fig. 19: Cytoarchitectonic border of IFG2 and Fo6 (A) with quantified border detection and dot blot illustrating the position of significant peaks plotted against the block size

Brain code: BC20. Section number: 6496. Hemisphere: left. Roman numbers indicate the cortical layers. Scale bar: 500µm. Notice that layer II is less dense with a clear border to layer III in Fo6 (Wojtasik et al. 2020) compared to IFG2. Layer III is loosely packed, and layer IV of Fo6 is not as broad as in IFG2. Fewer large pyramidal cells are present in layers V and VI, with a clear boundary to the white matter in Fo6 compared to IFG2. (B) Inverted GLI image with the identified border detection. A significant

border was marked by a pink line, along with the corresponding profile number at which each border was identified. (C) Dot blot illustrating block size and profile index. Dots suggest that the significant maxima of the MD function for different block sizes are found at profile positions where the cytoarchitectonic border lies between two areas.

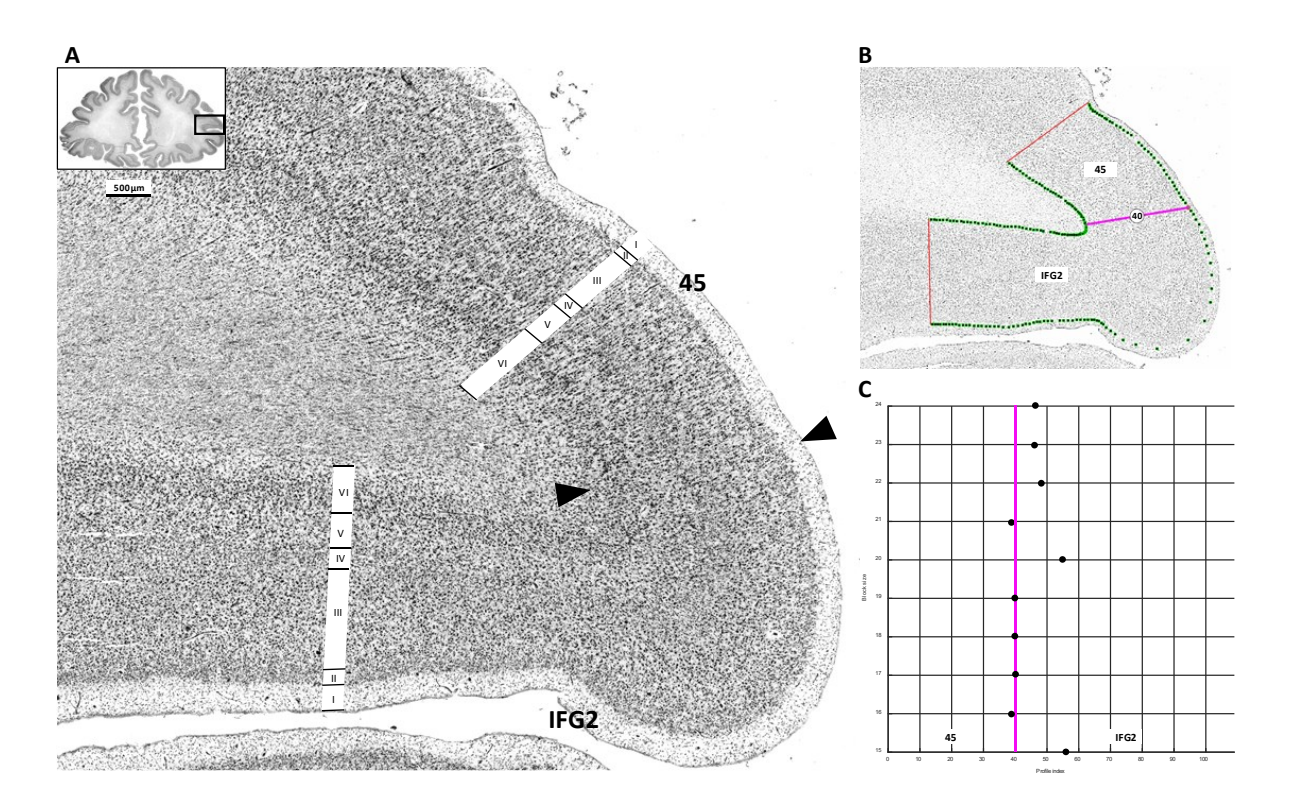


Fig. 20: Cytoarchitectonic border of IFG2 and area 45 (A) with quantified border detection and dot blot illustrating the position of significant peaks plotted against the block size

Brain code: BCO4. Section number: 6061. Hemisphere: right. Roman numbers indicate the cortical layers. Scale bar: 500µm. Notice that layer II is less dense in area 45 (Amunts et al. 1999), with a blurry transition to layer III. Large pyramidal cells in deeper layer III and layer V are more prominent, and cell size is larger in area 45 than in IFG2. Layer IV is less pronounced in area 45 than in IFG2. (B) Inverted GLI image with the quantified border detection. A significant border was marked by a pink line, along with the corresponding profile number at which each border was identified. (C) Dot blot depicting block size and profile index. Dots indicate that the significant maxima of the MD function for different block sizes are found at profile positions where the cytoarchitectonic border lies between two areas.

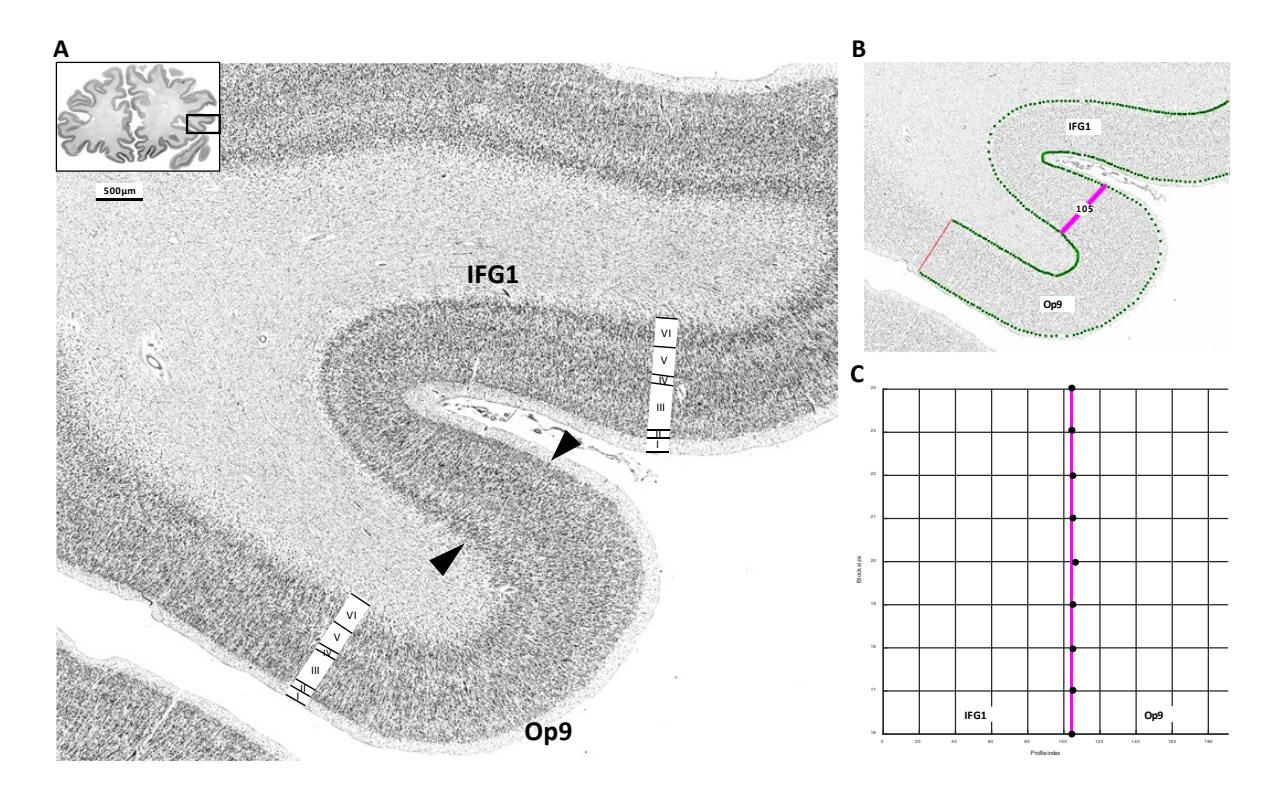


Fig. 21: Cytoarchitectonic border of IFG1 and Op9 (A) with quantified border detection and dot blot illustrating the position of significant peaks plotted against the block size

Brain code: BC08. Section number: 5521. Hemisphere: right. Roman numbers mark the laminar. Scale 500μm. Notice that Op9 (Saal 2019) has a less dense layer II, with no large pyramidal cells in deeper layer III compared to IFG1. Layer IV of Op9 has a blurred border to layers III and V, and is not as broad as in IFG1. (B) Inverted GLI image with the identified border detection. A significant border was marked by a pink line, along with the corresponding profile number at which each border was identified. (C) Dot blot depicting block size and profile index. Dots indicate that the significant maxima of the MD function for different block sizes are found at profile positions where the cytoarchitectonic border lies between two areas.

3.2 Quantification of cytoarchitectonic differences and similarities of new areas and neighboring areas of the prefrontal cortex

Areas of the anterior prefrontal cortex - IMFS1, IMFS2, MFG3, IFG1 and IFG2 - were distinguished in a discriminant analysis using their GLI profiles (**Figure 22A**). The analysis revealed that while GLI profiles showed some interindividual variance, all identified areas form discrete clusters, which partially overlapped. Area IFG1 formed a cluster that was separated from IFG2. Cytoarchitectonically, area IFG2 was more similar to IMFS1 and MFG3 than to IMFS2. Similarly, area IMFS2 resembled IMFS1 more closely than MFG3, as indicated by the slight intersection. However, we consistently detected and verified the borders between these areas along their trajectories.

In the hierarchical cluster analysis, the newly defined areas (IMFS1, IMFS2, MFG3, IFG1, and IFG2) were compared with neighboring areas of the prefrontal cortex, including the frontal pole areas Fp1 (Bludau et al. 2014), Broca's areas 44 and 45 (Amunts et al. 2004), the lateral orbitofrontal cortex areas (Fo5 and Fo6) (Wojtasik et al. 2020), and other anterior prefrontal cortex areas (mfg1, mfg2, mfg4, and mfg5) (Bruno et al. 2022, Bruno et al. 2024). Areas IMFS1, IMFS1 and IFG2 shared cytoarchitectonic similarities with the lateral orbitofrontal cortex (Fo5, Fo6), while areas MFG3 and IFG1 exhibited greater similarity to the prefrontal cortex areas mfg5. Notably, all five areas were more distinct from other prefrontal cortex areas (mfg1, mfg2, and mfg4), Broca's region and the frontal pole area Fp1, based on the Euclidean distance measurements (Figure 22B).

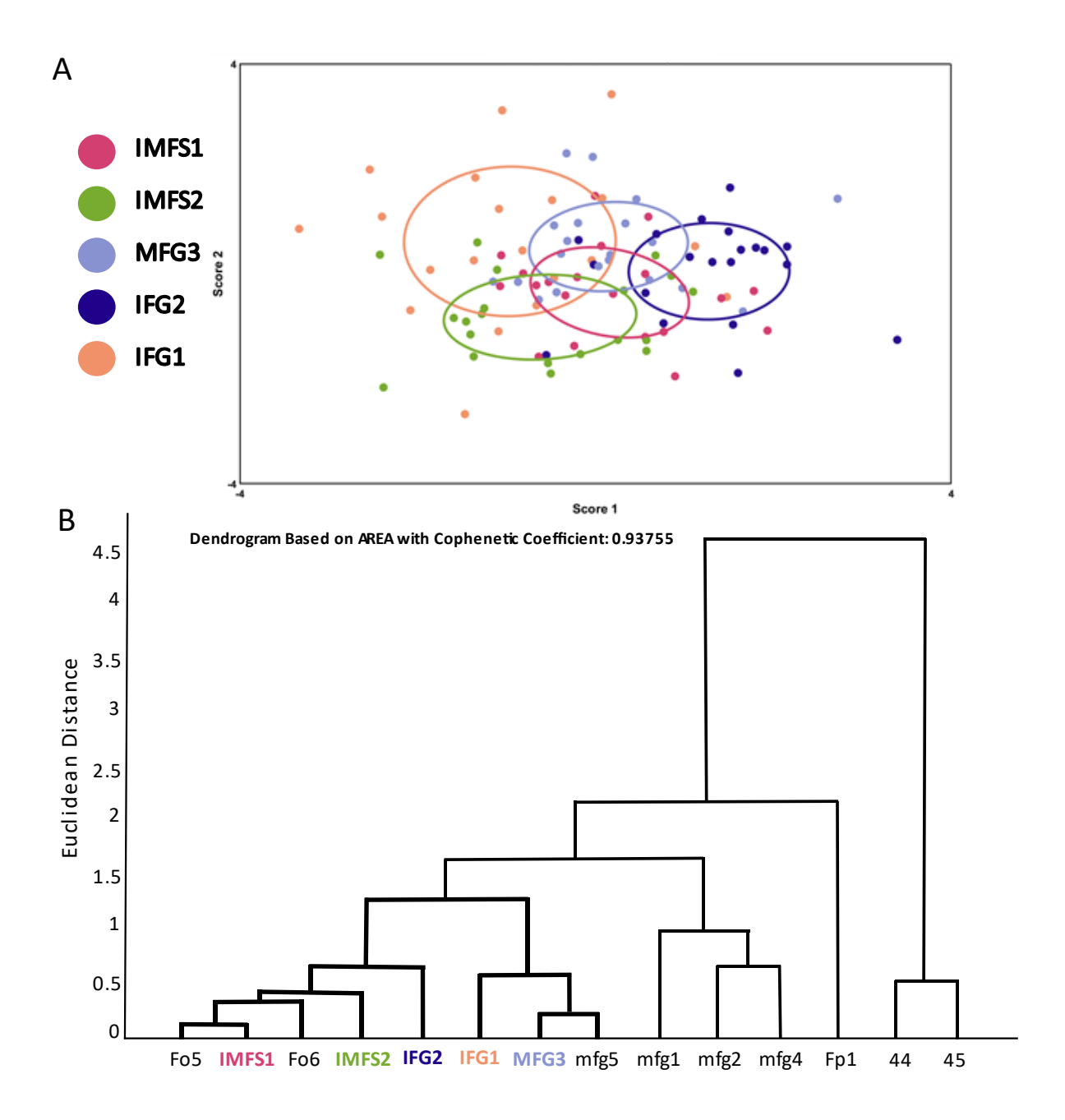


Fig. 22: Discriminant and cluster analysis of Gray Level Index profiles

The GLI profiles of the newly defined areas in the anterior prefrontal cortex were compared using discriminant analysis (A). Each area is represented by a set of 20 dots (2 hemispheres from 10 brains) and an ellipsoid, indicating the centroid for each area. The variance in dot localization reflects the cytoarchitectonic interindividual variability. The dendrogram from hierarchical cluster analysis (B) distinguishes the newly identified areas from Fp1 (Bludau et al. 2014), Broca's areas 44 and 45 (Amunts et al. 2004), the lateral orbitofrontal cortex (Fo5 and Fo6) (Wojtasik et al. 2020), and other anterior prefrontal cortex areas (mfg1, mfg2, mfg4, and mfg5) (Bruno et al. 2022, Bruno et al. 2024). The newly defined five areas form a distinguish cluster, reflecting structural differences from their adjacent areas in the prefrontal cortex. A high Euclidean distance along the y-axis indicates structural dissimilarity.

3.3 Individual localization of areas within single brains

The considerable intrasubject variability in sulcal patterns, localization, and the extent of new areas on the lateral surface was depicted in the 3D reconstruction of 10 individual brains (**Figure 23**). The main sulci were identified on the cortical surface of the lateral prefrontal cortex, including the central sulcus, precentral sulcus, superior frontal sulcus, inferior frontal sulcus, intermediate frontal sulcus, horizontal ramus and ascending ramus of the Sylvian fissure, and diagonal sulcus (ds).

3.3.1 Sulcal pattern

The sulcal pattern varied between individual brains and hemispheres. For example, the rostral origins of areas IMFS1 and IMFS2 always located at the imfs, and the imfs exhibited different shapes, such as a "Y" or "V" shape oriented in different directions (e.g., see Figure 23A, B, C) or a horizontal reversed "Z" shape (see Figure 23D left hemisphere) in individual brains.

Here we defined the imfs in a simplified way, since Amiez et al. determined the intermediate frontomarginal sulcus (ifms) in other literature as part of the vertical ramus of intermediate frontal sulcus (imfs-v). In fact, the sulcus "imfs" in our map encompassed the imfs-v and ifms in the nomenclature of Petrides (Petrides 2013), imfs-v in Amiez (Amiez et al. 2023), and infs-v and ifms in Petrides and Pandya (Petrides and Pandya 2012). Additionally, the inferior frontal sulcus also varied between individual brains. In some case, the ifs rostrally from the precentral sulcus and ended within the inferior frontal gyrus without connecting to any more rostral sulcus (see Figure 23B, E, J). In contrast, in other brains, the ifs can extend rostrally to connect with the intermediate frontal sulcus (see Figure 23I) or the lateral frontomarginal sulcus (see Figure 23G left hemisphere).

The horizontal branch and ascending branch of the Sylvian fissure, and the diagonal sulcus also exhibited different locations in different brains. In some brains, such as BC04 (see Figure 23B), the diagonal sulcus was not easily identifiable on the lateral surface, especially in the left hemisphere. The hs in the left hemisphere of BC09 (see Figure 23E) was located at the same position as the lateral orbital sulcus in other brains (e.g., the left hemisphere of BC10, Figure 23F). We also observed that the extent and shape of the middle and inferior frontal gyri varied among individuals, in combination with the variable locations of the sfs, ifs, imfs and hs.

3.3.2 The localization of areas

The location of the newly defined five areas is described in detail below. Area IMFS1 was primarily located within the depth of the vertical portion of the imfs, extending dorsally and caudally and partially onto the surface of middle frontal gyrus (for example, see BC01 Figure 23A).

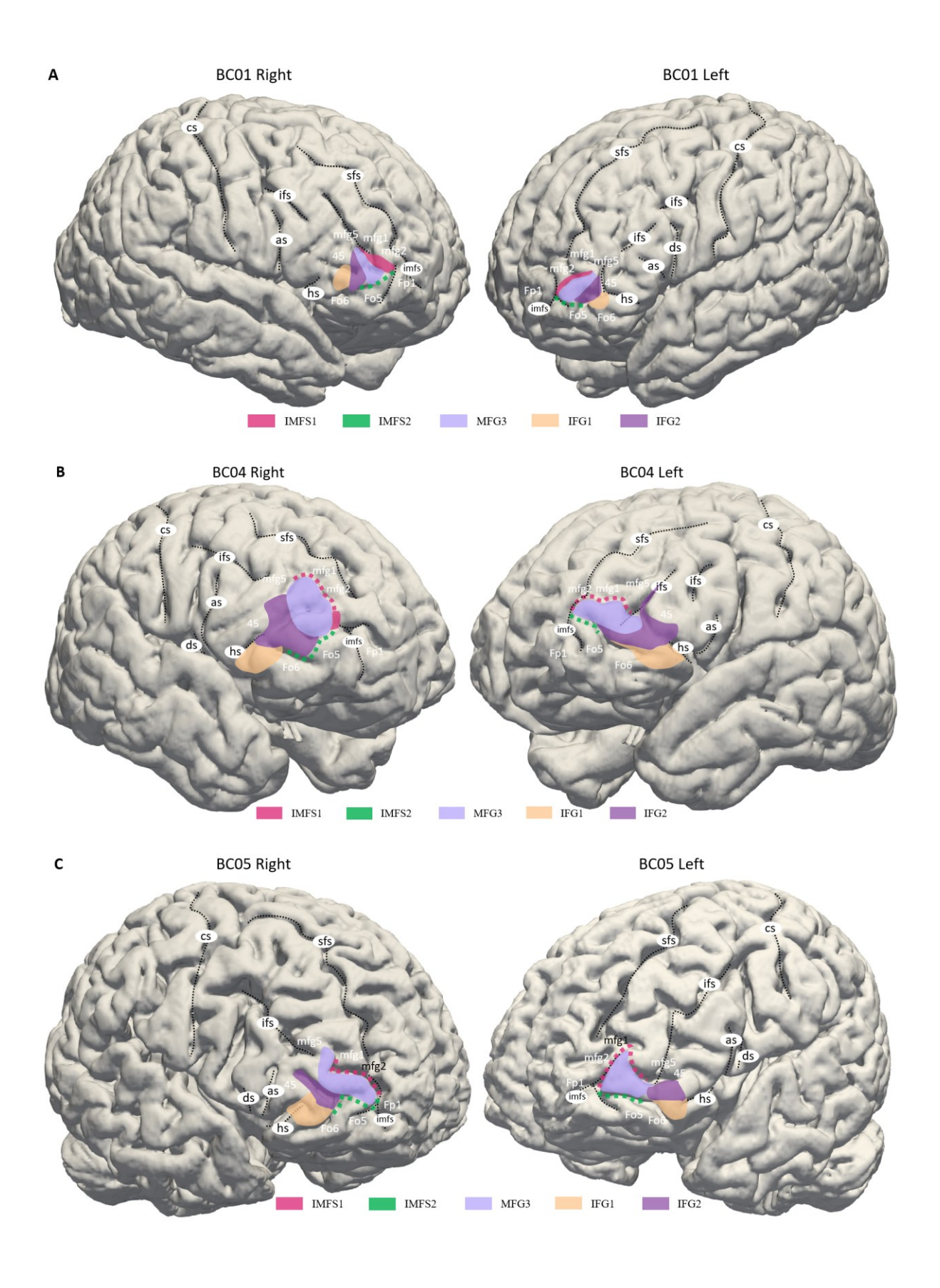
Area IMFS2 was located ventral to IMFS1, also within the depth of imfs but mainly extending ventrally and caudally (for example, see BC05 **Figure 23C**). Unlike IMFS1, IMFS2 was almost never visible on the brain's surface.

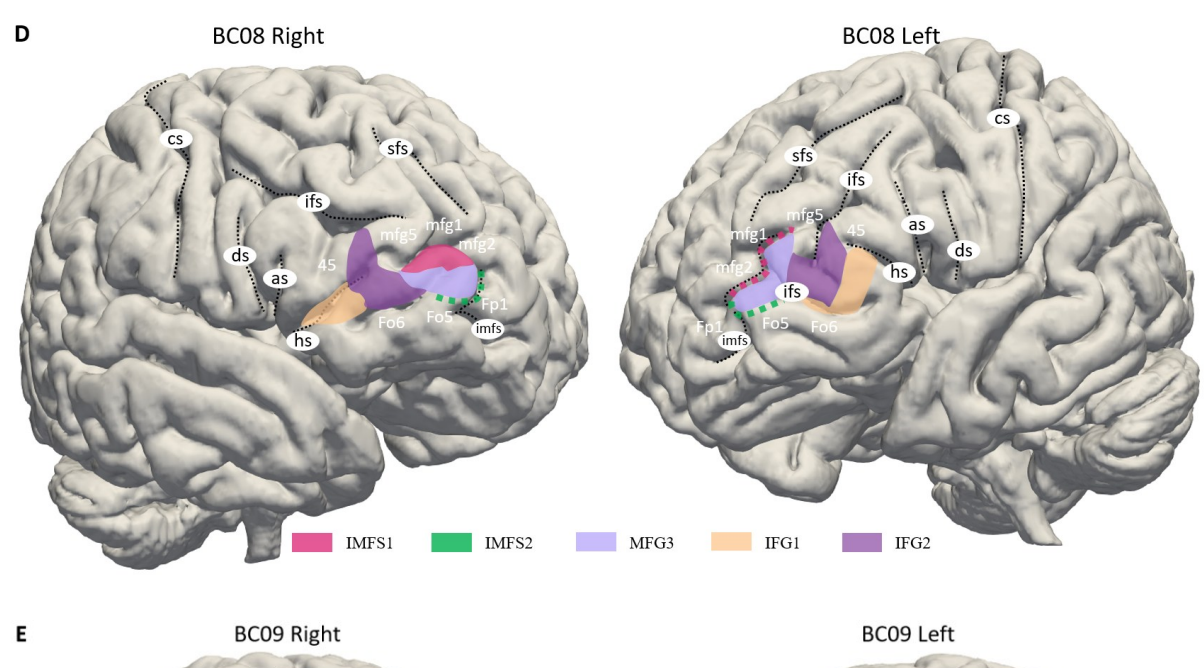
Area MFG3 was located ventral to IMFS1 but dorsal to IMFS2, primarily covering the surface of the anterior mfg and partially extending to the anterior portion of the inferior frontal sulcus (for example, see BC09 **Figure 23E**). Ventral to MFG3, area IFG2 mainly covered the surface of the anterior ifg and extended caudally to the ifs (for example, see BC20 **Figure 23I**).

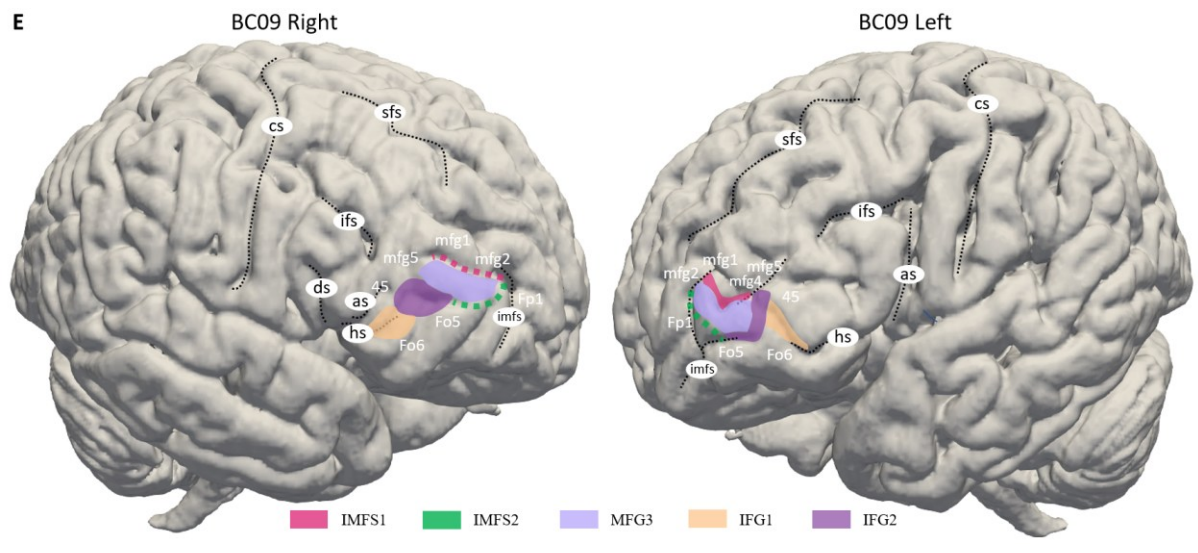
Adjacent to IFG2, area IFG1 was located on the surface of ifg and extended to the horizontal ramus of sylvian fissure (for example, see BC04 **Figure 23B**).

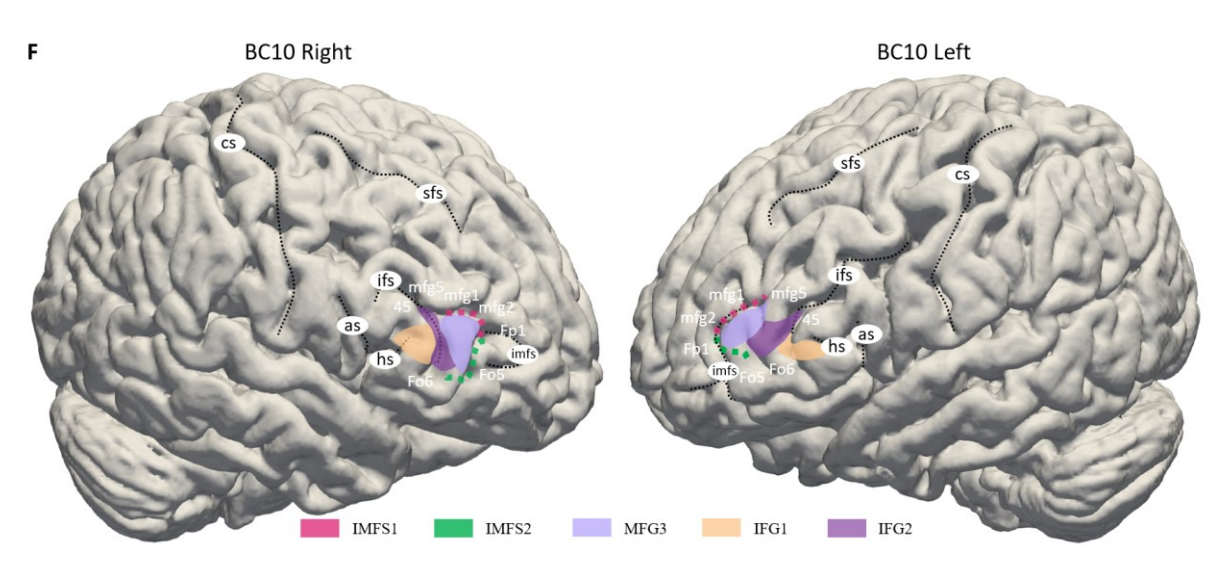
These five newly defined areas were connected with each other in the order IMFS1-MFG3-IFG2-IFG1 following a dorsal-to-ventral and rostral-to-caudal orientation. Moreover, area IMFS2 was connected to IMFS1 or MFG3 ventrally but never directly bordered IFG1 and IFG2. There was only one exception, where area IMFS1 did not connect to MFG3 in the right hemisphere of BC11 (see **Figure23G**).

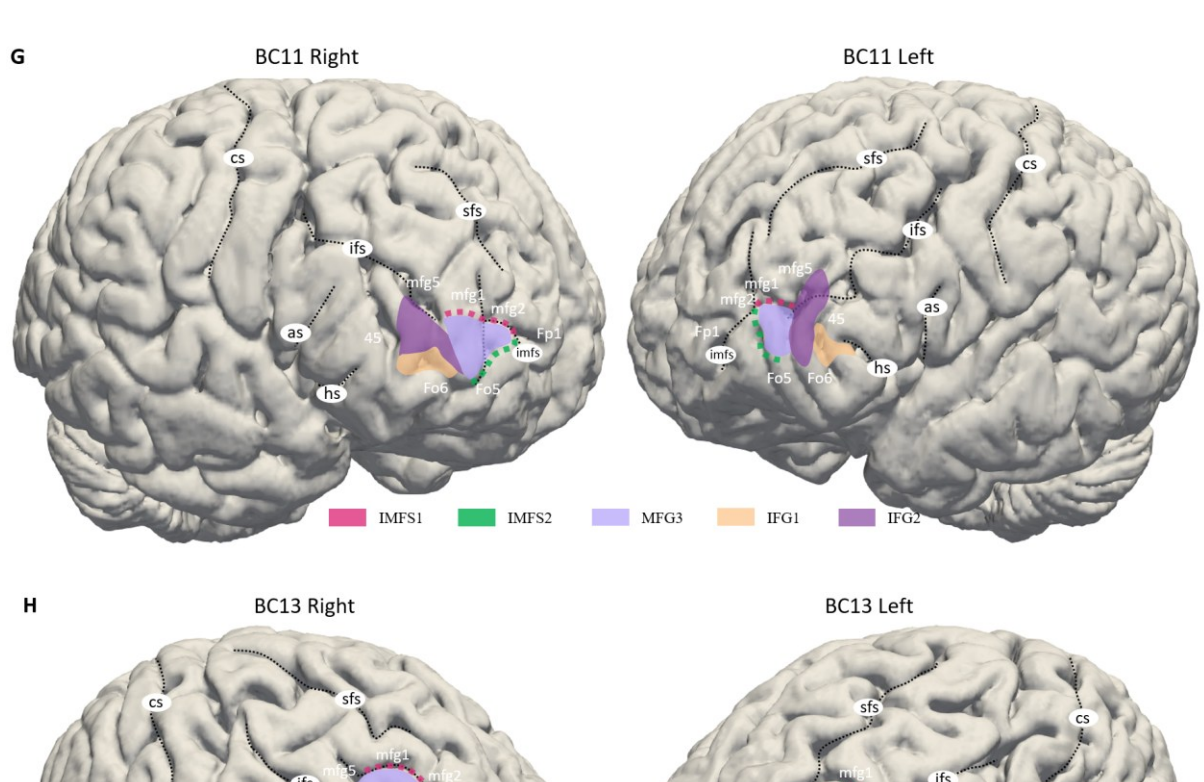
It was also clearly demonstrated that the shape and extent of these five newly defined areas varied significantly among individual brains. Analysis of the three-dimensional reconstructions indicated that the cytoarchitectonically defined borders between areas did consistently align with the contours of the sulci.

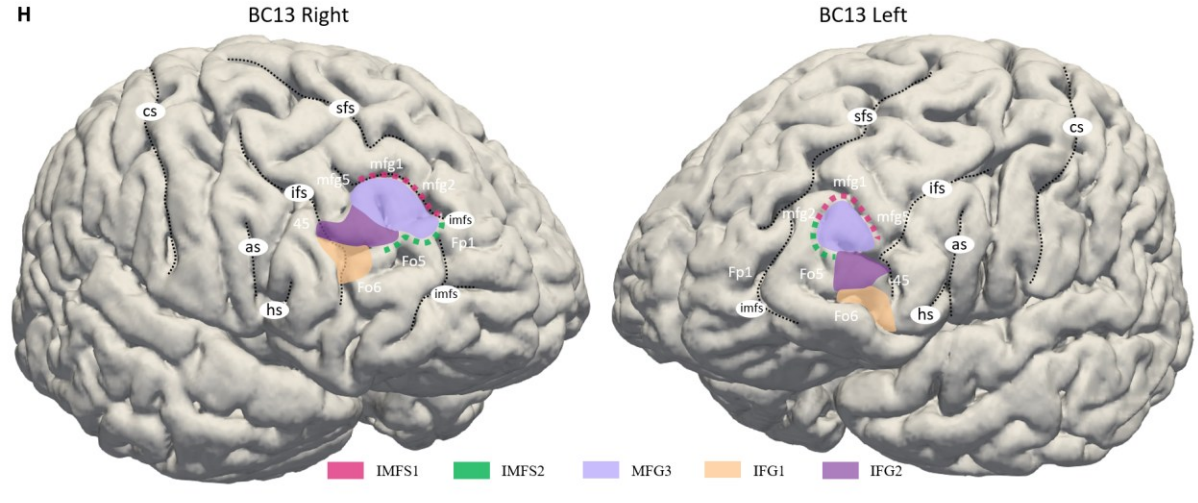


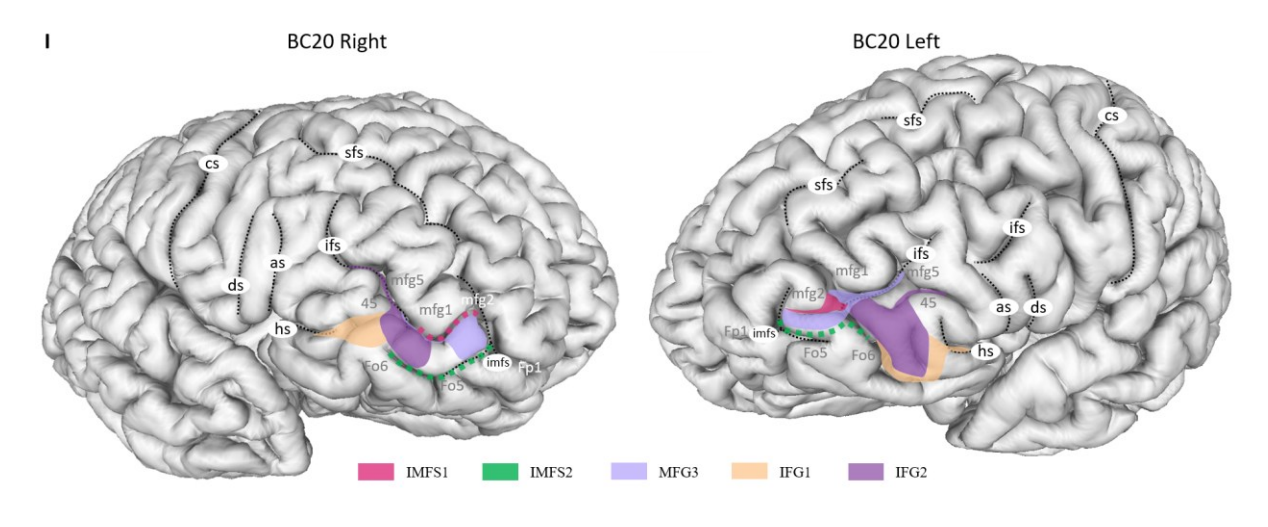












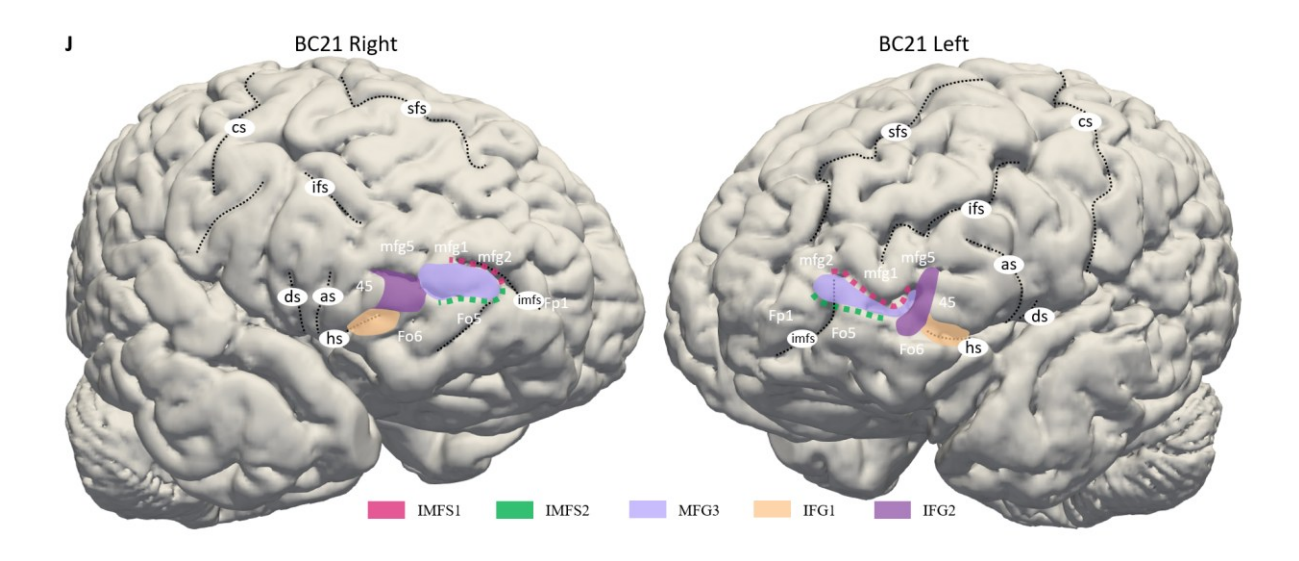


Fig. 23: Lateral views of 3D reconstructions of the areas mapped in ten individual brains

Pink and green dashed lines indicate that area IMFS1 and IMFS2 were located within the depth of the imfs and were not visible from the lateral surface view. The surroundings regions of the newly defined areas were also marked. BC20 and BC21 represent BigBrains (I, J). The main sulci for each hemisphere were labelled above with black dashed lines (A-J): cs, central sulcus; ifs, inferior frontal sulcus; sfs, superior frontal sulcus; imfs, intermediate frontal sulcus; as, ascending sulcus (ascending ramus of the lateral fissure); hs, horizontal sulcus (horizontal ramus of the lateral fissure); ds, diagonal sulcus. The nomenclature for the sulcus was based on (Petrides and Pandya 2012, Petrides 2018).

3.4 Probability maps and maximum probability maps

The high interindividual variability in the anterior part of the prefrontal cortex across individual brains and the location of the newly defined areas IMFS1, IMFS2, MFG3, IFG1, and IFG2 are shown in **Figure 24**. Cytoarchitectonic probability maps in the anatomical reference space MNI Colin27 (**Figure 24**) were calculated to quantify the interindividual variability in the stereotaxic localization and extent of these five anterior prefrontal cortex areas. The probability maps depicted the overlap of areas with a color gradient from red (high probability and low interindividual variability) to blue (low probability and high interindividual variability). The center of gravity for the newly defined anterior prefrontal cortex areas were listed in **Table 3** for both MNI Colin27 and ICBM152casym spaces.

IMFS2 was mainly located in the depth of the anterior imfs. IMFS1 originated from the imfs, extending dorsally to the sfs and partly onto the mfg. MFG3 was situated on the surface of the mfg and extended toward the ifs with a gradually decreasing probability. IFG2 began at the anterior ifs and extended into the anterior part of the ifg. IFG1 was also located on the anterior ifg, extending into the hs.

A non-overlapping surface representation of all newly defined anterior prefrontal cortex areas was provided by the MPM, showing the topography of these areas along with the cytoarchitecturally defined adjacent regions, including Fp1 (Bludau et al. 2014), the lateral orbitofrontal cortex Fo5 and Fo6 (Wojtasik et al. 2020), other anterior prefrontal cortex areas mfg1, mfg2, mfg4 and mfg5 (Bruno et al. 2022, Bruno et al. 2024), and Broca's areas 44 and 45 (Amunts et al. 2004), on the inflated brain surface of MNI Colin27 (Figure 25).

The newly generated maps are publicly available, free to share, and open for adaption under the Creative Commons license agreement. They can be downloaded at (atlases.ebrains.eu/viewer).

Area	Hemisphere	MNI Colin27 space		ICBM152casym space			
		×	У	Z	×	У	Z
IMFS1	Left	-31	52	12	-32	53	11
	Right	37	50	9	36	54	9
IMFS2	Left	-28	54	2	-29	55	1
	Right	32	53	2	30	57	3
MFG3	Left	-40	51	8	-40	52	6
	Right	44	48	8	43	51	8
IFG1	Left	-45	43	-3	-45	44	-5
	Right	52	38	-1	50	40	-2
IFG2	Left	-44	45	4	-45	46	3
	Right	48	42	6	46	44	5

Table 3: Center of gravity coordinates in MNI Colin27 space and ICBM152casym space of newly defined anterior prefrontal cortex areas separated by hemisphere

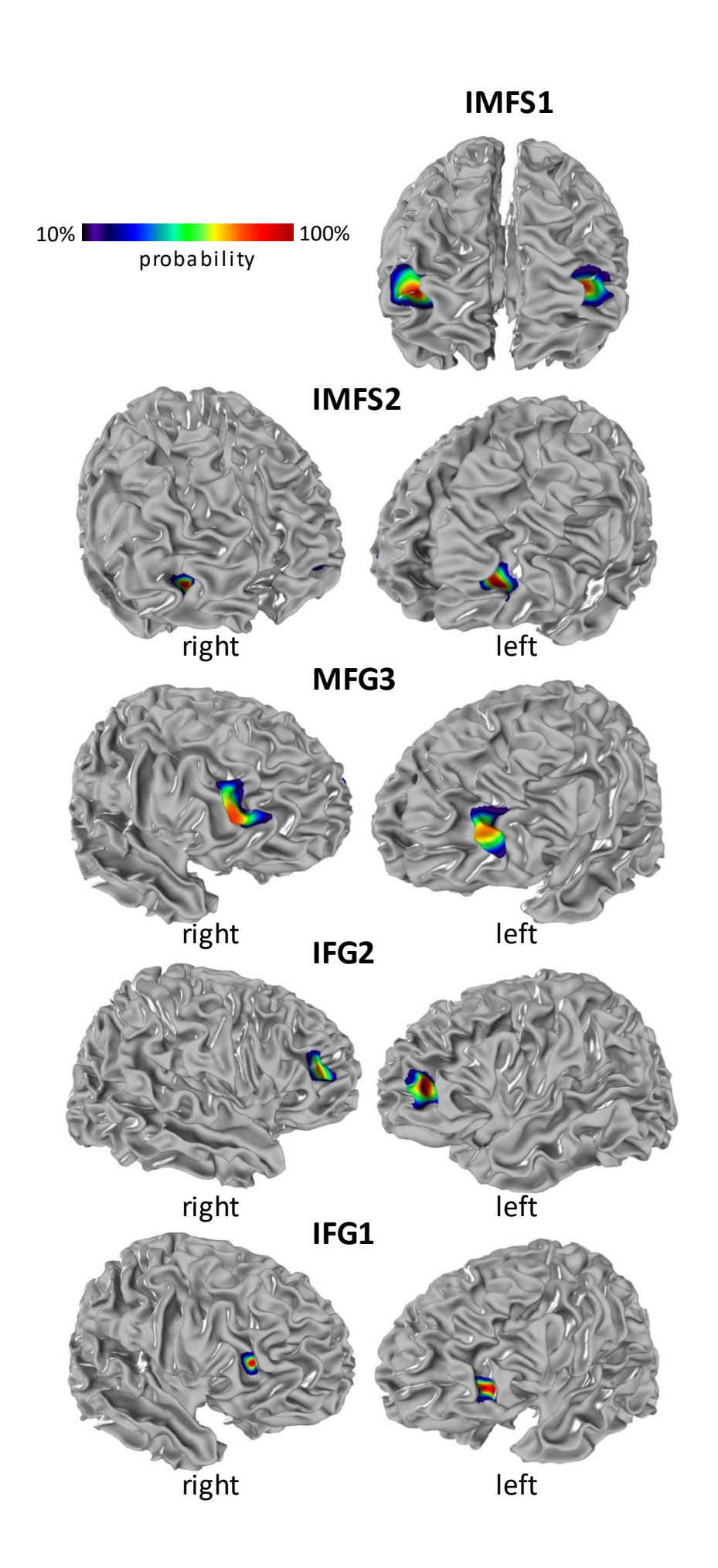


Fig. 24: Probability maps of the areas IFG1, IFG2, IMFS1, IMFS2, and MFG3

The probability maps are displayed on the individual anatomical template brain, MNI Colin27. These color-coded maps illustrate interindividual variability, with probability values ranging from 10% (violet-blue) to 100% (red).

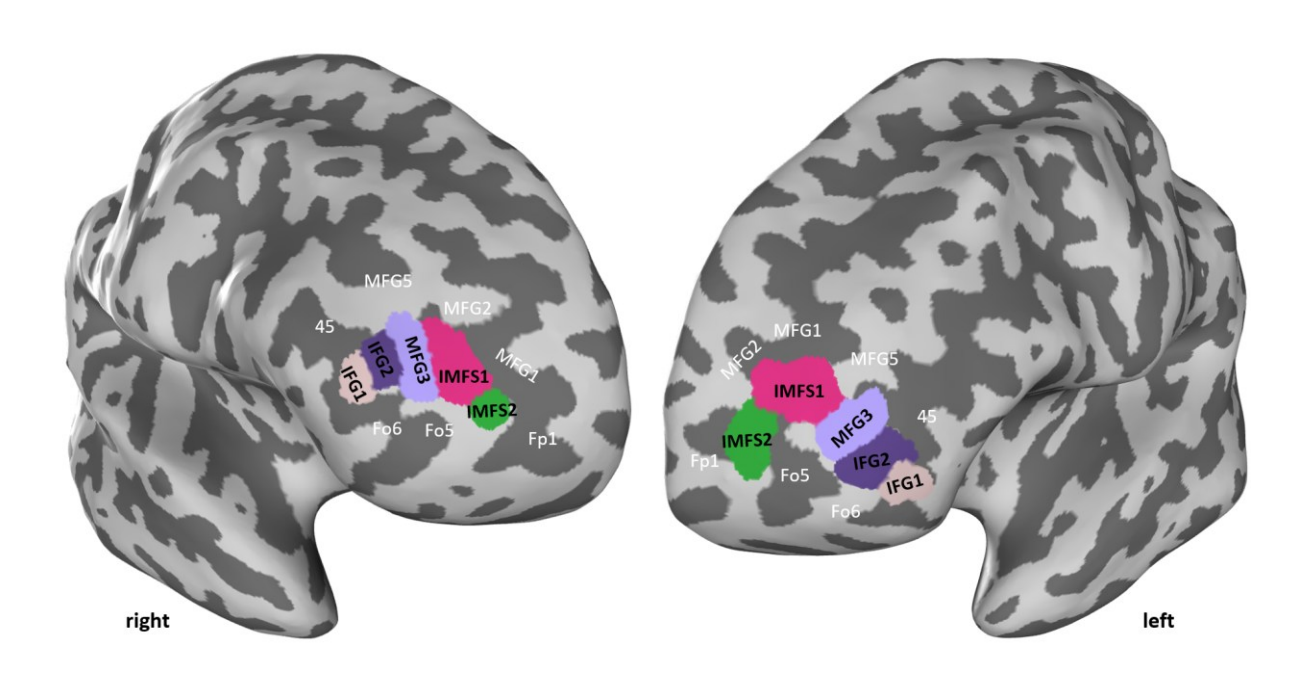


Fig. 25: Maximum probability Map of areas IFG1, IFG2, IMFS1, IMFS2, and MFG3, inflated views

The maximum probability maps are displayed in the inflated view of the MNI Colin27 brain in smooth-white-matter mode, highlighting the localization of specific areas on both gyri and sulci. The non-overlapping surface illustrates the position of the newly five defined areas alongside adjacent regions, including the frontal pole area (Fp1), the lateral orbitofrontal cortex areas (Fo5 and Fo6), other prefrontal cortex areas (MFG1, MFG2, MFG5), and Broca's area 45.

3.5 Volumes of areas IMFS1, IMFS2, MFG3, IFG1 and IFG2

The volumes of areas IMFS1, IMFS2, MFG3, IFG1, and IFG2 in each hemisphere of each brain were presented in **Table 4**, including the shrinkage correction factor for each post-mortem brain. The total volume for each brain was included in Supplementary Table 1. The shrinkage-corrected volumes of five areas showed that area MFG3 had the largest volume, followed by IFG2, IMFS1, IFG1 and IMFS2 (see **Table 4**). The shrinkage-corrected volumes of the five areas were analyzed to investigate interhemispheric and sex-related differences. To account for individual brain size variations, the shrinkage-corrected volumes were normalized to the corresponding total brain volume. Statistical comparisons were performed using a two-way ANOVA, with area and hemisphere as within-subject factors and sex as a between-subject factor. The analysis revealed no significant differences in volume between sexes or hemispheres (p>0.05).

The data showed a considerable variability between individual brains. According to the standard deviation of volume, which reflects individual variability, area IFG2 showed the highest variation.

Brain	Sex	Factor	Left (mm³)				Right (mm³)					
No.												
			IMFS1	IMFS2	MFG3	IFG1	IFG2	IMFS1	IMFS2	MFG3	IFG1	IFG2
BC01	F	1.7	329	181	436	77	260	392	243	502	168	138
BC04	М	1.9	376	249	953	642	1411	404	408	1061	1001	2146
BC05	F	2.2	377	982	450	160	322	618	1021	603	444	325
BC08	F	1.9	424	302	627	1213	868	162	167	271	986	602
BC09	F	1.5	797	680	717	206	422	607	330	836	305	337
BC10	F	1.7	1244	396	632	233	873	543	585	704	478	1344
BC11	М	2.2	894	377	842	121	549	679	472	742	378	962
BC13	М	2.3	778	156	691	306	330	423	516	1021	282	517
BC20	М	1.9	612	644	628	809	868	975	268	556	430	487
BC21	М	1.8	436	346	854	622	448	195	267	1182	359	615
Mean			627	431	683	439	635	500	427	748	483	747
SD			297	260	167	370	363	240	247	282	284	599

Table 4: Shrinkage corrected volumes of areas (mm³) of each hemisphere in 10 brains

Factor refers to the individual "Shrinkage factor". F, Female. M, Male. SD, standard deviation.

3.6 Functional characterization of the cytoarchitectonic areas by meta-analytic connectivity modelling

The maximum probability maps were used as VOIs to explore potential functions of the areas IMFS1, IMFS2, MFG3, IFG1, and IFG2 through meta-analytic connectivity modelling analysis. The present research revealed a greater number of experiments in the right hemisphere compared to the left hemisphere (see **Table 5**). It was also apparent that the experiment associated with areas IMFS1, MFG3, and IFG2 were more frequent than those associated with areas IMFG2 and IFG1. The numbers of experiments included in the analysis for each cytoarchitectonic area are listed in **Table 5**.

We obtained the preliminary identification of potential corresponding functions of each area in both hemispheres by using uncorrected p<0.05 (UC05) data. In order to address the potential false positive rate, we also performed FDR correction by multiple comparison to ensure greater statistical reliability of the identified functional categories. The relevant Behavioural Domains (BD) and PC for each hemisphere of each area were shown in **Figure 26** and **Figure 27**.

Area	Experiments	Subjects	Foci
IMFS1 left	588	8777	7985
IMFS1 right	615	8925	8490
IMFS2 left	128	1957	1855
IMFS2 right	139	2215	1869
MFG3 left	716	10659	9741
MFG3 right	925	13720	13093
IFG1 left	192	3089	2423
IFG1 right	644	9768	9099
IFG2 left	750	11214	10255
IFG2 right	755	11499	10682

Table 5: Number of experiments, subjects and activation foci located within the respective areas used for functional profiling

3.6.1 Behavioural Domains of areas IMFS1, IMFS2, MFG3, IFG1 and IFG2 on both hemispheres

The main Behavioural Domains (BD) for the newly defined five areas were primarily cognitive functions, including language, memory, reasoning, emotion, perception, and interoception. Area IMFS1 in the left hemisphere was associated with cognitive memory working, memory explicit, and inhibition of action, whereas the right hemisphere was mainly associated with perception, as well as working memory and action inhibition. The left IMFS2 was primarily associated with perceptual pain after the FDR correction. Before the FDR correction, both hemispheres of area IMFS2 were associated with working memory and explicit memory. MFG3 in the left hemisphere was also associated with working memory, while the right hemisphere was involved in other functions, including negative emotion such as anxiety, somesthetic pain, and inhibition of behaviour. We also observed that the two inferior frontal gyrus areas, IFG1 and IFG2, in the left hemisphere were involved in language functions. The left IFG1 was associated with language semantics, and the left IFG2 was not only related to language semantics but also closely linked to language phonology and orthography. The left IFG2 was also associated with memory function. By contrast, the right hemisphere of IFG1 differed significantly from the left hemisphere in its associated functions, which included negative emotions such as anxiety, as well as perception and interoception. The right hemisphere IFG2 was also involved in negative emotion (Emotion. Negative Disgust) as well as other cognitive functions, such as reasoning and working memory.

3.6.2 Paradigm Classes of areas IMFS1, IMFS2, MFG3, IFG1 and IFG2 on both hemispheres

The IMFS1 area in the right hemisphere was activated by the n-back experiment, Stroop task, Delayed Match to Sample (DMTS) tasks, and pain discrimination. In the left hemisphere, it was only activated by the n-back experiment (see **Figure 27**). The Paradigm Class of area IMFS2 was not involved in the Figure 25 after the FDR correction. Before the FDR correction, the left IMFS2 was activated by n-back (working memory), explicit memory, and recall tasks, while the right IMFS2 was activated not only by the same tasks as the left side but also by the task-switching experiment and affective pictures experiment.

The left MFG3 was activated by the n-back experiment and word generation (covert), while the right MFG3 was activated not only by the n-back experiment but also other tasks,

including pain discrimination, DMTS tasks, and cognitive control tasks such as inhibitory control or impulsivity control. In contrast to other areas, the IFG1 and IFG2 areas in the left hemisphere were primarily activated by language related experiments, such as semantic discrimination, phonological discrimination, and word generation. The left IFG2 was also activated by encoding process experiment. However, these two inferior frontal gyrus areas in the right hemisphere differed from the left hemisphere; they were activated not by the language experiments but by pain discrimination and the n-back experiment.

In summary, the function distribution of the areas IMFS1, IMFS2, MFG3, IFG1, and IFG2 was primarily associated with cognitive functions, emotional functions, and also perception. Different areas were associated with distinct functions, and evidence of functional lateralization between the hemispheres was also observed.

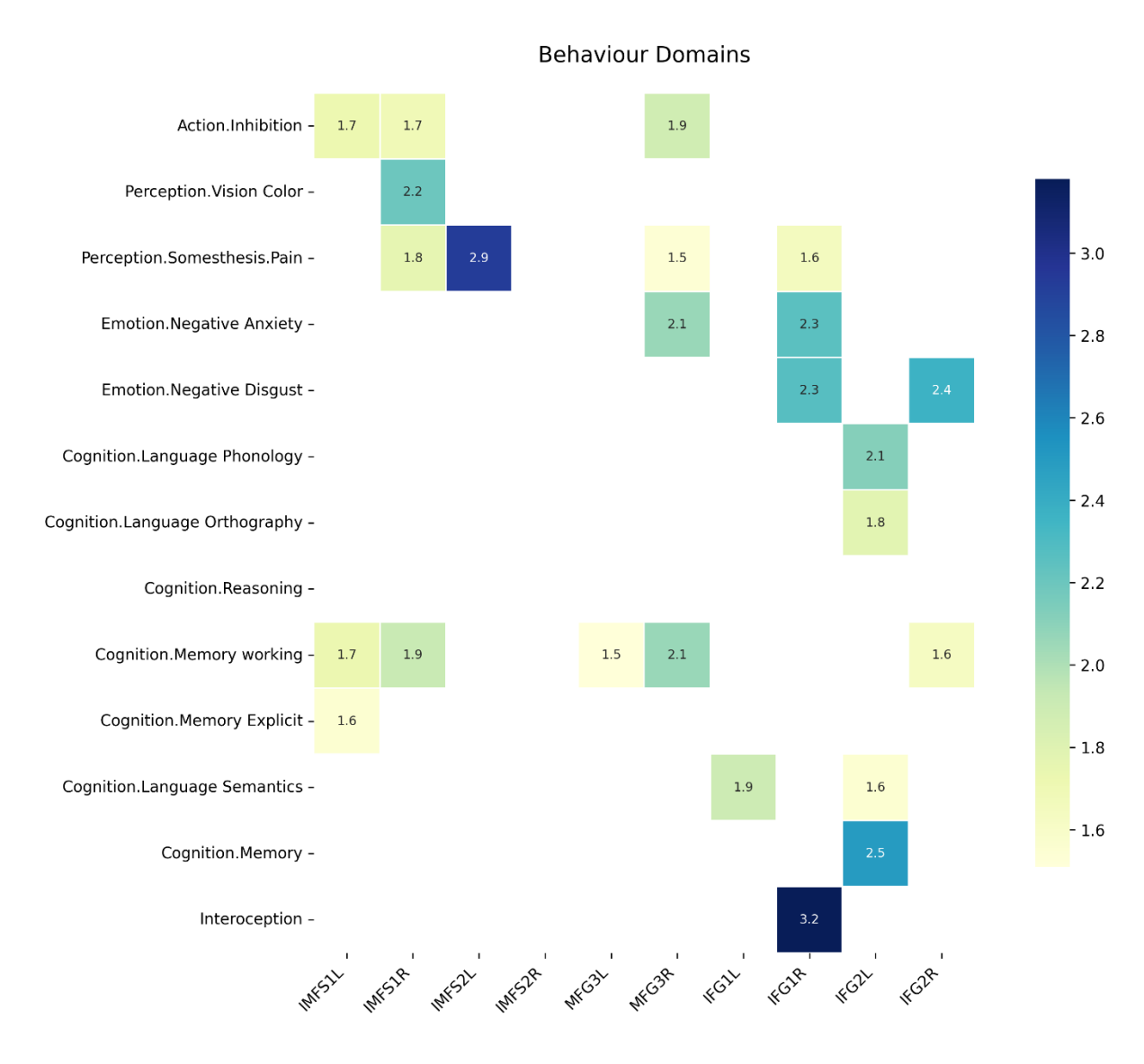


Fig. 26: Behavioural domains associated with areas IMFS1, IMFS2, MFG3, IFG1 and IFG2 of both hemispheres (L, R) with FDR corrected (p<0.05)

All the coloured squares represent items that were after corrected for multiple comparisons using the (FDR) with the likelihood ration. The intensity of the colour reflects the magnitude of the values, which also indicates the association with the corresponding functions. Higher values or darker colours denote a stronger association with the respective function.

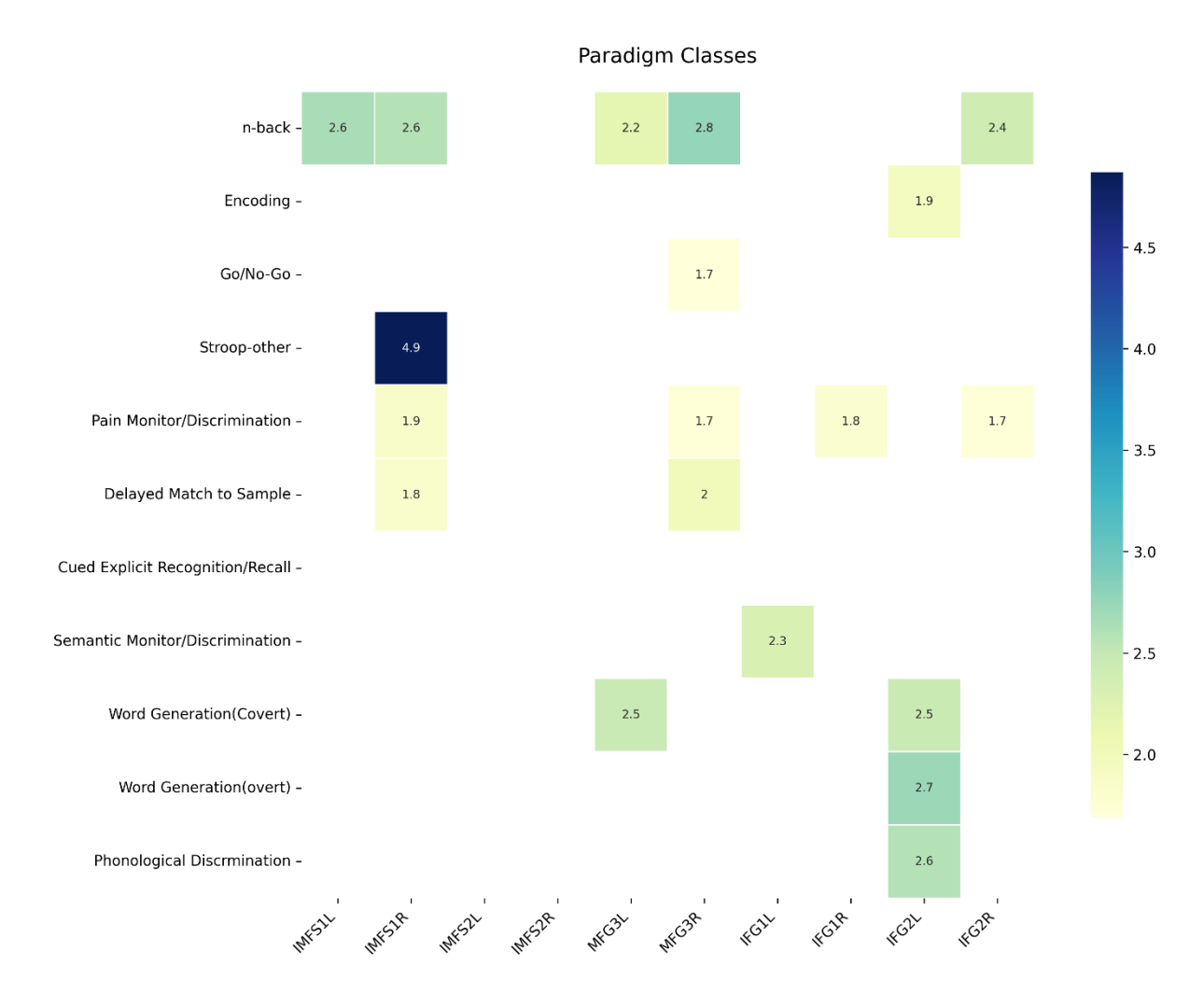


Fig. 27: Paradigm classes associated with areas IMFS1, IMFS2, MFG3, IFG1 and IFG2 of both hemispheres with FDR corrected (p<0.05)

Areas were activated by different paradigm classes as referenced in the BrainMap Database of neuroimaging studies. Converging results of both forward and reverse inference are represented by colored squares per hemisphere (p<0.05, FDR corrected). The colored squares with numbers represent the likelihood ratio. Darker colors indicate a higher likelihood ratio, and vice versa.

4 Discussion

This study identified five new cytoarchitectonically distinct areas (IMFS1, IMFS2, MFG3, IFG1, and IFG2) within the anterior lateral prefrontal cortex, extending the previous research of our group on mapping the frontal lobe using the observer-independent mapping method. This approach was used to map the new areas in a reproducible, quantifiable way based on statistical tests, resolving differences in architectonic definitions by different investigators found in classical maps. All areas were verified in both hemispheres of the anterior lateral prefrontal cortex, covering the region from the intermediate frontal sulcus to the horizontal ramus of the lateral fissure. This mapped region is adjacent to the previously mapped DLPFC areas (e.g., MFG1, MFG2, MFG4, and MFG5) of our research group (Bruno et al. 2022, Bruno et al. 2024). All five newly defined five areas replace previously unexplored gaps, the "GapMap Frontal-I" and dorsal part of "GapMap Frontal-to-Temporal-I" of the Julich-Brain Atlas (Amunts 2023). A new nomenclature was introduced to facilitate the localization of these areas, although the precise localization and extent of the new areas varied across individual brains in the 3D surface space. This variability was documented through 3D cytoarchitectonic probability maps constructed in both the ICBM152casym and MNI Colin27 reference spaces. These maps facilitate direct comparisons with results from functional imaging studies, providing a spatial framework for further functional characterization of this region. Functional analysis using MACM was performed as a first step in this direction, and to provide a preliminary understanding of the possible functions associated with each area.

4.1 The newly defined five areas in the context of previous cytoarchitectonic maps

As shown above, the localization and extent of areas varied significantly between previous cytoarchitectonic maps. The present study provides the three-dimensional probability maps in reference spaces, offering a finer subdivision of the human anterior lateral prefrontal cortex based on reliable and reproducible quantitative image analysis, which are improvement over former microstructural maps.

4.1.1 Comparison with the map of Petrides and Pandya

The cytoarchitectonic maps of Petrides and Pandya (1999) represent the most recent complete microstructural map of the dorsolateral prefrontal cortex; therefore, we focused on comparing our newly defined areas with this parcellation. In the cytoarchitectonic parcellation of Petrides and Pandya (1999), area 46 was primarily located on the middle frontal sulcus and the middle part of the middle frontal gyrus. It exhibited a uniform appearance with medium-sized pyramidal cells in layer III and a well-developed, broad layer IV. Layers V and VI lack large pyramidal cells. Area 9 covered the surface of the superior frontal gyrus, with large pyramidal cells in deep layer III and a poorly developed layer IV. Area 9/46 occupied the remainder of the middle frontal gyrus and could be divided into dorsal and ventral parts. The main cytoarchitecture features were large cells in deeper layer III and a well-developed layer IV (Petrides and Pandya 1999). A slight difference exists between the dorsal and ventral part of 9/46. The large pyramidal cells in the lower part of layer III were less densely packed, and layer IV was thinner in 9/46d compared with 9/46v. Area 10, which occupied the frontal pole, had an overall pale appearance with small- to medium-sized pyramidal cells in layer III, and layer IV was less developed compared to area 46 and 9/46. Area 47/12 covered the ventral most portion of the ventrolateral frontal region and extended as far as the lateral orbital sulcus. In area 47/12, layer III contained small and medium pyramidal cells in its upper part, and medium to somewhat larger pyramidal neurons in its lower part; layer IV was not as broad as in area 45, while the infragranular layers were more prominent than those of adjacent areas (Petrides and Pandya 2002). Compared to the newly defined areas, there were both differences and similarities. Area IMFS1 was primarily located in the depth of the intermediate frontal sulcus and partially extended into the middle frontal gyrus. Its cytoarchitectonic features were similar to area 46 while, although its localization

differed from that of area 46 in Petrides and Pandya (Petrides and Pandya 1999). Meanwhile, area MFG3 covered most of the middle frontal gyrus, with considerably large cells in deeper layer III and a well-developed layer IV, which corresponded to the cytoarchitecture and extent of area 9/46. Area IMFS2 was also situated in the depth of intermediate frontal sulcus, ventral to IMFS1. It exhibited a loosely packed layer III with medium to large pyramidal cells and a thinner layer IV. IMFS2's cytoarchitecture is similar to that of area 47/12.

Furthermore, areas IFG1 and IFG2 were located ventral to MFG3 and covered the anterior part of the inferior frontal gyrus. Area IFG2 was primarily characterized by densely arranged medium-sized cells in layer III, a well-defined layer IV, and a high cell density in layer VI. The localization of IFG2 corresponds to that of area 47/12, but there are slight differences in cytoarchitecture between the two, such as smaller cell sizes in deeper layer III of IFG2 compared to area 47/12. Area IFG1 was ventral to IFG2 and extended caudally to the hs, corresponding to part of area 47/12 in the maps of Petrides and Pandya (Petrides and Pandya 1999). However, the layer IV of IFG1 was thinner than that of area 47/12. Both IFG1 and IFG2 aligned with the position of area 47/12, but their microstructural differences were consistent with the description that layer IV was less developed in the more orbital part of area 47/12 compared to the more lateral part, as described by Petrides and Pandya (Petrides and Pandya 2002). Moreover, Brodmann (Brodmann 1909), Sarkissov et al. (Sarkissov et al. 1955), and Kononova (Kononova 1935) all indicated that the region designated as 47 or 47/12 is heterogenous and can be subdivided, with IFG1 and IFG2 possibly representing subdivision of this region.

4.1.2 Comparison with other classical maps

We also compared the maps in the present study with other historical maps. Based on the localization, areas IMFS1 and MFG3 are largely aligned with BA46 in Brodmann's map (1909); area IFG1 corresponds to BA47, while area IFG2 may be positioned in the ventral part of BA46 and BA10, with a portion connecting to BA47 (Brodmann 1909). However, because Brodmann's map is a schematic and two-dimensional, without accounting for deep sulci, direct comparison based solely on localization is not suitable, especially considering that almost 60-70% of the human cerebral cortex is buried in sulci (Willbrand et al 2024). For example, area IMFS2 was located in the depth of intermediate frontal sulcus and extended caudally. It does not correspond to any areas of Brodmann's areas but lies underneath and is covered by BA46. Furthermore, the cytoarchitecture of area IMFS2 does not exhibit characteristic corresponding to BA10 or BA46. These observations are consistent with those described in the maps of Sarkissov et al. (Sarkissov et al. 1955).

In the maps of Sarkissov et al. and Kononova, field 47 was divided into 5 formations, and these subdivisions differed in shape, extent, and microstructure. It formed the lower surface of the inferior frontal gyrus, extending downward from the hs and bordered anteriorly by area 45, which significantly differed from this region in Petrides and Pandya's map (Kononova 1935, Sarkissov et al. 1955, Petrides and Pandya 2002). The descriptions of region 47 are similar in both of these maps. Area 47⁵ was the lateral part of area 47, and the largest in extent, directly neighboring area 45. Area 47⁴ was ventral to 47⁵ and extended to the orbital surface.

In the map of Kononova, areas 47⁴ and 47⁵, along with area 45, sometimes extended to the anterior borders of the inferior frontal sulcus (Kononova 1938). Area 47⁵ exhibited radial striation with a large number of medium-sized cells, with almost no large cells in layers III, V, VI. Layer IV very well developed with a rich concentration of cells, and its borders with layer III and V were indistinct. Layer V was narrow, with the deeper part being brighter, while layer VI was wide and densely populated with medium-sized cells. The newly defined area IFG2 shared a similar cytoarchitecture with area 47⁵, although the localization of IFG2 was dorsal to hs, which distinguished it from area 47⁵. The most prominent characteristic of area 47⁴ was the large cells in the lower parts of layers III and V. Layer VI contained fewer cells in area 47⁴ than in area 47⁵. According to cytoarchitecture, area IFG1 showed a high similarity to area 47⁴. However, area IFG1 extended considerably into the depth of the hs, which lead to a

misalignment in the positions of areas IFG1 and 47⁴. The reason for this misalignment between the newly defined areas and previous maps could be due to individual variability and the complexity of the sulcus pattern in this region.

In previous studies conducted by our research group, nine cytoarchitectonic areas within the DLPFC (i.e., SFS1, SFS2, MFG1, MFG2, SFG2, SFG3, SFG4, MFG4, and MFG5) were identified using the reliable and reproducible cytoarchitectonic mapping approach. These areas correspond to parts of Brodmann area 9 and 46 (Bruno et al. 2022, Bruno et al. 2024). Areas MFG1, MFG2, MFG4, and MFG5 neighbor to the newly defined areas dorsally, and together, they form a finely parcellated DLPFC. Additional cytoarchitectonic subdivisions in the prefrontal cortex have been delineated, including the two frontal pole areas (Fp1 and Fp2), which align with Brodmann area 10 (Bludau et al. 2014), and four lateral orbitofrontal cortex (Fo4, Fo5, Fo6, and Fo7) (Wojtasik et al. 2020), which correspond to subdivisions of area 47/12 as described by Öngür et al.(Öngür et al 2003). Further detailed cytoarchitectonic parcellations, such as the subdivisions of Broca's area 44 and 45 based on the work of Amunts et al. (Amunts et al. 1999) have yet to be published. While some newly defined areas in the present study share similar cytoarchitectonic characteristics and may correspond to the same regions in earlier maps - for instance, MFG2 and IMFS1 align with BA46, while MFG3 and MFG5 align with the transitional area 46/9 - they remain distinguishable. Therefore, these studies, including the present work, contribute to a more precise, probabilistic map of the entire prefrontal cortex, addressing the interindividual variability in different brains.

4.1.3 Interpretation of the cluster analysis results

The discriminant analysis showed some overlaps between the newly defined five areas, but they can still be separated from each other. Cluster analysis demonstrated that the five new areas in the anterior prefrontal cortex were cytoarchitectonically similar to the lateral orbitofrontal cortex Fo5 and Fo6, as well as other anterior prefrontal cortex areas mfg5, than to areas of Broca's region or the frontal pole areas Fp1. In detail, IMFS1 clustered with Fo5, and MFG3 clustered with mfg5. Areas IMFS1, IMFS2, and IFG2 shared cytoarchitectural similarity with Fo5 and Fo6, while IFG1 and MFG3 showed similar cytoarchitecture to mfg5. Interestingly, Wojtasik et al. reported that the left Fo5 is associated with reward processing, language phonology, as well as working and explicit memory (Wojtasik et al. 2020) – functions

that overlap with the left IMFS1, which is also involved with working and explicit memory. Similarly, the right Fo5 is involved in explicit memory and perceptual pain, aligning with the right IMFS1 in terms of perceptual pain processing. The left Fo6 plays a role in the language semantics processing and negative emotional responses (e.g., disgust and anger), whereas the right Fo6 is involved in action inhibition and perceptual pain, the latter of which overlaps with the right IMFS1. Notably, IFG2 shares the same function with Fo5 on the left hemisphere, detailed in language phonology, while IMFS2 has no functional overlap with Fo6 despite their cytoarchitectonic closeness.

Moreover, findings from our research group indicate that MFG5 is related to behavioural control, working memory, and verbal input process (Bruno et al. 2024), partially overlapping with the functional role of MFG3, particularly in working memory. In contrast, IFG1 does not share any functional overlap with mfg5. Overall, cytoarchitectonically clustered areas or adjacent areas tend to share some common functions, suggesting potential correlations between structural organization and functional specialization. Further more functional interpretation will be described in Chapter 4.3. Combining our previous delineation work (Amunts et al. 2022), these results demonstrated that a comparably detailed microstructural parcellation of the lateral prefrontal existed. It is also reasonable to assume the existence of the functional segregation within this region.

4.2 Variability in brains

4.2.1 Sulcal variability

In humans, almost two-thirds of the neocortex are hidden away within the depths of the sulci (Braak 2012). Individual sulci exhibit considerable intersubject variability, and many sulci show one or several interruptions (Nieuwenhuys et al. 2008).

In the present study, the sulcal pattern not only varied among individuals but also differed between hemispheres within the same individual. Other studies, such as those by Ono et al. (Ono et al. 1990) and Willbrand et al. (Willbrand et al. 2024), have also reported the high variability in the sulcal pattern of the lateral prefrontal cortex across individuals and hemispheres, particularly the intermediate frontal sulcus and inferior frontal sulcus. Amiez et al. identified a sulcus, which they attributed to the intermediate frontomarginal sulcus (ifms), located ventral to the previous defined imfs-v, as part of vertical ramus of the intermediate frontal sulcus (Amiez et al. 2023). This variability further complicates the sulcal pattern, highlighting its intricate nature.

Moreover, in Willbrand et al.'s study, the dorsal and ventral components of the paraintermediate frontal sulcus (pimfs-d and pimfs-v) are functionally (Willbrand et al 2023). The pimfs-v is a key developmental, cognitive, and evolutionarily relevant feature that should be considered in future research investigating how the complex interactions among multiscale anatomical and functional properties of the brain contribute to abstract thought. Additionally, the pimfs exhibits substantial variability, which has been linked to individual differences in relational reasoning performance across various age groups (Willbrand et al. 2024). This leads us to the presence or absence of specific sulci or sulcal features may induce changes in gray or white matter, potentially forming the basis of cognitive process. This strong association between sulcal pattern variability and the corresponding functional organization may help explain the uniqueness of the human brain.

4.2.2 Volumetric variability

We noticed that the extent, volumes, and shape of the five newly defined areas varied considerably between brains and even hemispheres within the same brain even though

statistical comparisons of volumes between hemispheres and genders revealed no significant differences.

For example, the volume of area IFG2 on the right hemisphere seems larger than other areas within BC04. This can be explained by the extensive inferior frontal gyrus in the right hemisphere, which spanned from the as to the lateral orbital sulcus. In this hemisphere, the pars triangularis comprises two gyri, separated by the triangular sulcus and another deep sulcus; the latter extended ventrally to dorsally and directly connected to the posterior intermediate frontal sulcus. Additionally, the hs in this brain was deep and extends dorsally, merging directly with the intermediate frontal sulcus. Consequently, the dorsal part of the inferior frontal gyrus and the middle frontal gyrus were partially merged. The gyri rostral to the hs, corresponding to the pars orbitalis in the right hemisphere, were also larger and more complex compared to those in other brains. This unique structural organization of the ifg and sulcal pattern in the right hemisphere of BC04 likely accounts for the large volume of IFG2 in this region. Furthermore, the increased extent of the ifg and its partial fusion with the anterior mfg in the right hemisphere could explain why MFG3 also occupies a larger volume. The gyrus and sulcus pattern in the left hemisphere of BC04 was similar to that of the right hemisphere but still exhibited notable differences. While the ifg was relatively smaller, the region merged with the mfg remains substantial, contributing to the large volume of MFG3. Thus, both hemispheres of BC04 exhibited a combination of shared features and volumetric asymmetries. Other areas volumes also showed high variability between different brains, primarily due to anatomical differences in sulci (i.e., imfs, hs) and gyri (i.e., ifg and mfg). These findings support our previous conclusion that the volumes of these areas exhibit high variability, with asymmetries between hemispheres and a strong association between volumetric variability and anatomical topography.

Brain asymmetries are significant and should be considered even they might be subtle. Like individual variability, asymmetries are essential for evolution (Kuo and Massoud 2022). In humans and many other mammals, the two brain hemispheres exhibit varying degrees of structural and functional asymmetry. Hemisphere asymmetries are a fundamental aspect of nervous system architecture. The left hemisphere plays a crucial role in the cognitive systems prevalence of propositional and conscious processing modes (Ocklenburg et al 2016), while the right side characterize emotional system prevalence of automatic and unconscious

processing modalities (Gainotti 2024). The discussion of functional asymmetry will be discussed in a later chapter.

The hemispheric specialization was thought to arise from evolutionary, developmental, genetic, experiential, and pathological influences (Toga and Thompson 2003). Volumetric asymmetry of the inferior frontal region has been reported by Jernigan et al. (Jernigan et al 1991). The present study also suggest that the inferior frontal gyrus areas differ in volumes between hemispheres within the same brain. Another study analyzing cortical volume asymmetries, particularly in relation to cortical thickness, indicated a greater right-sided thickness in the inferior frontal gyrus (Luders et al 2006). Other studies have also demonstrated these asymmetries. For instance, significant asymmetries have been found in the distribution of gray and white matter in the frontal lobes (Good et al 2001), and the right frontal lobe extends further anteriorly than the left (Duboc et al 2015). A sex-specific effect on surface area asymmetry was observed, particularly within the frontal lobe, including the superior frontal gyrus and pars orbitalis of the left inferior frontal gyrus (Kong et al 2018). However, in our investigation, the sex did not have a significant effect on the volumetric differences between corresponding regions of the two hemispheres.

Altered hemispheric lateralization has been associated with various cognitive and neuropsychiatric disorders, including attention-deficit/hyperactivity disorder (ADHD), autism, and mood disorders (Kong et al. 2018). Therefore, recognition morphological differences between the hemisphere is crucial, as these differences may influence functional specialization, which will be discussed in the following section.

4.3 Structural-Functional properties of areas IMFS1, IMFS2, MFG3, IFG1 and IFG2

The cytoarchitectonic maps in the present study provided a spatial reference framework, enabling the localization of activation in functional imaging studies with respect to cytoarchitectonic areas. The MACM results indicated possible functional roles of the newly defined areas. Most of the associated functions are related to cognitive functions, emotions, perceptions, and language. Functional laterization was also observed between hemispheres for each area. Although many of these functional asymmetries are linked to language (Kuo and Massoud 2022), it is evident that such asymmetries extend beyond language, influencing other cognitive functions as well.

4.3.1 Relationship of structure and function of areas IMFS1, IMFS2, MFG3, IFG1 and IFG2

According to the MACM analysis results, area IMFS1 was primarily involved in cognitive functions, including working memory, explicit memory, action inhibition, and perceptual pain processing. Its activation has been observed in tasks related to cognitive control and sensory processing, such as the n-back task (working memory), the Stroop task (cognitive interference control), the DMTS task (short-term memory and recognition), and pain discrimination (sensory processing and evaluation). As discussed above in the section on the interpretation of the newly defined five areas in the context of previous cytoarchitectonic maps, area IMFS1 roughly aligns with part of areas 46 in the maps of Petrides and Pandya (Petrides and Pandya 1999) and Brodmann (Brodmann 1909). A group of studies focusing on the common function of area 46 indicated that this area was primarily involved in processing cognitive information, especially working memory (Rowe and Passingham 2001), attention (Lau et al 2004), task switching (Sohn et al 2000, Kim et al 2012), and planning (Tanji and Hoshi 2001, Nitschke et al 2017). BA46 was also activated during the suppression of eye movements to particular locations, and patients with lesions in the lateral prefrontal cortex, especially BA46, may exhibit a decreased ability to perform reflexive saccades (Ridderinkhof et al 2004). Given the potential functional heterogeneity within BA46 (Jung et al 2022), the cytoarchitecture and localization of area IMFS1 in the present study align with the anterior part of BA46, situated near BA10 and BA9. This anatomical positioning may explain its strong association with the working memory network. However, some functions that area IMFS1 could be associated with, such as action inhibition and perceptual pain, are not entirely consistent with the

functions of BA46 found in previous research. This discrepancy could be explained by: (1) most of area IMFS1 being located at the depth of the intermediate frontal sulcus, where its specific localization was not well represented in previous classical maps, which failed to reflect the deep sulcus pattern accurately, and (2) high variability between individual brains, which may result in extensive changes to the coordinates used in the MACM analysis.

Before FDR correction, the BD of area IMFS2 in both hemispheres were primarily associated with working memory and explicit memory, and this association was observed in both hemispheres. However, after FDR correction, these two BDs (working memory and explicit memory) in both hemispheres of area IMFS2 were no longer statistically significant, and only the perceptual pain function remained significant for the left IMFS2. The left hemisphere of area IMFS2 was activated during n-back tasks (working memory), explicit memory tasks, and recall tasks, while the right hemisphere of area IMFS2 was involved in other tasks, such as task switching and the affective picture experiment (prior FDR correction). The BD and PC of area IMFS2 exhibited similar function to BA46, including tasking switching and working memory, which could be due to the localization of IMFS2 being ventral to area IMFS1 and situated beneath and overlapping with BA46.

Area IMFS2 was also located at the depth of the intermediate frontal sulcus, which exhibited a similar cytoarchitecture to area 47/12 in the map of Petrides and Pandya (Petrides and Pandya 1999), while its localization did not correspond to any of Brodmann's areas. As the main associated function of the left IMFS2 was perceptual pain, and considering the similar microstructure between IMFS2 and area 47, studies had shown a relative increase in activity in the BA47 region when perceptual pain was modulated (Rainville et al 1997, Rainville et al 1999, Petrovic et al 2000, Villemure and Bushnell 2009). This may explain the specific functions related to the left IMFS2. The affective pictures experiment is used to study the emotional processing and has provided insights into the dimensional aspects of emotion, including anger, disgust, fear, sadness, and enjoyment (Mikels et al 2005). Several studies have demonstrated that BA47, or area 47/12, has a strong relationship with emotional processing, with reduced activation observed on the right side of the brain or bilaterally in patients with mania (Öngür and Price 2000, Badre and Wagner 2007, Uylings et al. 2010, Chen et al 2011). The right hemisphere of area IMFS2 was activated during the affective picture experiments (which was used in emotional processing), consistent with some of the functions

of area 47/12. However, although the cytoarchitecture and emotion-related functions of area IMFS2 were similar to area 47/12, the number of experiments included for MACM analysis of area IMFS2 was fewer than for other areas, particularly as no significance was found regarding the emotional function (affective pictures experiment) after FDR correction. More detailed experiments for this area need to be performed in future neuroimaging research.

In the left hemisphere, area MFG3 showed a predominant involvement in working memory, as evidenced by its activation during n-back tasks. In contrast, the right hemisphere of MFG3 displayed a multifunctional role, encompassing: (1) emotional processing, particularly of negative emotional states (e.g., anxiety-related responses); (2) pain processing, including perceptual pain and the discrimination of pain stimuli; (3) cognitive-behavioural regulation, which involves the inhibitory control of prepotent responses and modulation of impulsivity, supported by its engagement in cognitive control tasks (e.g., Go/No-Go) and delayed matchto-sample paradigms.

The area MFG3 may align with area 9/46 in the map of Petrides and Pandya (Petrides and Pandya 1999), and both of these two areas align with BA46 in Brodmann's map (Brodmann 1909), as discussed above. Several functional studies support this structural alignment. For example, the functional similarity between area MFG3 and BA46, as well as area 9/46, has been clearly demonstrated in previous studies, such as those on the working memory process (Petrides 1996). Townsend et al. indicated that the right area 9/46 showed significantly reduced activation in the bipolar subjects compared to control subjects (Townsend et al 2010). Another study using resting-state functional near-infrared spectroscopy (rs-fNIRS) demonstrated that BA46 was involved in the processing and modulation of pain signaling, with no hemisphere laterization observed (Luo et al 2024). Zheng et al. reported that BA46 in the right hemisphere showed significant correlations with the response inhibition process in the Go/No-Go and stop signals tasks (Zheng et al 2008), which was similar to the findings of Gondo et al., who used PET (Gondo et al 2000). Additionally, another study indicated that only the right hemisphere of BA46 showed activation in the DMTS experiment (Daniel et al 2016).

Area MFG3 in the left hemisphere was also activated by covert word generation paradigms. Its relationship with BA46 can be explained by the fact that BA46 is also activated in tasks involving the generation of words (Frith et al 1991). Therefore, the anatomical and functional

parcellation of area MFG3 aligns well with BA46 in the present study, even though discrepancies exist.

According to the description in above chapter 4.1, both IFG1 and IFG2 align with BA47 in Brodmann's map and area 47/12 in the map of Petrides and Pandya (Petrides and Pandya 1999). BA47, or area 47/12, has been implicated in various functions across multiple neuroimaging studies. Recent functional studies have demonstrated that left BA47 is involved in various language functions, including language comprehension (Turken and Dronkers 2011), semantic retrieval (Zhang et al 2004), encoding (Li et al 2000, Ardila et al 2017), phonological processing (McDermott et al 2003, De Carli et al 2007), grammatical processing (Ardila et al. 2017), syntactic processing (Tyler et al 2011), and selective attention to speech (Vorobyev et al 2004). BA47 has also been observed to play a role not only in language process but also in other domains, such as working memory (Friederici 2002), logical reasoning (Goel et al 1998), response inhibition (Deng et al 2017), and reward-punishment learning and decision-making (Elliott et al 2000, Rubinsztein et al 2001). In the present study, areas IFG1 and IFG2 in the left hemisphere were involved not only in language process but also exhibited distinct functional sub-specializations. Specifically, IFG1 was primarily engaged in semantic processing, whereas IFG2 contributed to phonological/orthographic decoding and word generation. Notably, left IFG2 showed additional involvement in cognitive memory systems and information encoding mechanisms, while right IFG2 was associated with logical reasoning and working memory process. These functions align with those described above for area 47/12.

A group of studies have demonstrated that BA47, or area 47/12, contributed to emotional processing on the right side of the brain or bilaterally in the patients with mania or bipolar depression (Öngür and Price 2000, Badre and Wagner 2007, Altshuler et al 2008, Uylings et al. 2010, Chen et al. 2011), and that BA47 is involved in general mechanisms underlying the evaluation of emotion (Lee and Siegle 2012). Interestingly, both the right hemisphere of IFG1 and IFG2 showed preferential engagement in negative emotional processing (e.g., anxiety, disgust), which closely resembled the activity observed in area 47/12.

In the present study, the right IFG1 was also involved in interoceptive awareness. A study has reported that inferior frontal gyrus, along with the anterior insula and frontal operculum, forms a node of the saliency network for interoceptive input (Engelen et al 2023), suggesting that IFG1 could be the corresponding region; however, this study did not specify a particular

region of the inferior frontal gyrus associated with this interoceptive function. Moreover, the right IFG1 was also related to perceptual pain recognition and the discrimination of pain stimuli. Coen et al. indicated that BA47 was activated, lateralized to the right hemisphere, during painful stimulation (Coen et al 2009), indicating a deeper relationship between IFG1 and area 47/12.

These functional alignments between BA47 or area 47/12 and the research areas (IFG1, IFG2) in the present study further support the possibility that IFG1 and IFG2 may be subregions of BA47. At the same time, the present study revealed functional differences between these two areas, which not only validate the plausibility of our microstructural and functional subdivision results but also provide new evidence for their distinct functions.

Beyond the former discussion in Chapter 4.1.3, other examples might also support potential relationships between structure organization and functional specialization. For example, both IFG1 and MFG3 in the right hemisphere were involved in perceptual pain processing and negative emotions (e.g., anxiety), despite each having distinct functional associations. Notably, these two areas were also cytoarchitectonically close, as indicated by the cluster analysis. The observation supports the hypothesis that structural similarity may contribute to functional similarity (Sebenius et al 2024). However, another pair of cytoarchitectonically similar areas, IMFS2 and IFG2, did not exhibit any statistically significant functional overlap. This suggests that while structural architecture may constrain functional organization (Park and Friston 2013), it does not fully determine it. Indeed, although functional networks are influenced by anatomical connections, the precise extent to which structural features shape function remains unclear (Honey et al 2010). Studies on neural connectivity indicate that functional connectivity cannot be solely explained by anatomical substrate (Batista-García-Ramó and Fernández-Verdecia 2018). A comprehensive understanding of human brain function requires a detailed elucidation of its structural organization. Future investigations integrating anatomical and physiological studies, particularly those examining neuronal circuits and connections, are essential to delineate the fundamental principles governing cortical and functional connectivity (Sporns and Zwi 2004). Thus, while cytoarchitectonic similarity may contribute to functional resemblance, it does not unequivocally determine it.

4.3.2 Functional lateralization

It is easily noticeable that the functional profiles of areas IMFS1, IMFS2, MFG3, IFG1, and IFG2 exhibit distinct hemispheric lateralization. For instance, the most prominent functional lateralization was observed in language-related functions in the left hemisphere and emotional processing on the opposite side for areas IFG1 and IFG2.

In the history of neuroscience, functional segregation has been discussed since the 19th century, and the view that the two hemispheres of the human brain evolved to specialize in certain cognitive and behavioural functions has been widely accepted (Hugdahl 2000), especially with the development of brain imaging techniques, such as PET and fMRI (Nitschke et al. 2017). Broca's areas, corresponding to Brodmann's area 44 (pars opercularis of the left inferior frontal gyrus) and 45 (pars triangularis), serve as classical examples of language functions lateralization (Foundas et al 1996, Amunts et al. 1999), with the majority of this lateralization occurring in the left hemisphere of the brain. In some cases, language lateralization occurs in the right hemisphere, regardless of handedness (Knecht et al 2000, Wang et al 2019).

Anatomical asymmetries, such as larger left planum temporale and Broca's area compared to their right hemisphere counterparts, have been associated with certain aspects of language lateralization (Foundas 2001, Toga and Thompson 2003, Maingault et al 2016). However, Greve et al., using an automated surface-based technique to measure gray matter volume asymmetries, reported no significant volumetric differences in the pars opercularis and pars triangularis between participants with left- and right - hemisphere language dominance (Greve et al 2013). Two inferior frontal gyrus areas (IFG1 and IFG2) were primarily located in the anterior inferior frontal gyrus and exhibited a preference for language functions in the left hemisphere. Nevertheless, their volumetric comparisons between hemispheres did not reach statistical significance. These findings point to the necessity of larger samples to clarify the relationships of language lateralization and anatomical asymmetries.

In the right hemisphere, IFG1 and IFG2 demonstrated lateralization for emotional functions rather than language functions. The right hemisphere is known to dominate emotional processing (Coen et al. 2009). This was supported by a number of behavioural studies indicating that emotional processing was primarily associated with the left-side sensory inputs in healthy humans (Sackeim et al 1978, Levine and Levy 1986, Erhan et al 1998).

However, Wager et al. reported that the right-lateralization of emotional function was not strongly supported in their 65 neuroimaging studies on emotion (Wager et al 2003). Several other studies also failed to find evidence of emotional lateralization (Mammucari et al 1988, Caltagirone et al 1989, Mandal et al 1992, Kowner 1995). Given that the sample sizes in these studies were relatively small, their findings require further validation. In contrast, the current study, which involved a significantly larger sample, provides stronger evidence for right-hemisphere dominance in emotional processing.

The mechanisms underlying functional lateralization remain debated (Hopkins and Cantalupo 2008). One hypothesis is inter-hemispheric independence, suggesting that as the brain increased in size during evolution, functional lateralization developed to reduce excessive conduction delays between the hemispheres (Ringo et al 1994). According to this view, to optimize processing efficiency, regions exhibiting functional lateralization would be less strongly connected via the corpus callosum compared to non-lateralized regions (Markov et al 2013). Another hypothesis posits inter-hemispheric competition between lateralized regions in opposite hemispheres. It suggests that lateralized regions must inhibit one another via corpus callosum in order to establish more efficient connections (Karolis et al 2019). While these two hypotheses may partially explain the mechanism behind functional lateralization, a clear understanding of the underlying mechanisms remains elusive, as the brain functions as a whole.

Moreover, the brain is not only functionally specialized along the lateral axis between hemispheres, but also along the longitudinal axis. The latter is organized such that the frontal lobe serves as the site for complex "executive" functions, the temporal lobe is associated with memory functions, and the posterior parietal lobe is involved in attention processes (Hugdahl 2000).

As a concluding mark, there are limitations to this study. Firstly, while the meta-analytic approach has summarized thousands of task-related neuroimaging experiments, it remains limited because real-world behaviours are more complex and richer than in-scanner tasks. Secondly, the studies included in the meta-analytic lacked homogeneity in terms of tasks types, methods, and participant characteristics. For example, the experimental paradigms used to probe brain function may have systematically employed the same or similar material, which could have biased some of the asymmetries reported. Finally, the connectivity within

the newly defined areas, as well as their interactions with other brain regions, remains poorly understood. To better elucidate the functions of these areas, further investigation is required to examine the co-activation patterns within these areas and with other brain structures. This is critical, as these newly defined areas play a vital role in the cognitive functions of the human brain.

5 Conclusion

The newly defined five areas (IMFS1, IMFS2, MFG3, IFG1, and IFG2) were identified using an observer-independent approach in both hemispheres of ten post-mortem human brains. All of these areas were granular, yet they could be differentiated based on their distinct cytoarchitectonic characteristics. They were bordered by the previously mapped cytoarchitectonic regions delineated by our research group, including Fp1 rostrally; MFG1 and MFG2 dorsally; Fo5 and Fo6 ventrally; and MFG5, MFG4, and area 45 caudally. This anatomical context allowed for a more comprehensive characterization of the structural and functional organization of the lateral prefrontal cortex. The probability maps of these new areas demonstrated considerable interindividual variability while preserving high spatial precision. The resulting maximum probability maps helped resolve discrepancies in localization, areal extent of, and nomenclature observed in previous studies, thereby addressing limitations of earlier maps.

The functional profiles of these five new areas were characterized using the MACM analysis, revealing a diverse range of associations predominantly involving cognitive functions, language processing, perception, and emotional processing. IMFS1 was primarily associated with working memory, perceptual pain, and color perception. IMFS2 showed a strong association with perceptual pain. MFG3 was mainly linked to working memory, action inhibition, and negative emotional processing, particularly anxiety. The two inferior frontal areas, IFG1 and IFG2, exhibited a consistent pattern of hemispheric lateralization: both were associated with language related functions in the left hemisphere and emotional processing in the right hemisphere. Notably, right IFG1 was also involved in interoception awareness, indicating a potentially unique functional specialization.

The cytoarchitectonic maps of the five identified areas may serve as reference data for further integration with more explicit functional decoding, genetic brain architecture, and a more precise delineation to complement the functional parcellations (Dadi et al. 2020). These maps provide a structural-functional framework that could be valuable for the future neurosurgical procedures. For example, integrating the altas with functional imaging technologies (e.g., fMRI) into neuronavigation systems could potentially support the identification of individual anatomical variations, which may contribute to a more accurate localization of language-

related and executive subregions. This could, in turn, assist in refining resection boundaries for tumors or epileptic foci, potentially minimizing intraoperative functional risks.

These maps will be publicly available as part of the Julich Brain Cytoarchitectonic Atlas (https://julich-brain-atlas.de/) and the HBP Atlas, which are included within EBRAINS (https://ebrains.eu/services/human-brain-atlas).

6 References

Abutalebi, J., et al (2009). "Bilingual aphasia and language control: A follow-up fMRI and intrinsic connectivity study." <u>Brain and Language</u> **109**(2-3): 141-156.

Ahmari, S. E. and S. L. Rauch (2022). "The prefrontal cortex and OCD." <u>Neuropsychopharmacology</u> **47**(1): 211-224.

Altshuler, L., et al (2008). "Regional brain changes in bipolar I depression: a functional magnetic resonance imaging study." <u>Bipolar disorders</u> **10**(6): 708-717.

Amiez, C., et al (2023). "A revised perspective on the evolution of the lateral frontal cortex in primates." <u>Science Advances</u> **9**(20): eadf9445.

Amunts, K., et al (2007). "Gender-specific left-right asymmetries in human visual cortex." <u>Journal of Neuroscience</u> **27**(6): 1356-1364.

Amunts, K., et al (2022). "EBRAINS-Whole-brain parcellation of the Julich-Brain Cytoarchitectonic Atlas (v2. 9)." DOI: https://doi. org/10.25493/VSMK-H94. https://search. kg. ebrains.

eu/instances/Dataset/a8932c7e-063c-4131-ab96-996d843998e9. Zugegriffen 7.

Amunts, K., et al (2020). "Julich-Brain: A 3D probabilistic atlas of the human brain's cytoarchitecture." <u>Science</u> **369**(6506): 988-+.

Amunts, K., Mohlberg, H., Bludau, S., Caspers, S., Lewis, L. B., Eickhoff, S. B., & Pieperhoff, P. (2023). "Julich-Brain Atlas, cytoarchitectonic maps (v3.1) [Data set]."

Amunts, K., et al (1999). "Broca's region revisited: Cytoarchitecture and intersubject variability." <u>Journal of Comparative Neurology</u> **412**(2): 319-341.

Amunts, K., et al (2007). "Cytoarchitecture of the cerebral cortex—more than localization." Neuroimage **37**(4): 1061-1065.

Amunts, K., et al (2004). "Analysis of neural mechanisms underlying verbal fluency in cytoarchitectonically defined stereotaxic space—the roles of Brodmann areas 44 and 45." Neuroimage **22**(1): 42-56.

Amunts, K. and K. Zilles (2015). "Architectonic mapping of the human brain beyond Brodmann." Neuron **88**: 1086-1107.

Ardila, A., et al (2017). "Should Broca's area include Brodmann area 47?" <u>Psicothema</u> **29**(1): 73-77. Badre, D. and A. D. Wagner (2007). "Left ventrolateral prefrontal cortex and the cognitive control of memory." <u>Neuropsychologia</u> **45**(13): 2883-2901.

Bailey, P. (1951). "The isocortex of man." Urbana 3.

Batista-García-Ramó, K. and C. I. Fernández-Verdecia (2018). "What we know about the brain structure—function relationship." Behavioral Sciences **8**(4): 39.

Beck, E. (1949). "A cytoarchitectural investigation into the boundaries of cortical areas 13 and 14 in the human brain." <u>Journal of Anatomy</u> **83**(Pt 2): 147.

Behrens, T. E., et al (2003). "Non-invasive mapping of connections between human thalamus and cortex using diffusion imaging." <u>Nature Neuroscience</u> **6**(7): 750-757.

Bludau, S., et al (2014). "Cytoarchitecture, probability maps and functions of the human frontal pole." <u>Neuroimage</u> **93**: 260-275.

Bourgeois, J.-P., et al (1994). "Synaptogenesis in the Prefrontal Cortex of Rhesus Monkeys." <u>Cerebral</u> Cortex **4**(1): 78-96.

Braak, H. (2012). <u>Architectonics of the human telencephalic cortex</u>, Springer Science & Business Media.

Brodmann, K. (1909). <u>Vergleichende Lokalisationslehre der Grosshirnrinde in ihren Prinzipien</u> dargestellt auf Grund des Zellenbaues, Barth.

Brody, A. L., et al (2001). <u>Prefrontal-subcortical and limbic circuit mediation of major depressive disorder</u>. Seminars in clinical neuropsychiatry.

Bruno, A., et al (2022). "Cytoarchitecture, intersubject variability, and 3D mapping of four new areas of the human anterior prefrontal cortex." <u>Frontiers in Neuroanatomy</u> **16**.

Bruno, A., et al (2024). "New organizational principles and 3D cytoarchitectonic maps of the dorsolateral prefrontal cortex in the human brain." <u>Frontiers in Neuroimaging</u> **3**.

Bulut, T. (2022). "Meta-analytic connectivity modeling of the left and right inferior frontal gyri." cortex **155**: 107-131.

Caltagirone, C., et al (1989). "Posed emotional expression in unilateral brain damaged patients." cortex **25**(4): 653-663.

Campbell, A. W. (1905). <u>Histological studies on the localisation of cerebral function</u>, University Press.

Carlén, M. (2017). "What constitutes the prefrontal cortex?" Science 358(6362): 478-482.

Catani, M. (2019). "The anatomy of the human frontal lobe." Handb Clin Neurol 163: 95-122.

Chase, H. W., et al (2020). "Functional differentiation in the human ventromedial frontal lobe: a data-driven parcellation." <u>Human Brain Mapping</u> **41**(12): 3266-3283.

Chen, C. H., et al (2011). "A quantitative meta-analysis of fMRI studies in bipolar disorder." <u>Bipolar</u> disorders **13**(1): 1-15.

Coen, S. J., et al (2009). "Negative mood affects brain processing of visceral sensation." <u>Gastroenterology</u> **137**(1): 253-261. e252.

Convit, A., et al (2001). "Volumetric analysis of the pre-frontal regions: findings in aging and schizophrenia." <u>Psychiatry Research: Neuroimaging</u> **107**(2): 61-73.

Costafreda, S. G., et al (2006). "A systematic review and quantitative appraisal of fMRI studies of verbal fluency: role of the left inferior frontal gyrus." Human Brain Mapping **27**(10): 799-810.

Cox, S. R., et al (2014). "A systematic review of brain frontal lobe parcellation techniques in magnetic resonance imaging." <u>Brain Structure and Function</u> **219**: 1-22.

Crespo-Facorro, B., et al (1999). "Human frontal cortex: an MRI-based parcellation method." Neuroimage **10**(5): 500-519.

Dadi, K., et al (2020). "Fine-grain atlases of functional modes for fMRI analysis." <u>Neuroimage</u> **221**: 117126.

Daniel, T. A., et al (2016). "Delayed match-to-sample in working memory: A BrainMap meta-analysis." <u>Biological Psychology</u> **120**: 10-20.

De Carli, D., et al (2007). "Identification of activated regions during a language task." <u>Magnetic</u> resonance imaging **25**(6): 933-938.

Deng, W., et al (2017). "Separate neural systems for behavioral change and for emotional responses to failure during behavioral inhibition." Human Brain Mapping **38**(7): 3527-3537.

Duboc, V., et al (2015). "Asymmetry of the brain: development and implications." <u>Annual review of genetics</u> **49**(1): 647-672.

Eickhoff, S. B., et al (2012). "Activation likelihood estimation meta-analysis revisited." <u>Neuroimage</u> **59**(3): 2349-2361.

Eickhoff, S. B., et al (2010). "Anatomical and functional connectivity of cytoarchitectonic areas within the human parietal operculum." <u>Journal of Neuroscience</u> **30**(18): 6409-6421.

Eickhoff, S. B., et al (2009). "Coordinate-based activation likelihood estimation meta-analysis of neuroimaging data: A random-effects approach based on empirical estimates of spatial uncertainty." Human Brain Mapping **30**(9): 2907-2926.

Eickhoff, S. B., et al (2005). "A new SPM toolbox for combining probabilistic cytoarchitectonic maps and functional imaging data." Neuroimage **25**(4): 1325-1335.

Eickhoff, S. B., et al (2015). "Connectivity-based parcellation: Critique and implications." <u>Human</u> Brain Mapping **36**(12): 4771-4792.

Elliott, R., et al (2000). "Dissociable neural responses in human reward systems." <u>Journal of Neuroscience</u> **20**(16): 6159-6165.

Engelen, T., et al (2023). "Interoceptive rhythms in the brain." <u>Nature Neuroscience</u> **26**(10): 1670-1684.

Erhan, H., et al (1998). "Identification of emotion in a dichotic listening task: event-related brain potential and behavioral findings." <u>Brain and Cognition</u> **37**(2): 286-307.

Evans, A. C., et al (2012). "Brain templates and atlases." Neuroimage 62(2): 911-922.

Flechsig, P. (1927). "Meine Myelogenetische Hirnlehre: Mit Biographischer Einleitung."

Foundas, A. L. (2001). "The anatomical basis of language." <u>Topics in Language Disorders</u> **21**(3): 1-19. Foundas, A. L., et al (1996). "Pars triangularis asymmetry and language dominance." <u>Proceedings of the National Academy of Sciences</u> **93**(2): 719-722.

Fox, P. T. and J. L. Lancaster (2002). "Mapping context and content: the BrainMap model." <u>Nature</u> Reviews Neuroscience **3**(4): 319-321.

Friederici, A. D. (2002). "Towards a neural basis of auditory sentence processing." <u>Trends in cognitive sciences</u> **6**(2): 78-84.

Friederici, A. D., et al (2006). "The brain differentiates human and non-human grammars: Functional localization and structural connectivity." <u>Proceedings of the National Academy of Sciences</u> **103**(7): 2458-2463.

Frith, C. D., et al (1991). "Willed action and the prefrontal cortex in man: a study with PET."

<u>Proceedings of the Royal Society of London. Series B: Biological Sciences</u> **244**(1311): 241-246.

Fuster, J. (2015). The prefrontal cortex, Academic press.

Fuster, J. M. (1988). Prefrontal cortex. <u>Comparative neuroscience and neurobiology</u>, Springer: 107-109.

Fuster, J. M. (2002). "Frontal lobe and cognitive development." <u>Journal of neurocytology</u> **31**(3): 373-385.

Gainotti, G. (2024). "Does the right hemisphere retain functional characteristics typical of the emotional adaptive system? An evolutionary approach to the problem of brain asymmetries." Neuroscience & Biobehavioral Reviews: 105777.

Glasser, M. F., et al (2016). "A multi-modal parcellation of human cerebral cortex." <u>Nature</u> **536**(7615): 171-178.

Goel, V., et al (1998). "Neuroanatomical correlates of human reasoning." <u>Journal of Cognitive</u> Neuroscience **10**(3): 293-302.

Goldstein, A., et al (2025). "A unified acoustic-to-speech-to-language embedding space captures the neural basis of natural language processing in everyday conversations." <u>Nature Human Behaviour</u>: 1-15.

Gondo, Y., et al (2000). "The role of the prefrontal cortex in the go/no-go task in humans: a positron emission tomography study." <u>Japanese psychological research</u> **42**(1): 36-44.

Good, C. D., et al (2001). "A voxel-based morphometric study of ageing in 465 normal adult human brains." Neuroimage **14**(1): 21-36.

Greve, D. N., et al (2013). "A surface-based analysis of language lateralization and cortical asymmetry." <u>Journal of Cognitive Neuroscience</u> **25**(9): 1477-1492.

Haber, S. N., et al (2022). "Prefrontal connectomics: from anatomy to human imaging." Neuropsychopharmacology **47**(1): 20-40.

Hoffstaedter, F., et al (2014). "The role of anterior midcingulate cortex in cognitive motor control." Human Brain Mapping **35**(6): 2741-2753.

Honey, C. J., et al (2010). "Can structure predict function in the human brain?" <u>Neuroimage</u> **52**(3): 766-776.

Hopkins, W. D. and C. Cantalupo (2008). "Theoretical speculations on the evolutionary origins of hemispheric specialization." <u>Current Directions in Psychological Science</u> **17**(3): 233-237.

Hugdahl, K. (2000). "Lateralization of cognitive processes in the brain." <u>Acta psychologica</u> **105**(2-3): 211-235.

Hyde, K. L., et al (2011). "Functional MRI Evidence of an Abnormal Neural Network for Pitch Processing in Congenital Amusia." <u>Cerebral Cortex</u> **21**(2): 292-299.

Jernigan, T. L., et al (1991). "Cerebral structure on magnetic resonance imaging in language-and learning-impaired children." <u>Archives of neurology</u> **48**(5): 539-545.

Jones, L. B. (2001). "Recent cytoarchitechtonic changes in the prefrontal cortex of schizophrenics." <u>Front. Biosci</u> **6**: E148-E153. Jones, S. E., et al (2000). "Three-dimensional mapping of cortical thickness using Laplace's equation." <u>Human Brain Mapping</u> **11**(1): 12-32.

Judaš, M., et al (2012). "Brodmann's map of the human cerebral cortex—or Brodmann's maps?" <u>Translational Neuroscience</u> **3**(1): 67-74.

Jung, J., et al (2022). "Subregions of DLPFC display graded yet distinct structural and functional connectivity." <u>Journal of Neuroscience</u> **42**(15): 3241-3252.

Karolis, V. R., et al (2019). "The architecture of functional lateralisation and its relationship to callosal connectivity in the human brain." Nature Communications **10**(1): 1417.

Kim, C., et al (2012). "Domain general and domain preferential brain regions associated with different types of task switching: A meta-analysis." <u>Human Brain Mapping</u> **33**(1): 130-142.

Kim, J.-H., et al (2010). "Defining functional SMA and pre-SMA subregions in human MFC using resting state fMRI: functional connectivity-based parcellation method." <u>Neuroimage</u> **49**(3): 2375-2386.

Klaus, J. and G. Hartwigsen (2019). "Dissociating semantic and phonological contributions of the left inferior frontal gyrus to language production." Human Brain Mapping **40**(11): 3279-3287.

Knecht, S., et al (2000). "Language lateralization in healthy right-handers." Brain 123(1): 74-81.

Koenigs, M. and J. Grafman (2009). "The functional neuroanatomy of depression: distinct roles for ventromedial and dorsolateral prefrontal cortex." <u>Behavioural brain research</u> **201**(2): 239-243.

Kolb, B. (2024). "Patricia Goldman-Rakic: a pioneer and leader in frontal lobe research." <u>Frontiers in</u> Human Neuroscience **17**.

Kolk, S. M. and P. Rakic (2022). "Development of prefrontal cortex." <u>Neuropsychopharmacology</u> **47**(1): 41-57.

Kong, X.-Z., et al (2018). "Mapping cortical brain asymmetry in 17,141 healthy individuals worldwide via the ENIGMA Consortium." <u>Proceedings of the National Academy of Sciences</u> **115**(22): E5154-E5163.

Kononova, E. (1935). "The variability of structure of the cortex of the brain: inferior frontal gyrus of adult man." <u>Brain Res Inst Publ</u> 1: 49-118.

Kononova, E. (1938). "Variability of the structure of the cerebral cortex." <u>The frontal region of adult</u> human **2**: 213-274.

Kowner, R. (1995). "Laterality in facial expressions and its effect on attributions of emotion and personality: a reconsideration." <u>Neuropsychologia</u> **33**(5): 539-559.

Kuo, F. and T. F. Massoud (2022). "Structural asymmetries in normal brain anatomy: A brief overview." Annals of Anatomy-Anatomischer Anzeiger **241**: 151894.

Laird, A. R., et al (2005). "BrainMap: the social evolution of a human brain mapping database." Neuroinformatics **3**: 65-77.

Lau, H. C., et al (2004). "Willed action and attention to the selection of action." <u>Neuroimage</u> **21**(4): 1407-1415.

Lee, K. H. and G. J. Siegle (2012). "Common and distinct brain networks underlying explicit emotional evaluation: a meta-analytic study." <u>Social cognitive and affective neuroscience</u> **7**(5): 521-534.

Levine, S. C. and J. Levy (1986). "Perceptual asymmetry for chimeric faces across the life span." <u>Brain and Cognition</u> **5**(3): 291-306.

Levy, R. (2023). "The prefrontal cortex: from monkey to man." Brain 147(3): 794-815.

Levy, R. (2024). "The prefrontal cortex: from monkey to man." Brain 147(3): 794-815.

Li, P.-C., et al (2000). "Left prefrontal cortex activation during semantic encoding accessed with functional near infrared imaging." <u>Hang tian yi xue yu yi xue gong cheng= Space Medicine & Medical</u> Engineering **13**(2): 79-83.

Luders, E., et al (2006). "Hemispheric asymmetries in cortical thickness." <u>Cerebral Cortex</u> **16**(8): 1232-1238.

Luo, Y., et al (2024). "Resting-state fNIRS reveals changes in prefrontal cortex functional connectivity during TENS in patients with chronic pain." <u>Scientific Reports</u> **14**(1): 29187.

Mahalanobis, P. C., et al (1949). "Anthropometric Survey of the United Provinces, 1941: A Statistical Study." <u>Sankhyā: The Indian Journal of Statistics (1933-1960)</u> **9**(2/3): 89-324.

Maingault, S., et al (2016). "Regional correlations between cortical thickness and surface area asymmetries: A surface-based morphometry study of 250 adults." <u>Neuropsychologia</u> **93**: 350-364. Mammucari, A., et al (1988). "Spontaneous facial expression of emotions in brain-damaged patients." <u>cortex</u> **24**(4): 521-533.

Mandal, M., et al (1992). "Role of cerebral hemispheres and regions in processing hemifacial expression of emotion: evidence from brain-damage." <u>International journal of neuroscience</u> **63**(3-4): 187-195.

Markov, N. T., et al (2013). "Cortical high-density counterstream architectures." <u>Science</u> **342**(6158): 1238406.

McDermott, K. B., et al (2003). "A procedure for identifying regions preferentially activated by attention to semantic and phonological relations using functional magnetic resonance imaging." Neuropsychologia **41**(3): 293-303.

Merker, B. (1983). "Silver staining of cell bodies by means of physical development." <u>J Neurosci</u> Methods **9**(3): 235-241.

Mikels, J. A., et al (2005). "Emotional category data on images from the International Affective Picture System." <u>Behavior research methods</u> **37**: 626-630.

Minkova, L., et al (2017). "Gray matter asymmetries in aging and neurodegeneration: A review and meta-analysis." <u>Human Brain Mapping</u> **38**(12): 5890-5904.

Mizuno, K., et al (2008). "The neural basis of academic achievement motivation." <u>Neuroimage</u> **42**(1): 369-378.

Nieuwenhuys, R., et al (2007). <u>The human central nervous system: a synopsis and atlas</u>, Springer Science & Business Media.

Nieuwenhuys, R., et al (2008). "The Human Central Nervous System." (No Title).

Nitschke, K., et al (2017). "A meta-analysis on the neural basis of planning: Activation likelihood estimation of functional brain imaging results in the tower of London task." <u>Human Brain Mapping</u> **38**(1): 396-413.

Ocklenburg, S., et al (2016). "Intrahemispheric white matter asymmetries: the missing link between brain structure and functional lateralization?" Reviews in the Neurosciences **27**(5): 465-480. Öngür, D., et al (2003). "Architectonic subdivision of the human orbital and medial prefrontal

cortex." <u>Journal of Comparative Neurology</u> **460**(3): 425-449.

Öngür, D. and J. L. Price (2000). "The organization of networks within the orbital and medial prefrontal cortex of rats, monkeys and humans." <u>Cerebral Cortex</u> **10**(3): 206-219.

Ono, M., et al (1990). Atlas of the cerebral sulci, Thieme.

Park, H.-J. and K. Friston (2013). "Structural and functional brain networks: from connections to cognition." <u>Science</u> **342**(6158): 1238411.

Passingham, R. E., et al (2002). "The anatomical basis of functional localization in the cortex." <u>Nature Reviews Neuroscience</u> **3**(8): 606-616.

Petralia, M. C., et al (2020). "Meta-analysis of transcriptomic data of dorsolateral prefrontal cortex and of peripheral blood mononuclear cells identifies altered pathways in schizophrenia." <u>Genes</u> **11**(4): 390.

Petrides, M. (1996). "Specialized systems for the processing of mnemonic information within the primate frontal cortex." <u>Philosophical Transactions of the Royal Society of London. Series B: Biological Sciences</u> **351**(1346): 1455-1462.

Petrides, M. (2005). "Lateral prefrontal cortex: architectonic and functional organization."

Philosophical Transactions of the Royal Society B: Biological Sciences 360(1456): 781-795.

Petrides, M. (2013). Neuroanatomy of language regions of the human brain, Academic Press.

Petrides, M. (2018). <u>Atlas of the morphology of the human cerebral cortex on the average MNI brain</u>, Academic Press.

Petrides, M. and D. Pandya (2002). "Comparative cytoarchitectonic analysis of the human and the macaque ventrolateral prefrontal cortex and corticocortical connection patterns in the monkey." European Journal of Neuroscience **16**(2): 291-310.

Petrides, M. and D. N. Pandya (1999). "Dorsolateral prefrontal cortex: comparative cytoarchitectonic analysis in the human and the macaque brain and corticocortical connection patterns." <u>Eur J Neurosci</u> **11**(3): 1011-1036.

Petrides, M. and D. N. Pandya (1999). "Dorsolateral prefrontal cortex: comparative cytoarchitectonic analysis in the human and the macaque brain and corticocortical connection patterns." <u>European Journal of Neuroscience</u> **11**(3): 1011-1036.

Petrides, M. and D. N. Pandya (2012). "The frontal cortex." <u>The human nervous system</u>: 988-1011. Petrides, M., et al (2012). "The prefrontal cortex: comparative architectonic organization in the human and the macaque monkey brains." cortex **48**(1): 46-57.

Petrovic, P., et al (2000). "Pain-related cerebral activation is altered by a distracting cognitive task." Pain **85**(1-2): 19-30.

Pirau, L. and F. Lui (2018). "Frontal lobe syndrome."

Preuss, T. M. and P. S. Goldman-Rakic (1991). "Myelo-and cytoarchitecture of the granular frontal cortex and surrounding regions in the strepsirhine primate Galago and the anthropoid primate Macaca." <u>Journal of Comparative Neurology</u> **310**(4): 429-474.

Preuss, T. M. and S. P. Wise (2022). "Evolution of prefrontal cortex." <u>Neuropsychopharmacology</u> **47**(1): 3-19.

Rainville, P., et al (1997). "Pain affect encoded in human anterior cingulate but not somatosensory cortex." <u>Science</u> **277**(5328): 968-971.

Rainville, P., et al (1999). "Cerebral mechanisms of hypnotic induction and suggestion." <u>Journal of Cognitive Neuroscience</u> **11**(1): 110-125.

Rajkowska, G. and P. S. Goldman-Rakic (1995). "Cytoarchitectonic Definition of Prefrontal Areas in the Normal Human Cortex: I. Remapping of Areas 9 and 46 using Quantitative Criteria." <u>Cerebral Cortex</u> **5**(4): 307-322.

Rajkowska, G. and P. S. Goldman-Rakic (1995). "Cytoarchitectonic Definition of Prefrontal Areas in the Normal Human Cortex: II. Variability in Locations of Areas 9 and 46 and Relationship to the Talairach Coordinate System." <u>Cerebral Cortex</u> **5**(4): 323-337.

Ray, K. L., et al (2015). "Co-activation based parcellation of the human frontal pole." <u>Neuroimage</u> **123**: 200-211.

Ridderinkhof, K. R., et al (2004). "Neurocognitive mechanisms of cognitive control: the role of prefrontal cortex in action selection, response inhibition, performance monitoring, and reward-based learning." <u>Brain and Cognition</u> **56**(2): 129-140.

Ringo, J. L., et al (1994). "Time is of the essence: a conjecture that hemispheric specialization arises from interhemispheric conduction delay." Cerebral Cortex **4**(4): 331-343.

Robinson, J. L., et al (2010). "Metaanalytic connectivity modeling: delineating the functional connectivity of the human amygdala." <u>Human Brain Mapping</u> **31**(2): 173-184.

Rowe, J. B. and R. E. Passingham (2001). "Working memory for location and time: activity in prefrontal area 46 relates to selection rather than maintenance in memory." <u>Neuroimage</u> **14**(1): 77-86.

Rubinsztein, J. S., et al (2001). "Decision-making in mania: a PET study." <u>Brain</u> **124**(12): 2550-2563. Saal, M. (2019). Two new areas in the human frontal operculum: cytoarchitecture, stereotaxic maps and brain function.

Saal, M., et al (2021). "Probabilistic cytoarchitectonic map of Area OP9 (Frontal Operculum) (v6.2) [Data set]." EBRAINS. DOI: 10.25493/9TCJ-JZ3.

Sackeim, H. A., et al (1978). "Emotions are expressed more intensely on the left side of the face." <u>Science</u> **202**(4366): 434-436.

Salat, D. H., et al (2001). "Selective preservation and degeneration within the prefrontal cortex in aging and Alzheimer disease." <u>Archives of neurology</u> **58**(9): 1403-1408.

Sarkissov, S., et al (1955). "Atlas of the cytoarchitectonics of the human cerebral cortex." <u>Moscow:</u> <u>Medgiz</u> **20**.

Schleicher, A., et al (1999). "Observer-independent method for microstructural parcellation of cerebral cortex: A quantitative approach to cytoarchitectonics." <u>Neuroimage</u> **9**(1): 165-177.

Schleicher, A., et al (2009). "Quantitative Architectural Analysis: A New Approach to Cortical Mapping." <u>Journal of Autism and Developmental Disorders</u> **39**(11): 1568-1581.

Schleicher, A., et al (2005). "Quantitative architectural analysis: a new approach to cortical mapping." <u>Anatomy and Embryology</u> **210**(5-6): 373-386.

Schleicher, A. and K. Zilles (1990). "A QUANTITATIVE APPROACH TO CYTOARCHITECTONICS - ANALYSIS OF STRUCTURAL INHOMOGENEITIES IN NERVOUS-TISSUE USING AN IMAGE ANALYZER." <u>Journal of Microscopy-Oxford</u> **157**: 367-381.

Sebastian, A., et al (2016). "Dissociable attentional and inhibitory networks of dorsal and ventral areas of the right inferior frontal cortex: a combined task-specific and coordinate-based meta-analytic fMRI study." <u>Brain Structure and Function</u> **221**: 1635-1651.

Sebenius, I., et al (2024). "Structural MRI of brain similarity networks." <u>Nature Reviews</u> Neuroscience: 1-18.

Shi, Y., et al (2012). "Human cerebral cortex development from pluripotent stem cells to functional excitatory synapses." <u>Nature Neuroscience</u> **15**(3): 477-486.

Sohn, M.-H., et al (2000). "The role of prefrontal cortex and posterior parietal cortex in task switching." Proceedings of the National Academy of Sciences **97**(24): 13448-13453.

Sporns, O. and J. D. Zwi (2004). "The small world of the cerebral cortex." <u>Neuroinformatics</u> **2**: 145-162.

Suda, A., et al (2020). "Functional organization for response inhibition in the right inferior frontal cortex of individual human brains." <u>Cerebral Cortex</u> **30**(12): 6325-6335.

Suga, M., et al (2010). "Reduced gray matter volume of Brodmann's Area 45 is associated with severe psychotic symptoms in patients with schizophrenia." <u>European archives of psychiatry and clinical neuroscience</u> **260**: 465-473.

Tanji, J. and E. Hoshi (2001). "Behavioral planning in the prefrontal cortex." <u>Current opinion in</u> neurobiology **11**(2): 164-170.

Tau, G. Z. and B. S. Peterson (2010). "Normal development of brain circuits." Neuropsychopharmacology **35**(1): 147-168.

Teffer, K. and K. Semendeferi (2012). "Human prefrontal cortex: evolution, development, and pathology." <u>Progress in brain research</u> **195**: 191-218.

Toga, A. W. and P. M. Thompson (2003). "Mapping brain asymmetry." <u>Nature Reviews Neuroscience</u> **4**(1): 37-48.

Townsend, J., et al (2010). "fMRI abnormalities in dorsolateral prefrontal cortex during a working memory task in manic, euthymic and depressed bipolar subjects." <u>Psychiatry Research:</u> Neuroimaging **182**(1): 22-29.

Turken and N. F. Dronkers (2011). "The neural architecture of the language comprehension network: converging evidence from lesion and connectivity analyses." <u>Frontiers in System Neuroscience</u> **5**: 1. Tyler, L. K., et al (2011). "Left inferior frontal cortex and syntax: function, structure and behaviour in patients with left hemisphere damage." <u>Brain</u> **134**(2): 415-431.

Uylings, H. B., et al (2010). "3-D Cytoarchitectonic parcellation of human orbitofrontal cortex: Correlation with postmortem MRI." Psychiatry Research: Neuroimaging **183**(1): 1-20.

Villemure, C. and M. C. Bushnell (2009). "Mood influences supraspinal pain processing separately from attention." <u>Journal of Neuroscience</u> **29**(3): 705-715.

Vingerhoets, G., et al (2003). "Multilingualism: an fMRI study." Neuroimage 20(4): 2181-2196.

Vogt, S., et al (2007). "Prefrontal involvement in imitation learning of hand actions:: Effects of practice and expertise." <u>Neuroimage</u> **37**(4): 1371-1383.

von Economo, C. F. and G. N. Koskinas (1925). <u>Die cytoarchitektonik der hirnrinde des erwachsenen</u> <u>menschen</u>, J. Springer.

Vorobyev, V. A., et al (2004). "Linguistic processing in visual and modality-nonspecific brain areas: PET recordings during selective attention." <u>Cognitive Brain Research</u> **20**(2): 309-322.

Wager, T. D., et al (2003). "Valence, gender, and lateralization of functional brain anatomy in emotion: a meta-analysis of findings from neuroimaging." <u>Neuroimage</u> **19**(3): 513-531.

Walker, A. E. (1940). "A cytoarchitectural study of the prefrontal area of the macaque monkey." <u>Journal of Comparative Neurology</u> **73**(1): 59-86.

Wang, S., et al (2019). "Brain functional organization associated with language lateralization." <u>Cerebral Cortex</u> **29**(10): 4312-4320.

Ward Jr, J. H. (1963). "Hierarchical grouping to optimize an objective function." <u>Journal of the American statistical association</u> **58**(301): 236-244.

Willbrand, E. H., et al (2023). "Neuroanatomical and functional dissociations between variably present anterior lateral prefrontal sulci." <u>Journal of Cognitive Neuroscience</u> **35**(11): 1846-1867. Willbrand, E. H., et al (2024). "Sulcal variability in anterior lateral prefrontal cortex contributes to variability in reasoning performance among young adults." <u>Brain Structure and Function</u> **229**(2): 387-402

Wojtasik, M., et al (2020). "Cytoarchitectonic Characterization and Functional Decoding of Four New Areas in the Human Lateral Orbitofrontal Cortex." Frontiers in Neuroanatomy **14**.

Wree, A., et al (1982). "ESTIMATION OF VOLUME FRACTIONS IN NERVOUS-TISSUE WITH AN IMAGE ANALYZER." <u>Journal of Neuroscience Methods</u> **6**(1-2): 29-43.

Wu, L., et al (2025). "Right inferior frontal cortex and preSMA in response inhibition: An investigation based on PTC model." <u>Neuroimage</u> **306**: 121004.

Yokoyama, C., et al (2015). "Dysfunction of ventrolateral prefrontal cortex underlying social anxiety disorder: A multi-channel NIRS study." <u>NeuroImage: Clinical</u> **8**: 455-461.

Yucel, K., et al (2008). "Anterior cingulate volumes in never-treated patients with major depressive disorder." <u>Neuropsychopharmacology</u> **33**(13): 3157-3163.

Zald, D. H. (2007). "Orbital versus dorsolateral prefrontal cortex: anatomical insights into content versus process differentiation models of the prefrontal cortex." <u>Annals of the New York Academy of Sciences</u> **1121**(1): 395-406.

Zhang, J. X., et al (2004). "Semantic processing of Chinese in left inferior prefrontal cortex studied with reversible words." <u>Neuroimage</u> **23**(3): 975-982.

Zhang, L., et al (2020). "Sex difference in glia gene expression in the dorsolateral prefrontal cortex in bipolar disorder: Relation to psychotic features." <u>Journal of psychiatric research</u> **125**: 66-74.

Zheng, D., et al (2008). "The key locus of common response inhibition network for no-go and stop signals." <u>Journal of Cognitive Neuroscience</u> **20**(8): 1434-1442.

Zilles, K. and K. Amunts (2010). "Centenary of Brodmann's map—conception and fate." <u>Nature Reviews Neuroscience</u> **11**(2): 139-145.

Zilles, K., et al (1997). "Quantitative analysis of sulci in the human cerebral cortex: development, regional heterogeneity, gender difference, asymmetry, intersubject variability and cortical architecture." <u>Human Brain Mapping</u> **5**(4): 218-221.

7 Appendix

Supplementary. Table 1: The corrected total volume for each whole brain.

Brain No.	TotalVol (mm³)
BC01	1308140
BC04	1140504
BC05	1106589
BC08	1178295
BC09	1075581
BC10	1013566
BC11	1338178
BC13	1195736
BC20	1348837
BC21	1364826
Mean	1207025
SD	125878

SD, standard deviation.

Acknowledgement

Three years have passed so quickly since the first day I arrived in Germany. Pursuing a PhD here has been a significant milestone in my life.

First and foremost, I extend my deepest gratitude to my supervisor, Prof. Dr. med. Katrin Amunts, for unveiling the mysteries of the human brain to me. I am deeply honored to have pursued my scientific career in her distinguished research group. Her visionary mentorship guided me through the complexities of human brain research while respecting my autonomy. I am profoundly grateful for her balanced approach to supervision - meticulously refining the technical details of my work while fostering resilience through personal challenges. The thoughtful critiques she provided during our discussions systematically strengthened the precision and reproducibility of my experimental designs. Her exceptional ability to integrate groundbreaking science with compassionate leadership serves as an inspiring model that I will carry forward. Contributing to her pioneering work in advancing neuroscience and brain health has been the greatest honor of my early scientific career. Vielen Dank, Professor Amunts, for making this journey not only intellectually transformative and but also personally enriching.

Secondly, I extend my heartfelt gratitude to my PhD co-supervisor, Prof. Dr. med. Michael Sabel, for his steadfast academic stewardship. His rigorous review of my research proposals and annual reports has been instrumental in shaping the scientific rigor of this work, while his trust in my scholarly independence has allowed me to cultivate essential research autonomy. Vielen Dank, Prof. Sabel.

To my daily primary mentor, Dr. rer. nat. Sabine Helene Ruland, whose sharp insights transformed vague ideas into concrete scientific advancements - your scientific acumen, often delivered with witty remarks, never ceased to amaze me. Special appreciation goes to Dr. rer. nat. Ariane Bruno for establishing the methodological foundations during the early stage of my doctoral journey. The research habits I developed under your patient guidance remains my academic compass. Vielen Dank, dear Sabine and Ariane.

This journey would not have been possible without crucial technical support: To Sebastian, whose expertise in statistics and MATLAB provided indispensable solutions for time-sensitive analyses; To Hartmut, whose mastery in 3D reconstruction, coupled with an exceptional

collaborative spirit, proved invaluable to this research; To Felix from INM-7, whose expertise and generous support were indispensable in helping to perform the MACM analysis, his patience in clarifying complex computational aspects and his willingness to engage in in-depth discussions made a profound impact on the quality of this research. Vielen Dank, dear Sebastian, Hartmut, and Felix.

To my other cherished colleagues, Natallia, Olga, Daniel, Andrea, Ihsane, Meiqi, Mingxian, and Yuanyuan, your intellectual companionship transformed solitary research into a journey of collaborative discovery. Special thanks to the administrative lifeline extended by Janine, Anna, Steffie, and Chantal in our institute, along with Jessica from the medical faculty, deserves particular recognition for their meticulous responsiveness and unwavering support. Vielen Dank, dear you guys.

Beyond academia, I extend my deepest gratitude and heartfelt appreciation: To my parents, my grandmother, my younger brother Yu, my cousin Qitong and Lijie, and all my family members - your unwavering transcontinental faith in my choices has been the anchor of my resilience; To my best friends in China, Wenjing Guo, Xue Liu, Tingting Han, Fengpei Li, and Miss Ni - your limitless spiritual support and unwavering encouragement have brightened my world across time zones and vast mountains; To my German friends, Joerg, Daniel, and Julian - your warm inclusivity transformed foreign soil into a welcoming home, I will always cherish the beautiful memories we created in our apartment; To my other Chinese friends in Germany, Mengshu, Yangyan, Ruiyun, Yongmin, Lulu, and Jing — your companionship has made this journey not just fulfilling but also immensely joyful. Thank you all!

This doctoral journey has been an extraordinary chapter in my life, filled with challenges, growth, and countless moments of discovery. Looking back, I am grateful not only for the academic and scientific progress I have made but also for the profound personal transformation this journey has brought.

Finally, I extend my deepest gratitude to myself – for the perseverance, resilience, and dedication I have shown throughout these years. You did a great job navigating the complexities of the doctoral project while taking care of yourself in a foreign country. Fortunately, and thankfully, I did not walk this journey. This period has been more than just an academic pursuit; it has been a journey of self-discovery. Through the highs and lows, I

have gradually come to understand myself better and learn the invaluable lesson of self-love – an unexpected yet profoundly precious experience.

Last but not the least, I would like to express my heartfelt appreciation to Gabriel José García Márquez, Miguel de Cervantes Saavedra, Liu Cixin, Moyan, and Hermann Karl Hesse – although we have never met, your literary masterpieces stand as timeless beacons of human civilization. Your works have been my refuge, a source of inspiration and solace during moments of solitude and contemplation.

It takes a village to raise a PhD candidate – this village has my eternal gratitude.